

2011

Charmed Hadron Spectrum and Interactions

Liuming Liu

College of William & Mary - Arts & Sciences

Follow this and additional works at: <https://scholarworks.wm.edu/etd>



Part of the [Physics Commons](#)

Recommended Citation

Liu, Liuming, "Charmed Hadron Spectrum and Interactions" (2011). *Dissertations, Theses, and Masters Projects*. Paper 1539623577.

<https://dx.doi.org/doi:10.21220/s2-7per-0c68>

This Dissertation is brought to you for free and open access by the Theses, Dissertations, & Master Projects at W&M ScholarWorks. It has been accepted for inclusion in Dissertations, Theses, and Masters Projects by an authorized administrator of W&M ScholarWorks. For more information, please contact scholarworks@wm.edu.

Charmed Hadron Spectrum and Interactions

Liuming Liu

Tianmen, Hubei, China

Master of Science, Peking University, 2005

Bachelor of Engineering, Wuhan University, 2002

A Dissertation presented to the Graduate Faculty
of the College of William and Mary in Candidacy for the Degree of
Doctor of Philosophy

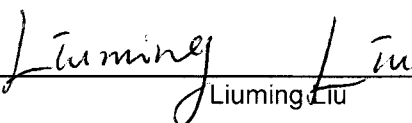
Department of Physics

The College of William and Mary
January, 2011

APPROVAL PAGE

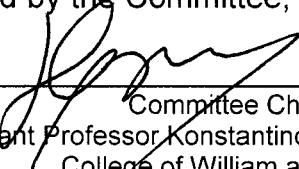
This Dissertation is submitted in partial fulfillment of
the requirements for the degree of

Doctor of Philosophy

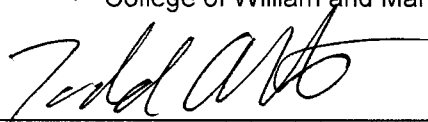


Liuming Liu

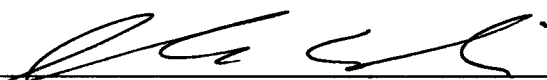
Approved by the Committee, September, 2010




Committee Chair
Assistant Professor Konstantinos Orginos, Physics
College of William and Mary



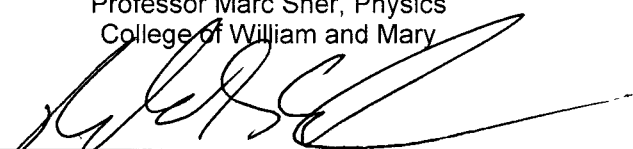
Professor Todd Averett, Physics
College of William and Mary



Associate Professor Joshua Erlich, Physics
College of William and Mary



Professor Marc Sher, Physics
College of William and Mary



Dr. Robert Edwards, Senior Staff Scientist, Theory Group
Thomas Jefferson National Accelerator Facility

ABSTRACT PAGE

Studying hadrons containing heavy quarks in lattice QCD is challenging mainly due to finite lattice spacing effects. To control the discretization errors, $m_Q a$ is required to be much less than 1, where m_Q is the quark mass and a is the lattice spacing. For currently accessible lattice spacings, the charm quark mass doesn't satisfy this requirement. One approach to simulate heavy quarks on the lattice is non-relativistic QCD, which treats heavy quark as a static source and expand the lattice quark action in powers of $\frac{1}{m_Q a}$. Unfortunately, the charm quark is not heavy enough to justify this expansion. Another is Heavy Quark Effective Theory (HQET) matched on QCD. Non-relativistic QCD and HQET are mainly used for bottom quark. Relativistic heavy-quark action, which incorporates both small mass and large mass formulations, is better suited to study the charm quark sector. The discretization errors can be reduced systematically following Symanzik improvement.

In this work, we use the relativistic heavy quark action to study the charmed hadron spectrum and interactions in full lattice QCD. For the light quarks we use domain-wall fermions in the valence sector and improved Kogut-Susskind sea quarks. The parameters in the heavy quark action are tuned to reduce lattice artifacts and match the charm quark mass and the action is tested by calculating the low-lying charmonium spectrum.

We compute the masses of the spin-1/2 singly and doubly charmed baryons. For the singly charmed baryons, our results are in good agreement with experiment within our systematics. For the doubly charmed baryon Ξ_{cc} , we find the isospin-averaged mass to be $M_{\Xi_{cc}} = 3665 \pm 17 \pm 14_{-78}^{+0}$ MeV; the three given uncertainties are statistical, systematic and an estimate of lattice discretization errors, respectively. In addition, we predict the mass splitting of the (isospin-averaged) spin-1/2 Ω_{cc} with the Ξ_{cc} to be $M_{\Omega_{cc}} - M_{\Xi_{cc}} = 98 \pm 9 \pm 22 \pm 13$ MeV (in this mass splitting, the leading discretization errors are also suppressed by $SU(3)$ symmetry). Combining this splitting with our determination of $M_{\Xi_{cc}}$ leads to our prediction of the spin-1/2 Ω_{cc} mass, $M_{\Omega_{cc}} = 3763 \pm 19 \pm 26_{-79}^{+13}$ MeV.

We calculate the scattering lengths of the charmed mesons with the light pseudoscalar mesons. The calculation is performed for four different light quark masses and extrapolated to the physical point using chiral perturbation formulas to next-to-next-to-leading order. The low energy constants are determined and used to make predictions. We find relatively strong attractive interaction in DK channels, which is closely related to the structure of $D_{sJ}(2317)$ state. The scattering of charmonium with light hadrons is also studied. Particularly, we find very weak attractive interaction between J/Ψ and nucleon, in this channel the dominate interaction is attractive gluonic van der Waals and it could lead to molecular-like bound states.

Table of Contents

List of Tables	v
List of Figures	ix
Acknowledgements	xiv
1 Introduction	1
1.1 Overview of particle physics	1
1.1.1 Fundamental particles	1
1.1.2 Quark model	2
1.1.3 Physics beyond quark model	15
1.2 Standard model	16
1.3 Quantum Chromodynamics	17
1.3.1 QCD Lagrangian	17
1.3.2 Asymptotic freedom	18
1.4 Organization of this dissertation	19
2 Lattice QCD and Numerical Methods	21
2.1 Euclidean space-time	21
2.2 Lattice discretization	22
2.3 Fermion fields on lattice	23
2.3.1 Discretization of free fermions	23

2.3.2	Fermion action with external gauge fields	24
2.3.3	Fermion doubling problem	25
2.3.4	Wilson fermions	27
2.3.5	Chiral fermions	28
2.4	Gauge fields on lattice	31
2.4.1	The Wilson gauge action	31
2.4.2	The wilson loop	32
2.5	Monte Carlo Method	33
2.6	Simulation of fermions	37
2.7	Data analysis	38
2.7.1	Statistical analysis for uncorrelated data	39
2.7.2	Statistical analysis in the presence of autocorrelation	40
2.7.3	Data blocking methods	41
2.7.4	Data fitting	42
3	Effective Field Theory	45
3.1	Heavy quark effective theory	46
3.1.1	Derivation of the effective lagrangian	46
3.1.2	$1/m_Q$ expansion	49
3.1.3	Hadron masses	51
3.2	Chiral perturbation theory	53
3.2.1	Chiral symmetry in QCD	54
3.2.2	Effective chiral Lagrangian	56
3.2.3	Heavy baryon chiral perturbation theory (HB χ PT)	58
3.2.4	χ PT for baryons containing a heavy quark	62
3.2.5	χ PT for Heavy mesons	65

4	Lattice Setup and Computational Techniques	67
4.1	Lattice Setup	67
4.1.1	Light-Quark Action	67
4.1.2	Heavy-Quark Action	69
4.2	Extracting Baryon Masses from Correlation Functions	72
4.2.1	Spectral representation of correlation functions	72
4.2.2	Effective mass	76
4.2.3	Extracting excited states	77
4.3	Extracting Scattering Length Using Lüscher's Finite Volume Technique	79
5	Charmed Baryon Spectrum	84
5.1	Introduction	84
5.2	Charmed Hadron Spectrum: Numerical Results	87
5.3	Heavy- and Light-Quark Mass Extrapolation	88
5.3.1	Scale setting with f_π	91
5.3.2	Charm-Quark Mass Extrapolation	93
5.3.3	Light-Quark Mass Extrapolation	99
5.3.4	Discretization Errors and Mass Splittings	106
5.4	Discussion and Conclusions	110
6	Charmed Hadron Interaction	116
6.1	Introduction	116
6.2	Scattering of charmed mesons (D, D_s) with light pseudoscalar mesons (π, K)	117
6.2.1	Numerical results	119
6.2.2	Discussion	126
6.3	Scattering of charmonium with light hadrons	127

7 Conclusions	134
Bibliography	137

List of Tables

1.1	The fundamental particles and their properties.	2
1.2	Quantum numbers of quarks and antiquarks.	6
1.3	Flavor content of the SU(3) mesons.	7
1.4	Flavor wave functions of SU(3) decuplet baryons.	9
1.5	Flavor wave functions of SU(3) octet baryons.	9
1.6	Spin wave functions of the states formed by 3 spin $\frac{1}{2}$ objects.	10
1.7	The flavor wave functions of the baryons containing at lease on charm quark in SU(4) 20-plet which is symmetric under the interchange of quark labels.	12
1.8	The flavor wave functions of the charmed baryons in $\bar{4}$ -plet.	13
1.9	The flavor wave functions of the baryons containing at lease on charm quark in SU(4) 20-plet which has mixed symmetry under the interchange of quark labels.	14
4.1	The parameters of the configurations and domain-wall propagators used in this work. The subscript l denotes light quark, and s denotes the strange quark. The superscript “dwf” denotes domain-wall fermion.	69
4.2	Speed of light for charmed mesons.	71

5.1	Charmed baryon masses in lattice units with 2 values of m_0 (indicated as $m_1 = 0.2034$ and $m_2 = 0.2100$) in Eq. (4.2). The first uncertainty is statistical and the second is systematic from the different choice of fitting ranges (presented in square brackets). The m007, m010, m020, m030 indicate the four ensembles listed in Table 4.1.	89
5.2	Charmonium masses in lattice units with $m_1 = 0.2034$ and $m_2 = 0.2100$.	89
5.3	Values of m_π and f_π calculated in Ref. [1]. For all ensembles the staggered strange-quark mass is $am_s = 0.050$ while the domain-wall strange-quark mass is $am_s^{\text{dwf}} = 0.081$	90
5.4	Values of l_4 needed for chiral extrapolations of M_h/f_π . The different values of l_4 are determined through the different choices of fitting range, also listed.	92
5.5	Low-lying charmonium spectrum of χ_{c0} , χ_{c1} and h_c . The experimental values are taken from the Particle Data Group [2].	97
5.6	Fit to Λ_c and Σ_c masses with NLO continuum formulae.	101
5.7	Fit to Ξ_c and Ξ'_c masses with NLO continuum formulae.	102
5.8	Fit to $J = 1/2$ Ξ_{cc} mass with the NLO continuum heavy-hadron formula.	103
5.9	Fit to $J = 1/2$ Ω_c and Ω_{cc} masses with NLO continuum heavy-hadron formulae.	104
5.10	Direct light/heavy quark mass extrapolation of the $J = 1/2$ charmed baryon spectrum.	106

5.11	Resulting charmed spectrum, extrapolated in the light-quark mass to the physical $m_\pi^{\text{phys}}/f_\pi^{\text{phys}}$ point. In (a) we display the mass splittings of the baryons related by $SU(3)$ and large N_c symmetry. As discussed in detail in the text, the first uncertainty is statistical, the second is systematic and the third is our estimate of discretization errors. These are the central results of this work. In (b), we display our resulting baryon spectrum determined using the experimental values of $M_{\Lambda_c}^{\text{exp}}$ and $M_{\Sigma_c}^{\text{exp}}$, combined with our splittings in (a). For the Ω_{cc} , we use our extrapolated value of $M_{\Xi_{cc}}$ given the present uncertainty in the experimental value. In (c), we present the results of our direct mass extrapolations, including our estimated discretization errors. The results from the two methods are consistent at the one-sigma level.	111
5.12	Summary of existing charmed baryon published calculations from lattice QCD. Please refer to the above references and references within for more details.	113
6.1	The values of m_π , m_K , m_η , f_π , f_K , m_D and m_{D_s} in lattice units. . .	124
6.2	The results of fitting the scattering lengths to the χ PT formulas. . . .	124
6.3	The scattering lengths extrapolated to the physical light quark masses. "Fit1" fits all four ensembles. "Fit2" fits the lightest three ensembles. "Fit3" fits the lightest two ensembles. The uncertainty presented in the parentheses is statistical.	125
6.4	Scattering lengths of $D\pi(I = 1/2)$, $DK(I = 0)$, $DK(I = 1)$ and D_sK predicted from chiral fits. Statistical errors are presented in the parentheses.	126

6.5 Fitted energy shifts of the scattering of $\eta_c - N$, $\eta_c - \rho$, $J/\Psi - \rho$ and $J/\Psi - N$. All values are in lattice units. The statistical errors are indicated in the parentheses. 129

List of Figures

1.1	Weight diagram of the fundamental representation $\mathbf{3}$. The arrows shows how u, d, s are related by the U -spin, V -spin and isospin. . . .	6
1.2	SU(4) multiplets of baryons made of u, d, s and c quarks. (a) is the 20-plet with mixed symmetry. (b) is the symmetric 20-plet. (c) is the $\bar{4}$ -plet.	13
2.1	The link variables $U_\mu(n)$	24
2.2	Domain wall fermions.	30
2.3	The plaquette U_p is composed by the four link variables. The arrows show the direction of the link variables.	32
3.1	Tree level and one-loop diagrams which contribute to the masses of the charmed baryons with $s_l = 0$. The single, double, dashed lines correspond to $s_l = 0$ baryons, $s_l = 1$ baryons and mesons respectively.	64
3.2	Tree level and one-loop diagrams which contribute to the masses of the charmed baryons with $s_l = 1$. The single, double, dashed lines correspond to $s_l = 0$ baryons, $s_l = 1$ baryons and mesons respectively.	65
4.1	S-function plot.	82

5.1	Sample effective-mass plots and corresponding fits to the correlation functions. The smaller error bands are statistical and the larger error bands are statistical and systematic (determined by varying fit range) added in quadrature.	90
5.2	The (blue) filled circles represent the lattice data and the (red) star is the physical point, converted to lattice units using $a^{-1} = 1588$ MeV with a 2% error bar added for the scale setting. The error bands are the 68% confidence intervals in the resulting chiral extrapolation from the lightest two points (a) and a fit to all four lattice points (b). . . .	93
5.3	Spin-averaged mass of η_c and J/Ψ on the different ensembles. The blue points and purple points indicate the masses at m_1 and m_2 respectively. The red line indicates the experimental value. The left panel displays the results from the lattice spacing $a^{-1} = 1588$ MeV used on all ensembles. This method was used to tune the charm-quark mass on the m007 ensemble. The right panel displays the masses scaled by f_π on the lattice and extrapolated to f_π^{phys} , as discussed in the text.	94
5.4	The masses of χ_{c0} , χ_{c1} and h_c as functions of m_π/f_π . The blue points are our numerical values. The pink shaded regions show the standard deviation allowed regions of quadratic fit. The blue shaded regions show the standard deviation allowed regions of quartic fit. The red points are experimental values.	96
5.5	Extrapolation of the hyperfine splitting. The blue points are the lattice data. The red point is the experimental value. The blue band is the quadratic fit with Eq. 5.4, while the pink band is the quartic fit with Eq. 5.4.	98

5.6	NLO HH χ PT extrapolation of M_{Λ_c} and M_{Σ_c} (a) as well as $M_{\Sigma_c} - M_{\Lambda_c}$ (b).	101
5.7	NLO HH χ PT extrapolation of M_{Ξ_c} and $M_{\Xi'_c}$ (a) as well as $M_{\Xi'_c} - M_{\Xi_c}$ (b).	102
5.8	NLO HH χ PT extrapolation of $M_{\Xi_{cc}}$	103
5.9	NLO HH χ PT extrapolation of M_{Ω_c} (a) and $M_{\Omega_{cc}}$ (b).	105
5.10	Ratio of extrapolated masses to experimentally measured masses. The first point represents the HH χ PT fit, the second point is a fit with Eq. (5.25), the third with Eq. (5.26) and the fourth with Eq. (5.27). . .	106
5.11	Polynomial extrapolations of of $J = 1/2$ mass splittings amongst heavy-quark- $SU(3)$ multiplets with Eq. (5.27).	109
5.12	Ratio of extrapolated mass splittings to experiment [2]. The first point is a fit with Eq. (5.25), the second with Eq. (5.26) and the third with Eq. (5.27).	109
5.13	Comparison among charmed baryon mass splittings of dynamical lat- tice calculations. The results of Na et al. are taken from Ref. [3]. . .	112
5.14	A summary of charmed baryon masses in MeV calculated using LQCD. We show both of our methods for obtaining the spectrum, the direct mass extrapolation (Liu et al. 1) and also using the extrapolated mass splittings, combined with $M_{\Lambda_c}^{\text{exp}}$ and $M_{\Sigma_c}^{\text{exp}}$ (Liu et al. 2). These results are taken from Table 5.11. The other results, displayed for comparison, are taken from Table 5.12.	113

5.15	Comparison of theoretical predictions for doubly charmed baryons of spin 1/2. “LQCD” is the lattice QCD calculation done in this work with solid error bars for the statistical error and dashed bars for the total error including the estimated systematic; “QM” is taken from a recent quark-model calculation [4]; “RTQM” is the result of relativistic three-quark model [5]; “RQM” and “HQET” are from the relativistic quark model [6] and the heavy-quark effective theory [7] respectively; “PM” is the result of a potential model [8]; note that there is no error estimation done in these calculations. “SR” and “FHT” are based on the sum rules of nonrelativistic QCD [9] and the Feynman-Hellmann theorem [10] respectively, where rough uncertainties are estimated. . .	115
6.1	Effective energy shifts plots of the scattering channels $D_s - \pi$, $D_s - K$, $D - \bar{K}(I = 0)$, $D - \bar{K}(I = 1)$, $D - \pi(I = 3/2)$. All plots are for ensemble m007. The grey bars show the fitted energy shifts and the fitting ranges. The height of the grey bars show the statistical errors.	120
6.2	Effective energy shifts of the scattering of charmonium (η_c and J/Ψ) with light hadrons (ρ and nucleon). All plots are for ensemble m007. The grey bars indicate the fitted energy shifts and the fitting ranges. The height of the grey bars show the statistical errors.	130
6.3	The scattering lengths of charmonium with light hadron fitted to Eq. 6.40. The blue points are the values from lattice calculation. The blue bands indicate the standard deviation allowed regions of the fits.	133

To my parents for all their love and support.

ACKNOWLEDGEMENTS

I owe my deepest gratitude to my advisor, Prof. Kostas Orginos. With his enthusiasm, his inspiration and his great efforts, he made my experience here invaluable. He provided me with many helpful suggestions, important advices and constant encouragement during the course of this work. This thesis would not have been possible without him.

Special thanks are due to Dr. Andre Walker-Loud. He was always willing to help and taught me many things. He provided valuable suggestions that greatly improved the quality of this study.

I also would like to show my gratitude to Dr. Huey-Wen Lin for her valuable contributions to this work and her instructive advices during my research.

Sincere thanks are extended to Prof. Todd Averett, Dr. Robert Edwards, Prof. Joshua Erlich and Prof. Marc Sher for carefully reading my thesis and giving constructive suggestions.

I would like to thank Dr. David Richards, Prof. William Detmold, Dr. Christopher Aubin, Dr. Christopher Thomas, Dr. Balint Joo, Dr. Jozef Dudek, Dr. Bernhard Musch and all the other collaborators for useful discussions. I wish to extend my warmest thanks to all those who have helped me with my work at the College of William and Mary and the Jefferson Laboratory.

Last but not least, I would like to thank my advisor during my study at Peking University: Prof. Chuan Liu, who was the first person who led me into the world of Lattice QCD.

I am financially supported by Jefferson Science Associates, under U.S. DOE Contract No. DE-AC05-06OR23177. The calculations of this work were performed using Chroma software suite, on computer clusters at Jefferson Laboratory (USQCD SciDAC supported) and the College of William and Mary (Cyclades cluster supported by the Jeffress Memorial Trust grant J-813).

CHAPTER 1

Introduction

1.1 Overview of particle physics

1.1.1 Fundamental particles

One of the main goals of physics is to identify the fundamental building blocks of the universe and the mechanisms that describe their interactions. In the early 20th century atoms were considered as the smallest and indivisible constituents of matter. The Rutherford experiment of large angle scattering of alpha particles off a gold foil suggested that atoms have substructure: a positively-charged nucleus surrounded by a cloud of negative electrons. Later it was discovered that the nucleus consists of positively-charged protons and neutral neutrons. From the 1950s a large number of particles were found in experiments. People began to realize that they are not fundamental but consist of some smaller elements. Around 1968, an experiment at SLAC, in which electrons were scattered off protons, gave the first clear hint that smaller point-like particles existed inside the proton. The electrons were scattered with large transfers of momentum more frequently than expected, suggesting that the proton contained discrete scattering centres within.

	quarks		leptons	
1st generation	u (up)	d (down)	e (electron)	ν_e (e neutrino)
2nd generation	c (charm)	s (strange)	μ (muon)	ν_μ (μ neutrino)
3rd generation	t (top)	b (bottom)	τ (tau)	ν_τ (τ neutrino)
electric charge	$2/3$	$-1/3$	-1	0
spin	$1/2$	$1/2$	$1/2$	$1/2$

Table 1.1: The fundamental particles and their properties.

In 1964, Gell-Mann and Zweig proposed that the proton and the other elementary particles known at that time are in fact built from more basic entities named “quarks”. Today, protons and neutrons are classified as members of a family named baryons which consist of three valence quarks. Another type of particles like pions consists of a quark and an antiquark, which are called mesons. Baryons and mesons are generally called hadrons.

Together with the leptons, the quarks are considered the fundamental particles of nature. The quarks and leptons as well as their properties are listed in Table 1.1. The six types of quarks, called six *flavors*, are split into three generations, with the first generation being the lightest, and the third the heaviest. So are the leptons.

1.1.2 Quark model

Color charge

The quarks have an additional degree of freedom called *color*. Each flavor of quark comes in three colors, which will be labeled as $i = 1, 2, 3$, or red, green and blue, mimicking the three fundamental colors. These three color states form a basis in a 3-dimensional complex vector space. A general color state of a quark is then a vector in this space, which can be rotated by 3×3 unitary matrices. All such

transformations form the Lie group of $SU(3)$. The 3-dimensional color space forms a fundamental representation of $SU(3)$ group, usually denoted as $\mathbf{3}$.

The quarks have anti-particles, called antiquarks. The antiquarks have the same spin and mass as the quarks, but with opposite electric charges. The color states of an antiquark form a representation space of $SU(3)$ where the vectors are transformed according to the complex conjugate $SU(3)$ matrix. We denote this representation as $\bar{\mathbf{3}}$.

In the quark model [11, 12, 13] all hadrons are colorless or white, that is to say the color wave functions of hadrons are $SU(3)$ singlets. According to the multiplication rules of $SU(3)$ group, we have

$$\mathbf{3} \otimes \bar{\mathbf{3}} = \mathbf{1} \oplus \mathbf{8}, \quad (1.1)$$

$$\mathbf{3} \otimes \mathbf{3} \otimes \mathbf{3} = \mathbf{1} \oplus \mathbf{8} \oplus \mathbf{8}' \oplus \mathbf{10}, \quad (1.2)$$

where $\mathbf{1}$ is a color singlet. Thus a color singlet can be formed either by a quark-antiquark pair or by three quarks. The hadrons made of quark-antiquark pair are called mesons while the hadrons made of three quarks are called baryons. The color wave function of a meson is $\frac{1}{\sqrt{3}} \sum_{i=1}^3 q_1^i \bar{q}_2^i$, where i is the color indices, q and \bar{q} are quark and anti-quark fields respectively, the subscripts indicate the flavors. For baryons, the color wave function is $\frac{1}{\sqrt{6}} \epsilon_{i_1 i_2 i_3} q_1^{i_1} q_2^{i_2} q_3^{i_3}$.

$SU(3)$ flavor symmetries

The hadrons that consist of the three flavors of quark(u, d, s) can be nicely classified in the $SU(3)$ group. The three flavors form a basis of the fundamental repre-

sentation of SU(3) group:

$$u = \begin{pmatrix} 1 \\ 0 \\ 0 \end{pmatrix}, \quad d = \begin{pmatrix} 0 \\ 1 \\ 0 \end{pmatrix}, \quad s = \begin{pmatrix} 0 \\ 0 \\ 1 \end{pmatrix}. \quad (1.3)$$

A general state ψ , which is a complex 3-vector, transforms as

$$\psi' = U\psi, \quad (1.4)$$

where U is a 3 unitarity matrix. U can be composed from the eight generators(t_a) of SU(3) group:

$$U = \exp(-i\alpha_a t_a), \quad a = 1, 2, \dots, 8, \quad (1.5)$$

where α_a are coefficients. Canonically the generators are chosen as $t_a = \frac{1}{2}\lambda_a$, where λ_a are the Gell-Mann matrices

$$\begin{aligned} \lambda_1 &= \begin{pmatrix} 0 & 1 & 0 \\ 1 & 0 & 0 \\ 0 & 0 & 0 \end{pmatrix}, & \lambda_2 &= \begin{pmatrix} 0 & -i & 0 \\ i & 0 & 0 \\ 0 & 0 & 0 \end{pmatrix}, & \lambda_3 &= \begin{pmatrix} 1 & 0 & 0 \\ 0 & -1 & 0 \\ 0 & 0 & 0 \end{pmatrix} \\ \lambda_4 &= \begin{pmatrix} 0 & 0 & 1 \\ 0 & 0 & 0 \\ 1 & 0 & 0 \end{pmatrix}, & \lambda_5 &= \begin{pmatrix} 0 & 0 & -i \\ 0 & 0 & 0 \\ i & 0 & 0 \end{pmatrix}, & \lambda_6 &= \begin{pmatrix} 0 & 0 & 0 \\ 0 & 0 & 0 \\ 0 & 1 & 0 \end{pmatrix} \\ \lambda_7 &= \begin{pmatrix} 0 & 0 & 0 \\ 0 & 0 & -i \\ 0 & i & 0 \end{pmatrix}, & \lambda_8 &= \frac{1}{\sqrt{3}} \begin{pmatrix} 1 & 0 & 0 \\ 0 & 1 & 0 \\ 0 & 0 & -2 \end{pmatrix} \end{aligned} \quad (1.6)$$

The λ_1, λ_2 and λ_3 are expanded from Pauli matrices by simply adding zero ele-

ments on the third row and column. They form a $SU(2)$ subgroup, associated with a quantum number called *isospin*. Define the operators

$$I_3 = F_3, \quad I_{\pm} = F_1 \pm iF_2. \quad (1.7)$$

The u, d, s are the eigenstates of I_3 :

$$I_3 u = \frac{1}{2}u, \quad I_3 d = -\frac{1}{2}d, \quad I_3 s = 0. \quad (1.8)$$

u and d are related by I_{\pm} :

$$I_+ d = u, \quad I_- u = d. \quad (1.9)$$

Similarly the $\lambda_{6,7}$ exhibit an $SU(2)$ subgroup called U -spin and the $\lambda_{4,5}$ are related to a subgroup V -spin. Define the operators

$$U_{\pm} = F_6 \pm iF_7, \quad V_{\pm} = F_4 \mp iF_5. \quad (1.10)$$

We have

$$U_+ s = d, \quad U_- d = s, \quad V_+ u = s, \quad V_- s = u. \quad (1.11)$$

The F_8 is diagonal, it commutes with F_3 . Define the hypercharge operator $Y = \frac{2}{\sqrt{3}}F_8$. The u, d and s are the eigenstates of Y with eigenvalues $1/3, 1/3$ and $-2/3$ respectively. Figure 1.1 show the plot of the fundamental representation in $I_3 - Y$ space.

The anti-quarks form a conjugate representation of $SU(3)$, denoted as $\bar{\mathbf{3}}$. The I_3 and Y quantum numbers of the antiquark are opposite as those of quarks. In Table 1.2, we summarize the quantum numbers of quarks and antiquarks. Here B is baryon number. A quark has baryon number $1/3$ while an antiquark has baryon

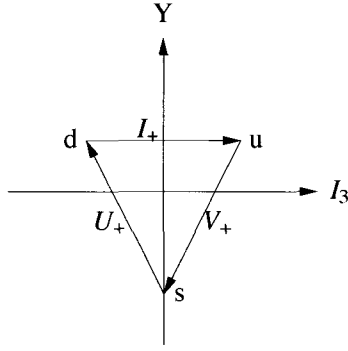


Figure 1.1: Weight diagram of the fundamental representation $\mathbf{3}$. The arrows shows how u, d, s are related by the U -spin, V -spin and isospin.

Quark	I	I_3	Y	B	S
u	$1/2$	$1/2$	$1/3$	$1/3$	0
d	$1/2$	$-1/2$	$1/3$	$1/3$	0
s	0	0	$-2/3$	$1/3$	1
\bar{u}	$1/2$	$-1/2$	$-1/3$	$-1/3$	0
\bar{d}	$1/2$	$1/2$	$-1/3$	$-1/3$	0
\bar{s}	0	0	$2/3$	$-1/3$	-1

Table 1.2: Quantum numbers of quarks and antiquarks.

number $-1/3$. S is strangeness. Only the s quark has non-zero strangeness.

Mesons

Mesons are constructed by combining a quark with an antiquark. Three flavors of quarks(u, d, s) combined with three antiquarks($\bar{u}, \bar{d}, \bar{s}$) yields nine combinations. In the framework of $SU(3)$, the multiplication of the fundamental representation $\mathbf{3}$ and its conjugate representation $\bar{\mathbf{3}}$ decomposes into a singlet and a octet, as shown in Eq. 1.1.

There are six combinations of a quark with a different flavor of anti-quark: $u\bar{d}, d\bar{u}, u\bar{s}, s\bar{u}, d\bar{s}, s\bar{d}$. All of them have definite quantum numbers of I and I_3 . While the combinations of a quark with its own antiquark($u\bar{u}, d\bar{d}, s\bar{s}$) don't have a definite isospin value. For example, $u\bar{u}$ has $I_3 = 0$ but can either a $I = 0$ or a $I = 1$ state.

	Quark content	I	I_3	Y	0^-	1^-
Octet	$u\bar{d}$	1	1	0	π^+	ρ^+
	$\frac{1}{\sqrt{2}}(u\bar{u} - d\bar{d})$	1	0	0	π^0	ρ^0
	$d\bar{u}$	1	-1	0	π^-	ρ^-
	$u\bar{s}$	1/2	1/2	1	K^+	K^{*+}
	$d\bar{s}$	1/2	-1/2	1	K^0	K^{*0}
	$\bar{d}s$	1/2	1/2	-1	\bar{K}^0	\bar{K}^{*0}
	$\bar{u}s$	1/2	-1/2	-1	K^-	K^{*-}
	$\frac{1}{\sqrt{6}}(u\bar{u} + d\bar{d} - 2s\bar{s})$	0	0	0	$\eta \cos \theta_P + \eta' \sin \theta_P$	$\phi \cos \theta_V + \omega \sin \theta_V$
Singlet	$\frac{1}{\sqrt{3}}(u\bar{u} + d\bar{d} + s\bar{s})$	0	0	0	$\eta \cos \theta_P - \eta' \sin \theta_P$	$\phi \cos \theta_V - \omega \sin \theta_V$

Table 1.3: Flavor content of the SU(3) mesons.

Quantum mechanically, the states $u\bar{u}$, $d\bar{d}$ and $s\bar{s}$ are linear superpositions of the $I = 0$ and $I = 1$ states. However, the pure I states can be got from the linear combinations of these states.

It is quite straightforward to write down the SU(3) singlet: $\frac{1}{\sqrt{3}}(u\bar{u} + d\bar{d} + s\bar{s})$, which is an isoscalar. Since the isospin of s and \bar{s} is zero, the isovector contains no $s\bar{s}$: $\frac{1}{\sqrt{2}}(u\bar{u} - d\bar{d})$. The third possible combination of $u\bar{u}$, $d\bar{d}$ and $s\bar{s}$ is orthogonal to these two states: $\frac{1}{\sqrt{6}}(u\bar{u} + d\bar{d} - 2s\bar{s})$. This state is an isoscalar of the SU(3) octet.

Table 1.3 summarizes the flavor functions of the SU(3) mesons and their quantum numbers, as well as the corresponding physical particles. As shown in the last two rows of the table, the physical isoscalars ($\eta, \eta', \phi, \omega$) are the mixtures of the two SU(3) isoscalars. The mixing angles θ_P and θ_V have to be determined experimentally.

Baryons

The baryons are constructed from 3 quarks, antibaryons from 3 antiquarks. This prescription automatically satisfies the rules for assignment of baryon number. For now we ignore the heavy flavors, each of the quarks can be any of the three flavors: u, d, s . There are 10 combinations of three quarks if we ignore the order in which the quarks are selected. They are $uuu, uud, udd, ddd, uus, uds, dds, uss, dss, sss$. We

can always define a symmetric state whatever the three quark content may be. For example, if the quark content is $q_1q_2q_3$, the state $\frac{1}{\sqrt{6}}(q_1q_2q_3 + q_1q_3q_2 + q_2q_1q_3 + q_2q_3q_1 + q_3q_1q_2 + q_3q_2q_1)$ is invariant under the interchange of the quark labels. Hence there are 10 such symmetric states. If at least two quarks are different, we can write a mixed symmetric states, there are 8 of them(uds comes in two ways since there are two choices for the “different quarks”). If all three quarks are different we can form an antisymmetric state under the interchange of any pair of quarks. There are one such state. These symmetry properties can be easily seen in the multiplication rules of the $SU(3)$ group:

$$\mathbf{3} \otimes \mathbf{3} \otimes \mathbf{3} = \mathbf{1}(A) \oplus \mathbf{8}(M, S) \oplus \mathbf{8}(M, A) \oplus \mathbf{10}(S) \quad (1.12)$$

Here (A) means antisymmetry. (M, S) and (M, A) means mixed symmetry, one is symmetric and the other is antisymmetric under the permutation of the first two labels(P_{12}) but having no symmetry under P_{23} or P_{13} . (S) means symmetry.

In Table 1.4 we list the flavor wave functions of the 10 symmetric states and the corresponding physical particles. The flavor wave functions of the mixed symmetric states are listed in Table 1.5. Note that Σ_0 and Λ_0 both have quark content uds , in Σ_0 the ud quarks have isospin 1 while in Λ_0 they have isospin 0.

The antisymmetric state is

$$\Psi(A) = \frac{1}{\sqrt{6}}(uds + dsu + sud - usd - dus - sdu). \quad (1.13)$$

In the ground state multiplet, this state is forbidden by Fermi statistics.

The complete wave function of a baryon, which contains color, space, spin and flavor part, is antisymmetric under the interchange of any two quarks due to the requirement of Fermi statistics. The color wave function is antisymmetric as we have

Particles	$\Psi(S)$
Δ^{++}	uuu
Δ^+	$\frac{1}{\sqrt{3}}(uud + udu + duu)$
Δ^0	$\frac{1}{\sqrt{3}}(udd + dud + ddu)$
Δ^-	ddd
Σ^{*+}	$\frac{1}{\sqrt{3}}(uus + usu + suu)$
Σ^{*0}	$\frac{1}{\sqrt{6}}(uds + usd + sud + sdu + dsu + dus)$
Σ^{*-}	$\frac{1}{\sqrt{3}}(dds + dsd + sdd)$
Ξ^{*0}	$\frac{1}{\sqrt{3}}(uss + sus + ssu)$
Ξ^{*-}	$\frac{1}{\sqrt{3}}(dss + sds + ssd)$
Ω^-	sss

Table 1.4: Flavor wave functions of SU(3) decuplet baryons.

Particles	$\Psi(M, S)$	$\Psi(M, A)$
P	$\frac{1}{\sqrt{6}}[(ud + du)u - 2uud]$	$\frac{1}{\sqrt{2}}(ud - du)u$
N	$-\frac{1}{\sqrt{6}}[(ud + du)d - 2ddu]$	$\frac{1}{\sqrt{2}}(ud - du)d$
Σ^+	$\frac{1}{\sqrt{6}}[(us + su)u - 2uus]$	$\frac{1}{\sqrt{2}}(us - su)u$
Σ^0	$\frac{1}{2\sqrt{3}}[(ds + sd)u + (us + su)d - 2(ud + du)s]$	$\frac{1}{2}[(ds - sd)u + (us - su)d]$
Σ^-	$\frac{1}{\sqrt{6}}[(ds + sd)d - 2dds]$	$\frac{1}{\sqrt{2}}(ds - sd)d$
Λ^0	$\frac{1}{\sqrt{2}}[(ds + sd)u - (us + su)d]$	$\frac{1}{2\sqrt{3}}[(sd - ds)u + (us - su)d - 2(du - ud)s]$
Ξ^0	$-\frac{1}{\sqrt{6}}[(us + su)s - 2ssu]$	$\frac{1}{\sqrt{2}}(ds - sd)s$
Ξ^-	$-\frac{1}{\sqrt{6}}[(ds + sd)s - 2ssd]$	$\frac{1}{\sqrt{2}}(us - su)s$

Table 1.5: Flavor wave functions of SU(3) octet baryons.

	$S_z = \frac{3}{2}$	$S_z = \frac{1}{2}$	$S_z = -\frac{1}{2}$	$S_z = -\frac{3}{2}$
$\Phi(\mathcal{S}), S = \frac{3}{2}$	$\uparrow\uparrow\uparrow$	$\frac{1}{\sqrt{3}}(\uparrow\uparrow\downarrow + \uparrow\downarrow\uparrow + \downarrow\uparrow\uparrow)$	$\frac{1}{\sqrt{3}}(\uparrow\downarrow\downarrow + \downarrow\uparrow\downarrow + \downarrow\downarrow\uparrow)$	$\downarrow\downarrow\downarrow$
$\Phi(\mathcal{M}, \mathcal{S}), S = \frac{1}{2}$		$\frac{1}{\sqrt{6}}[(\uparrow\downarrow + \downarrow\uparrow)\uparrow - 2\uparrow\uparrow\downarrow]$	$-\frac{1}{\sqrt{6}}[(\uparrow\downarrow + \downarrow\uparrow)\downarrow - 2\downarrow\downarrow\uparrow]$	
$\Phi(\mathcal{M}, \mathcal{A}), S = \frac{1}{2}$		$\frac{1}{\sqrt{2}}(\uparrow\downarrow - \downarrow\uparrow)\uparrow$	$-\frac{1}{\sqrt{2}}(\uparrow\downarrow - \downarrow\uparrow)\downarrow$	

Table 1.6: Spin wave functions of the states formed by 3 spin $\frac{1}{2}$ objects.

stated above. The space wave function is symmetric for the ground state. Thus the combination of the spin and flavor part should be symmetric.

Combing 3 spin- $\frac{1}{2}$ particles results in 8 independent states. Four of them have total spin $\frac{3}{2}$ and are symmetric under permutations of any two quarks. Another four states have total spin $\frac{1}{2}$, they have mixed symmetry. A spin $\frac{1}{2}$ object forms a basis of the fundamental representation of SU(2) group, thus combing three such objects can be symbolized as

$$\mathbf{2} \otimes \mathbf{2} \otimes \mathbf{2} = \mathbf{4}(S) \oplus \mathbf{2}(M, S) \oplus \mathbf{2}(M, A) \quad (1.14)$$

We display the spin wave functions in Table 1.6.

For the decuplet, the spin and flavor wave function is $\Psi(S)\Phi(S)$, it is clear that this wave function is symmetric under quark interchanges. For the octet, one have to combine the (M, S) and (M, A) wave functions properly to make a symmetric wave function. One possible combination is $\frac{1}{\sqrt{2}}(\Psi(M, S)\Phi(M, S) + \Psi(M, A)\Phi(M, A))$. It is easy to check that this combination is symmetric under the permutation of any pair of quarks.

SU(4) Multiplets

Baryons made of u, d, s and c quarks belong to SU(4) multiplets. Since the mass of the c quark is much larger than the masses of the u, d, s quark, the SU(4) flavor symmetry is badly broken. But studying the quark content of the baryons in the framework of SU(4) group is the clearest way to see what charmed baryons should exist. The u, d, s and c quark form a basis of the fundamental representation of the

SU(4) group. Similar to the SU(3) case, the baryons are categorized into different multiplets according to

$$\mathbf{4} \otimes \mathbf{4} \otimes \mathbf{4} = \mathbf{20}(S) \oplus \mathbf{20}(M, S) \oplus \mathbf{20}(M, A) \oplus \bar{\mathbf{4}}(A). \quad (1.15)$$

It is quite straightforward to construct the symmetric flavor wave functions. The flavor wave functions of the baryons containing at least one charm quark in $\mathbf{20}(S)$ multiplet are listed in Table 1.7. As we have stated, the combination of flavor and spin wave function has to be symmetric for the ground states. So the $\mathbf{20}(S)$ multiplet has total spin $\frac{3}{2}$. The flavor-spin wave function is $\Psi(S)\Phi(S)$, where $\Psi(S)$ is the flavor wave functions in Table 1.7 and $\Phi(S)$ is the spin wave function in Table 1.6. These states and the states in SU(3) decuplet all have the same J^P value $\frac{3}{2}^+$.

Table 1.8 presents the flavor wave functions of the charmed baryons in $\bar{\mathbf{4}}$ -plet. Since there isn't an antisymmetric spin wave function, we can't form a symmetric flavor-spin wave function for the ground states. The lowest states appear at the first excited states with $J^P = \frac{1}{2}^-$.

The flavor wave functions of the $\mathbf{20}(M, S)$ and $\mathbf{20}(M, A)$ multiplets can be constructed from the corresponding SU(3) multiplets. The structure of the Λ_c and Σ_c should be much like the Λ and Σ . The Λ_c differs from the Λ only by the replacement of the s quark with a c quark. Same with the Σ_c and Σ . The Λ_c and Ξ_c belong to the same SU(3) subgroup $\bar{\mathbf{3}}$, so the wave function of Ξ_c can be obtained from the wave function of Λ_c by replacing a light quark with a s quark. the Σ_c, Ξ'_c and Ω_c belong to a SU(3) subgroup $\mathbf{6}$, it is easy to get the wave function of Ξ'_c and Ω_c from the wave function of Σ_c . Table 1.9 summarizes the flavor wave functions of the $\mathbf{20}(M, S)$ and $\mathbf{20}(M, A)$ multiplets. To get a symmetric flavor-spin wave function, one has to combine the flavor wave function and the spin wave function as

Particles	$\Psi(S)$
Ω_{ccc}^{++}	ccc
Ω_{cc}^{*+}	$\frac{1}{\sqrt{3}}(scc + csc + ccs)$
Ξ_{cc}^{*+}	$\frac{1}{\sqrt{3}}(dcc + cdc + ccd)$
Ξ_{cc}^{*++}	$\frac{1}{\sqrt{3}}(ucc + cuc + ccu)$
Ω_c^{*0}	$\frac{1}{\sqrt{3}}(ssc + scs + css)$
Ξ_c^{*0}	$\frac{1}{\sqrt{6}}(dsc + dcs + sdc + scd + cds + csd)$
Ξ_c^{*+}	$\frac{1}{\sqrt{6}}(usc + ucs + suc + scu + cus + csu)$
Σ_c^{*0}	$\frac{1}{\sqrt{3}}(ddc + dcd + cdd)$
Σ_c^{*+}	$\frac{1}{\sqrt{6}}(udc + ucd + cud + cdu + duc + dcu)$
Σ_c^{*++}	$\frac{1}{\sqrt{3}}(uuc + ucu + cuu)$

Table 1.7: The flavor wave functions of the baryons containing at least one charm quark in SU(4) 20-plet which is symmetric under the interchange of quark labels.

$\frac{1}{\sqrt{2}}(\Psi(M, S)\Phi(M, S) + \Psi(M, A)\Phi(M, A))$. These state has $J^P = \frac{1}{2}^+$.

Fig. 1.2 shows the SU(4) multiplets of baryons. (a) is the 20-plet with mixed flavor symmetry. The lowest level is the SU(3) octet. The middle level is the singly-charmed baryons. It splits into two SU(3) multiplets, a $\bar{\mathbf{3}}$ and a $\mathbf{6}$. The $\bar{\mathbf{3}}$ multiplet, which includes Λ_c^+ , Ξ_c^0 and Ξ_c^+ , is antisymmetric under the interchange of light quarks. The $\mathbf{6}$ multiplet, which includes Σ_c^0 , Σ_c^+ , Σ_c^{++} , $\Xi_c'^0$, $\Xi_c'^+$ and Ω_c^0 , is symmetric under the interchange of the two light quarks. The prime is used to distinguish the Ξ_c in the $\mathbf{6}$ from the ones in the $\bar{\mathbf{3}}$. (b) is the 20-plet with a SU(3) decuplet on the lowest level. (c) is the $\bar{\mathbf{4}}$ -plet.

The $J^P = \frac{1}{2}^+$, $\frac{3}{2}$ and $\frac{1}{2}^-$ singly charmed baryons have been well established in experiments. There is also evidence of the existence of a doubly charmed baryon Ξ_{cc} . In this work we will calculate the masses of $J^P = \frac{1}{2}$ singly and doubly charmed baryons in lattice QCD.

Particles	$\Psi(M, S)$	$\Psi(M, A)$
Ω_{cc}^+	$-\frac{1}{\sqrt{6}}[(cs + sc)c - 2ccs]$	$\frac{1}{\sqrt{2}}(sc - cs)c$
Ξ_{cc}^+	$-\frac{1}{\sqrt{6}}[(cd + dc)c - 2ccd]$	$\frac{1}{\sqrt{2}}(dc - cd)c$
Ξ_{cc}^{++}	$-\frac{1}{\sqrt{6}}[(cu + uc)c - 2ccu]$	$\frac{1}{\sqrt{2}}(uc - cu)c$
Ω_c^0	$\frac{1}{\sqrt{6}}[(cs + sc)s - 2ssc]$	$\frac{1}{\sqrt{2}}(sc - cs)s$
Ξ_c^0	$\frac{1}{2}[(sc + cs)d - (dc + cd)s]$	$\frac{1}{2\sqrt{3}}[(cs - sc)d + (dc - cd)s - 2(sd - ds)c]$
Ξ_c^+	$\frac{1}{2}[(sc + cs)u - (uc + cu)s]$	$\frac{1}{2\sqrt{3}}[(cs - sc)u + (uc - cu)s - 2(su - us)c]$
$\Xi_c'^0$	$\frac{1}{2\sqrt{3}}[(dc + cd)s + (sc + cs)d - 2(sd + ds)c]$	$\frac{1}{2}[(dc - cd)s + (sc - cs)d]$
$\Xi_c'^+$	$\frac{1}{2\sqrt{3}}[(uc + cu)s + (sc + cs)u - 2(su + us)c]$	$\frac{1}{2}[(uc - cu)s + (sc - cs)u]$
Σ_c^0	$\frac{1}{\sqrt{6}}[(dc + cd)d - 2ddc]$	$\frac{1}{\sqrt{2}}(dc - cd)d$
Σ_c^+	$\frac{1}{2\sqrt{3}}[(dc + cd)u + (uc + cu)d - 2(ud + du)c]$	$\frac{1}{2}[(dc - cd)u + (uc - cu)d]$
Σ_c^{++}	$\frac{1}{\sqrt{6}}[(uc + cu)u - 2uuc]$	$\frac{1}{\sqrt{2}}(uc - cu)u$
Λ_c^+	$\frac{1}{2}[(dc + cd)u - (uc + cu)d]$	$\frac{1}{2\sqrt{3}}[(cd - dc)u + (uc - cu)d - 2(du - ud)c]$

Table 1.9: The flavor wave functions of the baryons containing at least one charm quark in SU(4) 20-plet which has mixed symmetry under the interchange of quark labels.

1.1.3 Physics beyond quark model

Quark model provides a convenient framework for classifying hadrons. Most of the experimentally observed hadron states fit into this scheme quite neatly. However, the quark model is only a phenomenological model. It is not derived from the underlying theory of the strong interactions – Quantum Chromodynamics. Hence the quark model spectrum is not necessarily the same as the physical spectrum of QCD.

One type of “non-conventional” hadrons are mesons with “exotic” J^{PC} quantum numbers. In the quark model, mesons are $q\bar{q}'$ bound states. If the orbital angular momentum of the $q\bar{q}'$ is L , then the parity $P = (-1)^{L+1}$. The angular momentum J is given by the relation $|L - S| < J < |L + S|$, where S is the spin of the meson which can be 0 or 1. The C -parity is $(-1)^{L+S}$. Thus the J^{PC} value of a meson can be $0^{++}, 0^{-+}, 1^{++}, 1^{--}, 1^{+-}, \dots$, but can never be $0^{--}, 0^{+-}, 1^{-+}, 2^{+-}, 3^{-+}, \dots$. Any state with these “exotic” quantum numbers is beyond quark model, but is not excluded in QCD.

Another type of “non-conventional” hadrons have ordinary quantum numbers but do not fit the quark model easily. For example, below 2GeV, seven $J^{PC} = 0^{++}$ scalar mesons have been observed in experiments: $f_0(600)$, $f_0(980)$, $f_0(1370)$, $f_0(1500)$, $f_0(1710)$, $f_0(1810)$. Within this mass range the quark model can only accommodate four scalars at most. Thus the quark content of some of these states can not be $q\bar{q}'$.

In the past several years there have been observed some charmonium-like states, such as $X(3872)$ [14, 15, 16, 17], $Y(3940)$ [18], $Y(4140)$ [19], $Y(4260)$ [20] etc., which have unexpected and puzzling nature. The structure of them remains ambiguous. Lattice calculations of the charmed meson scattering and the extraction of the phase shifts may help resolve the underlying structure of these states.

1.2 Standard model

There are three types of forces in nature: gravity, the electroweak force and the strong force. The electroweak and strong forces can be described in terms of unitary groups. Physicists write this combination of gauge groups as $SU(3) \times SU(2) \times U(1)$. This model is called the Standard Model.

The Standard Model consists of two types of elementary particle: bosons (force carriers) and fermions (particles that make up matter). In the quantum gauge theory described by the group $SU(N)$, there are $N^2 - 1$ gauge bosons. The group $SU(3)$ is the gauge group of the theory of the strong force known as Quantum Chromodynamics (QCD). The massless gauge boson of this theory is known as the gluon. The group $SU(3)$ has eight generators, and this means that there are eight types of gluons predicted by the theory.

The $SU(2) \times U(1)$ is the gauge groups of the electroweak theory which unifies the electromagnetic force and weak force. The gauge bosons in the electroweak theory are the massless photon and the massive W^\pm and Z^0 . The gauge bosons acquire their mass by interacting with a scalar field called the Higgs field when spontaneous symmetry breaking happens. This is so the called "Higgs mechanism". The resulting theory has massive gauge bosons but still retains the nice properties of a fully gauge invariant theory where the gauge bosons would normally be massless. The explicit remaining gauge symmetry is the $U(1)$ of electromagnetism.

The Standard Model is confirmed by experiments very well as of today, except that the Higgs boson has not been observed. However, it is widely recognized that this model is not complete, it fails to integrate the gravity. In this work we mainly use quantum chromodynamics to extract the physical observables.

1.3 Quantum Chromodynamics

Quantum chromodynamics(QCD) is considered as the underlying theory of the strong interaction. QCD is a non-abelian gauge theory with gauge group SU(3), in which the quark fields in the fundamental representation are coupled to the gauge fields in the adjoint representation. In this section, we will give a brief review of QCD.

1.3.1 QCD Lagrangian

The Lagrangian of QCD is given by

$$L(x) = \sum_f \bar{\psi}_f(x)(i\gamma^\mu D_\mu - m_f)\psi_f(x) - \frac{1}{4}\text{Tr}[F_{\mu\nu}(x)F^{\mu\nu}(x)], \quad (1.16)$$

where repeated indices are summed over. The γ^μ are the Dirac γ -matrices. The ψ_f are quark fields with flavor f and mass m_f . The covariant derivative is

$$D_\mu = \partial_\mu - igA_\mu, \quad A_\mu = \sum_a t^a A_\mu^a. \quad (1.17)$$

where g is the gauge coupling constant, A_μ^a are the gluon fields, a runs from 1 to 8 corresponding 8 kinds of gluons, t^a is the generators of the SU(3) group.

The gauge field tensor is defined by

$$[D_\mu, D_\nu] = -igF_{\mu\nu} \quad (1.18)$$

The quark field $\psi(x)$ transform according to

$$\psi(x) \rightarrow \psi'(x) = U(x)\psi(x), \quad (1.19)$$

where $U(x)$ is a 3×3 unitary matrix, which can be represented as

$$U(x) = 1 + i\alpha^a(x)t^a + \mathcal{O}(\alpha^2). \quad (1.20)$$

The transformation law for A_μ is

$$A_\mu(x) \rightarrow A_\mu(x)' = U(x)(A_\mu(x) + \frac{i}{g}\partial_\mu)U^\dagger(x). \quad (1.21)$$

Therefore

$$\begin{aligned} D_\mu\psi(x) &\rightarrow [\partial_\mu - igU(x)A_\mu U^\dagger(x) + U(x)(\partial_\mu U^\dagger(x))]U(x)\psi(x) \\ &= \partial_\mu(U(x)\psi(x)) - igU(x)A_\mu\psi(x) + U(x)\partial_\mu\psi(x) - \partial_\mu(U(x)\psi(x)) \\ &= U(x)(\partial - igA_\mu)\psi(x) = U(x)D_\mu\psi(x). \end{aligned} \quad (1.22)$$

In the second line we used $\partial_\mu\psi(x) = (\partial_\mu U^\dagger(x))U(x)\psi(x) + U^\dagger(x)\partial_\mu(U(x)\psi(x))$.

From the above equation it is easy to see that the covariant derivative transforms as $D_\mu \rightarrow U(x)D_\mu U^\dagger(x)$ and the commutator transforms as $[D_\mu, D_\nu] \rightarrow U(x)[D_\mu, D_\nu]U^\dagger(x)$.

Therefore the gauge field tensor transforms according to

$$F_{\mu\nu} \rightarrow U(x)F_{\mu\nu}U^\dagger(x). \quad (1.23)$$

Using Eq. 1.22 and Eq. 1.23 one can immediately show that the Lagrangian $L(x)$ is gauge invariant.

1.3.2 Asymptotic freedom

The dominant qualitative feature of QCD seen in perturbative theory is asymptotic freedom. The coupling constant decreases as the momentum scale k increases.

This means that the perturbation theory can be applied when the processes only involve high momentum or short distance.

To one loop order the beta function for N_c colors and N_f flavors is

$$\beta(g) = \frac{\partial g}{\partial \ln \mu} = -\frac{g^3}{16\pi^2} \left(\frac{11}{3} N_c - \frac{2}{3} N_f \right). \quad (1.24)$$

The coupling constant is

$$g^2(k) = \frac{g^2}{1 + \frac{g^2}{(4\pi)^2} \left(\frac{11}{3} N_c - \frac{2}{3} N_f \right) \log(k^2/\Lambda^2)}, \quad (1.25)$$

where Λ is the cut off energy of the theory.

For a theory with $N_c = 3$ and $N_f = 6$, Eq. 1.25 clearly implies the asymptotic freedom. On the other hand, it also implies that the coupling constant increases at lower momentum or longer distance. The value of Λ expresses a scale where the interaction becomes strong and the perturbation theory fails.

1.4 Organization of this dissertation

The basic knowledge about lattice QCD is reviewed in Chapter 2. We describe how the quark fields and gauge fields are formulated on lattice and how to calculate observables numerically using Monte-Carlo method. The statistical data analysis methods are also introduced. We describe how to analyze the statistical error and how to fit the quantities of interest from the simulated data.

In chapter 3, we introduce the heavy quark effective theory and chiral perturbation theory. The masses of charmed baryons are given in the framework of heavy quark effective theory. Chiral perturbation theory for heavy hadrons is described, which allows us to extrapolate the quantities calculated at unphysical light quark masses to the physical point.

Chapter 4 describes the ensembles we use in this work. The actions for heavy quark and light quark are discussed. We also describe how to extract the spectrum and scattering lengths from the correlation functions.

Chapter 5 presents the details of the calculations of the charmed baryon masses with careful analysis of systematics.

In Chapter 6, we calculate the scattering lengths of the scattering processes which involve charmed mesons and charmonium.

We conclude by summarizing the main results of this work and discussing the future outlook of heavy hadron physics.

CHAPTER 2

Lattice QCD and Numerical Methods

The strong interaction has a feature of confinement which is inherently non-perturbative. Lattice QCD(LQCD) is the only known way to study the strong interaction at low energy scale quantitatively. In this chapter I present the basic knowledge of lattice field theory. I review how to represent the gauge fields and fermions on the lattice. For the details of lattice QCD theory, see any of the text books [21, 22, 23] and the references therein. The Monte-Carlo simulation method as well as the methods to analyze statistical data are also presented in this chapter.

2.1 Euclidean space-time

In this work we will work in Euclidean space-time instead of Minkowski space-time. The positions and momenta in Euclidean space-time are related to those in Minkowski space-time as:

$$\begin{aligned}x_4^{(E)} &= ix_0^{(M)}, & k_i^{(E)} &= -k_i^{(M)}, & i &= 1, 2, 3, \\p_4^{(E)} &= ix_0^{(M)}, & p_i^{(E)} &= -p_i^{(M)}, & i &= 1, 2, 3,\end{aligned}\tag{2.1}$$

where the superscripts (E) and (M) denotes the Euclidean space-time and Minkowski space-time respectively.

With this definition, the metric becomes $\delta_{\mu,\nu} = \text{diag}(1, 1, 1, 1)$. The covariant and contravariant components of a Euclidean vector are identical: $x_\mu^{(E)} = x^{\mu(E)}$. The scalar product is

$$x \cdot y = x_1y_1 + x_2y_2 + x_3y_3 + x_4y_4. \quad (2.2)$$

The Euclidean time is purely imaginary. The path integral representation of the partition function becomes explicitly convergent which makes numerical calculation and theoretical analysis much easier. The transformation from a real time to imaginary time is called Wick rotation. The legitimacy of Wick rotation is beyond the scope of this thesis. The key point is that the Hamiltonian of the system has no pole on the first sheet, therefore the $+i\epsilon$ prescription enables the Wick rotation to imaginary time axis. See reference [24, 25] for more information.

Since in the rest of this thesis only Euclidean quantities will be involved we will omit the superscript (E).

2.2 Lattice discretization

The conventional regularization schemes are based on the perturbative expansion, when a divergence is met in a particular diagram, a counter term is introduced to eliminate this divergence. For the QCD theory at low-energy region, we need a non-perturbative regulator. The lattice is such a tool which directly removes all wavelengths less than the lattice spacing.

The lattice method was introduced by Kenneth Wilson in 1974 [26]. The idea is to replace the continuum space by a 4D finite lattice:

$$x_\mu = an_\mu, \quad n_\mu = 0, 1, 2, \dots, N-1 \quad \text{for } i = 1, 2, 3, 4. \quad (2.3)$$

where a is the lattice spacing which has the physical dimension of length. We assume the lattice is periodic, that is to identify n_i with $n_i + N$. The size of the lattice is N^4 .

The finite lattice spacing provides a cutoff removing the ultraviolet infinities. The Fourier transforms on lattice are periodic in momentum space with periodicity is $2\pi/a$. Therefore all momenta can be restricted in the range $(-\pi/a, +\pi/a)$ and the momentum cutoff is π/a .

2.3 Fermion fields on lattice

2.3.1 Discretization of free fermions

In lattice QCD the fermions are placed at the lattice sites. We denote the fermion fields by $\psi(n)$, where n is a integer-valued 4-vector labeling the lattice position. For convenience we omit the lattice spacing a . The actual physical position of the fermions is $x = an$.

In the continuum the action for a free fermion is given by

$$S_f^0[\psi, \bar{\psi}] = \int d^4x \bar{\psi}(x) (\gamma_\mu \partial_\mu + m) \psi(x) \quad (2.4)$$

To formulate this action on the lattice we need to discretize the integral over space-time and the derivative. The integral is replaced by a sum over the discretized space-time Λ . The derivative is discretized by the symmetric expression

$$\partial_\mu \psi(x) \rightarrow \frac{1}{2a} (\psi(n + \hat{\mu}) - \psi(n - \hat{\mu})), \quad (2.5)$$

where $\hat{\mu}$ indicates the unit vector at μ direction.

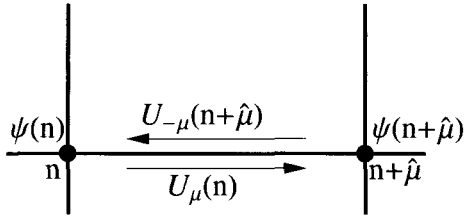


Figure 2.1: The link variables $U_\mu(n)$

Therefore, the lattice action of the free fermion reads

$$S_f^0[\psi, \bar{\psi}] = a^4 \sum_{n \in \Lambda} \bar{\psi}(n) \left(\sum_{\mu=1}^4 \gamma_\mu \frac{\psi(n + \hat{\mu}) - \psi(n - \hat{\mu})}{2a} + m\psi(n) \right) \quad (2.6)$$

2.3.2 Fermion action with external gauge fields

As in continuum QCD, gauge fields have to be introduced to keep the fermion action invariant under the local gauge transformations. On lattice we introduce a gauge field $U_\mu(n)$ with a direction μ . The gauge fields $U_\mu(n)$ live on the links of the lattice as shown in Fig. 2.1. The hermitian conjugate of $U_\mu(n)$ is the link variable in negative μ direction

$$U_\mu^\dagger(n) = U_{-\mu}(n + \hat{\mu}). \quad (2.7)$$

Define the gauge transformation of the link variables by

$$U_\mu(n) \rightarrow U'_\mu(n) = \Omega(n)U_\mu(n)\Omega(n + \hat{\mu})^\dagger. \quad (2.8)$$

In the above equation $\Omega(n)$ is an element of SU(3) group. The gluon fields $U_\mu(n)$ is also an element of SU(3) group. This is different with the continuum theory where gluon fields are elements of Lie algebra.

The fermion fields transform according to

$$\psi(n) \rightarrow \psi'(n) = \Omega(n)\psi(n), \quad \bar{\psi}(n) \rightarrow \bar{\psi}'(n) = \bar{\psi}(n)\Omega(n)^\dagger. \quad (2.9)$$

Consider the term $\bar{\psi}(n)\psi(n + \hat{\mu})$ in Eq. 2.6, it is not invariant under SU(3) gauge transformation. However, if we insert a gluon field, the modified term $\bar{\psi}(n)U_\mu(n)\psi(n + \hat{\mu})$ is gauge invariant:

$$\begin{aligned} \bar{\psi}(n)U_\mu(n)\psi(n + \hat{\mu}) &\rightarrow \bar{\psi}'(n)U'_\mu(n)\psi'(n + \hat{\mu}) \\ &= \bar{\psi}(n)\Omega(n)^\dagger\Omega(n)U_\mu(n)\Omega(n + \hat{\mu})^\dagger\Omega(n + \hat{\mu})\psi(n + \hat{\mu}) \\ &= \bar{\psi}(n)U_\mu(n)\psi(n + \hat{\mu}) \end{aligned} \quad (2.10)$$

We can now generalize the free fermion action 2.6 to the so-called naive fermion action for fermions in an external gauge field U :

$$S_f[\psi, \bar{\psi}, U] = a^4 \sum_{n \in \Lambda} \bar{\psi}(n) \left(\sum_{\mu=1}^4 \frac{U_\mu(n)\psi(n + \hat{\mu}) - U_{-\mu}(n)\psi(n - \hat{\mu})}{2a} + m\psi(n) \right). \quad (2.11)$$

2.3.3 Fermion doubling problem

The propagator of a lattice fermion has 16 poles. That is to say, the naive discretization gives rise to 15 unwanted poles, the so-called doublers. For simplicity, we use free fermion theory to exemplify this problem.

Rewrite the free fermion action (2.6) as

$$S_f[\psi, \bar{\psi}] = \sum_{m, n \in \Lambda} \bar{\psi}(m) D_{mn} \psi(n), \quad (2.12)$$

where D is the Dirac operator which is defined by

$$D_{mn} = \sum_{\mu=1}^4 \gamma_{\mu} \frac{\delta_{m,n-\hat{\mu}} - \delta_{m,n+\hat{\mu}}}{2} + m\delta_{m,n}. \quad (2.13)$$

Here we have set the lattice spacing a to 1.

To calculate the fermion propagator we introduce the external source $J(n)$ and $\bar{J}(n)$. The action is generalized to

$$S_f[\psi, \bar{\psi}, J, \bar{J}] = \sum_{m,n \in \Lambda} \bar{\psi}(m) D_{mn} \psi(n) - \sum_{m \in \Lambda} (\bar{J}(m) \psi(m) + \bar{\psi}(m) J(m)). \quad (2.14)$$

The partition function now depends on the sources

$$Z(J) = \int D\psi D\bar{\psi} \exp \left\{ - \left(\sum_{m,n \in \Lambda} \bar{\psi}(m) D_{mn} \psi(n) - \sum_{m \in \Lambda} (\bar{J}(m) \psi(m) + \bar{\psi}(m) J(m)) \right) \right\}. \quad (2.15)$$

This quantity is a generating function for the Green's functions, the fermion propagator is given by the differentiation with respect to the sources

$$\begin{aligned} \langle \psi(m) \bar{\psi}(n) \rangle &= \frac{1}{Z(0)} \int D\psi D\bar{\psi} e^{-S_f[\psi, \bar{\psi}]} \psi(m) \bar{\psi}(n) \\ &= \frac{1}{Z} \left\{ \frac{d}{d\bar{J}_m} \frac{d}{dJ_n} Z(J) \right\} \Big|_{J=0}. \end{aligned} \quad (2.16)$$

Complete the square and shifting the integration variables in (2.15) gives

$$Z(J) = \det D \exp \left\{ - \sum_{m,n \in \Lambda} \bar{J}(m) D_{mn}^{-1} J(n) \right\}, \quad (2.17)$$

where we have used the integration formula for Grassmann number

$$\int D\bar{\psi} D\psi e^{-\sum_{m,n \in \Lambda} \bar{\psi}(m) D_{mn} \psi(n)} = \det D \quad (2.18)$$

From Eq. 2.16 and Eq. 2.17 we get the fermion propagator to be

$$\langle \psi(m) \bar{\psi}(n) \rangle = D_{mn}^{-1}. \quad (2.19)$$

D can be inverted with a Fourier transform. For details of the Fourier transform on the lattice see reference [27]. Here we give the result:

$$D_{mn}^{-1} = \frac{1}{V} \sum_k \frac{e^{ip(m-n)}}{m + i \sum_{\mu} \gamma_{\mu} \sin p_{\mu}}. \quad (2.20)$$

The pole of the propagator in momentum space for massless fermions represents real particle states of the system. Due to the periodic nature of the sine function, this propagator has poles not only at $p = (0, 0, 0, 0)$ but also at the corner of the Brillouin zone, namely at $p = (\pi, 0, 0, 0)$ etc. In fact, in four dimensional space-time, there are 16 poles. Therefore the naive discretization of the continuum fermion action, which describe one species of fermions in the continuum, leads to 16 species of fermions on the lattice and they all survive the continuum limit. These extra degrees of freedom are called doublers.

2.3.4 Wilson fermions

In order to remove the doublers, Wilson suggest to add a second derivative term $-\frac{1}{2} \partial_{\mu} \partial_{\mu}$ in the action. The second derivative on the lattice is approximated by

$$f''(x) = \frac{f(x+a) + f(x-a) - 2f(x)}{a^2}. \quad (2.21)$$

The Wilson fermion action reads

$$\begin{aligned}
S_f[\psi, \bar{\psi}] = & \sum_{n \in \Lambda} \bar{\psi}(n) \left(\sum_{\mu=1}^4 \gamma_{\mu} \frac{\psi(n + \hat{\mu}) - \psi(n - \hat{\mu})}{2} + m\psi(n) \right. \\
& \left. - \sum_{\mu=1}^4 \frac{\psi(n + \hat{\mu}) + \psi(n - \hat{\mu}) - 2\psi(n)}{2} \right)
\end{aligned} \tag{2.22}$$

The propagator of is

$$\langle \psi(m) \bar{\psi}(n) \rangle = \frac{1}{V} \sum_k \frac{e^{ip(m-n)}}{m + i \sum_{\mu} \gamma_{\mu} \sin p_{\mu} + \sum_{\mu} (1 - \cos p_{\mu})}. \tag{2.23}$$

Comparing with the naive fermion propagator, there is an extra term $\sum_{\mu} (1 - \cos p_{\mu})$. Considering the dimension, we put back the lattice spacing a , this term becomes $a^{-1} \sum_{\mu} (1 - \cos p_{\mu})$. The value of this term is 0 at $p = (0, 0, 0, 0)$. While at other poles $p = (\pi, 0, 0, 0), (0, \pi, 0, 0), \dots$, this term goes to infinity when $a \rightarrow 0$. That is to say, the doublers receive extra mass values which goes to infinity in continuum limit. Therefore the physical state and the doublers decouple in the continuum limit.

2.3.5 Chiral fermions

The doubling problem poses a serious challenge for lattice fermions. In fact, this problem is intimately related to the chirality of fermions and the doubling problem is just a manifestation of the impossibility to define a fermion field theory of a single chirality non-perturbatively.

Nielsen and Ninomiya have proved a no-go theorem [28]. It states that it is impossible to construct a lattice fermion action $S_f = \sum_x \bar{\psi}_x D_{xy} \psi_y$ which satisfies the following conditions:

- (a) $\tilde{D}(p)$ is an analytic periodic function of the momenta p_{μ} with period $2\pi/a$.
- (b) For momenta far below the cutoff π/a , we have $\tilde{D}(p) = i\gamma_{\mu} p_{\mu}$ up to terms of order

ap^2 .

(c) $\tilde{D}(p)$ is invertible at all non-zero momenta (mod $2\pi/a$).

(d) D anti-commutes with γ_5 : $D\gamma_5 + \gamma_5 D = 0$.

Property (a) is necessary if we want D to be a local operator, (b) ensures that the correct continuum limit is obtained, (c) guarantees that there are no doublers and (d) is the requirement of chiral symmetry.

To avoid this theorem, Ginsparg and Wilson suggested a relation

$$\gamma_5 D + D\gamma_5 = aD\gamma_5 D \tag{2.24}$$

to replace the relation in property (d). At the continuum limit the right hand side of this equation goes to zero and the fermion propagator anti-commutes with γ_5 . Therefore the chiral symmetry is partly preserved.

Overlap fermions [29, 30] and domain wall fermions [31, 32, 33, 34] are two kinds of widely used fermions in lattice simulation which satisfy the Ginsparg-Wilson relation and the condition (a), (b), (c). In this work we use domain wall fermion for the light quarks in valence sector. Here we present some details of the domain wall fermion.

The domain wall formalism introduces a fifth dimension, labeled as s , of extent L_s and a mass parameter M_5 . The physical quark fields live on the 4-dimensional boundaries of the fifth coordinate. The left and right chiral components are separated on the corresponding boundaries, resulting in an action with chiral symmetry at finite lattice spacing as $L_s \rightarrow \infty$.

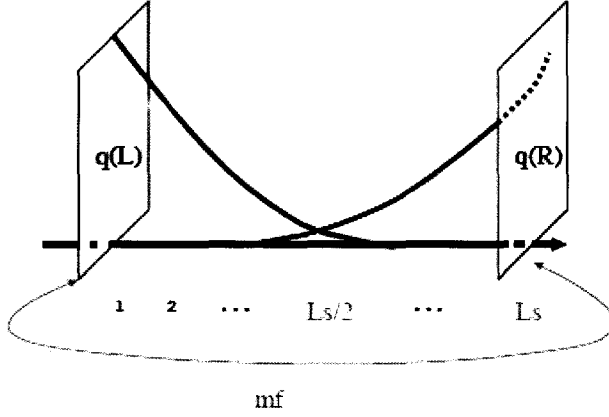


Figure 2.2: Domain wall fermions.

The domain wall fermion action is

$$\begin{aligned}
D_{x,s;x',s'} &= \delta_{s,s'} D_{x,x'}^{\parallel} + \delta_{x,x'} D_{s,s'}^{\perp}, \\
D_{x,x'}^{\parallel} &= \frac{1}{2} \sum_{\mu=1}^4 [(1 - \gamma_{\mu}) U_{x,\mu} \delta_{x+\hat{\mu},x'} + (1 + \gamma_{\mu}) U_{x',\mu}^{\dagger} \delta_{x-\hat{\mu},x'}] + (M_5 - 4) \delta_{x,x'} \\
D_{s,s'}^{\perp} &= \frac{1}{2} [(1 - \gamma_5) \delta_{s+1,s'} + (1 + \gamma_5) \delta_{s-1,s'} - 2\delta_{s,s'}] - \\
&\quad \frac{m_f}{2} [(1 - \gamma_5) \delta_{s,L_s-1} \delta_{0,s'} + (1 + \gamma_5) \delta_{s,0} \delta_{L_s-1,s'}]
\end{aligned} \tag{2.25}$$

Figure 2.2 illustrates the domain wall fermions. The two walls are coupled with a mass term $m_f \bar{q}q$, where m_f controls the bare quark mass. For finite L_s chiral symmetry is broken, leading to an additive renormalization of the mass, called residual mass m_{res} . The residual mass vanishes as $L_s \rightarrow \infty$.

2.4 Gauge fields on lattice

2.4.1 The Wilson gauge action

The gauge action is required to be gauge invariant. Before we construct the gauge action let's first discuss the transportation properties of the ordered product of a sequence of link variables along a path \mathcal{L} . Define

$$U_{\mathcal{L}} = U_{x_0, x_1} U_{x_1, x_2} \cdots U_{x_{n-1}, x_n}, \quad (2.26)$$

where x_0, x_1, \cdots, x_n are consecutive lattice sites along the path \mathcal{L} , $U_{x_i, x_{i+1}}$ denotes the gauge field lives on the link connecting the sites x_i and x_{i+1} .

Using Eq. 2.8, we get the transformation of $U_{\mathcal{L}}$:

$$U_{\mathcal{L}} \rightarrow U'_{\mathcal{L}} = \Omega_{x_0} U_{\mathcal{L}} \Omega_{x_n}^\dagger. \quad (2.27)$$

A natural way of constructing a gauge invariant term is to let the path \mathcal{L} to be a closed loop and then take the trace. When \mathcal{L} is closed, $x_0 = x_n$, thus

$$Tr[U'_{\mathcal{L}}] = Tr[\Omega_{x_0} U_{\mathcal{L}} \Omega_{x_0}^\dagger] = Tr[U_{\mathcal{L}}]. \quad (2.28)$$

The simplest closed path on the lattice is the so-called plaquette. The plaquette variable U_p is a product of the four gauge links along a plaquette p as shown in Fig. 2.3.

$$\begin{aligned} U_p &= U_\mu(n) U_\nu(n + \hat{\mu}) U_{-\mu}(n + \hat{\mu} + \hat{\nu}) U_{-\nu}(n + \hat{\nu}), \\ &= U_\mu(n) U_\nu(n + \hat{\mu}) U_\mu(n + \hat{\nu}) U_\nu(n)^\dagger. \end{aligned} \quad (2.29)$$

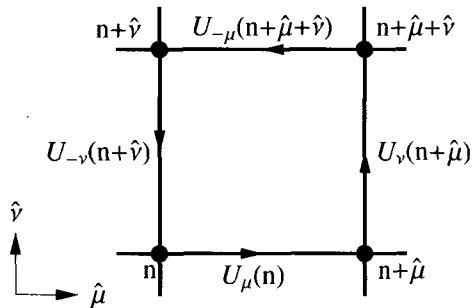


Figure 2.3: The plaquette U_p is composed by the four link variables. The arrows show the direction of the link variables.

In the second step we have used Eq. 2.7.

The Wilson gauge action is a sum over all plaquettes

$$S_g[U] = \frac{2}{g^2} \sum_p \text{Re Tr}[1 - U_p]. \quad (2.30)$$

The sum over all plaquette p is meant to include every plaquette only with one orientation. The factor $\frac{2}{g^2}$ is set to match the continuum action in the limit $a \rightarrow 0$.

The partition function of the pure gauge system is

$$Z = \int \prod_{x,\mu} DU_\mu(x) e^{-S_g[U]}, \quad (2.31)$$

where DU_μ is the invariant Haar measure for the gauge group.

2.4.2 The wilson loop

We have seen that the trace of the products of gauge fields along a closed path on a lattice is a gauge invariant quantity. A particular useful construction is called a

Wilson loop, which is defined as:

$$W(R, T) = \text{Tr} \left(\prod_{l=0}^{T-1} U_4(x+l\hat{4}) \prod_{k=0}^{R-1} U_i(x+T\hat{4}+k\hat{i}) \prod_{l=1}^T U_4^\dagger(x+(T-l)\hat{4}+R\hat{i}) \prod_{k=1}^R U_i^\dagger(x+(R-k)\hat{i}) \right). \quad (2.32)$$

The loop is a rectangle of dimensions T by R , T in temporal direction and R in spatial direction. For large T

$$W(R, T) \propto \exp(-V(R)T), \quad (2.33)$$

where $V(R)$ is the quark-antiquark potential. To see this, imagine that a quark-antiquark pair is created at some time with fixed distance R apart. The potential energy of the system is then $V(R)$. After some time separation T , the quark-antiquark pair is annihilated. The probability amplitude for this process is then proportional to $\exp(-V(R)T)$. On the other hand, this amplitude is precisely the average of the Wilson loop operator.

2.5 Monte Carlo Method

The expectation value of an observable is given by

$$\langle \mathcal{O} \rangle = \frac{1}{Z} \int DUD\psi D\bar{\psi} \mathcal{O}[\psi, \bar{\psi}, U] e^{-S_f[\psi, \bar{\psi}, U] - S_g[U]}, \quad (2.34)$$

where Z is the partition function

$$Z = \int DUD\psi D\bar{\psi} e^{-S_f[\psi, \bar{\psi}, U] - S_g[U]}. \quad (2.35)$$

On the lattice the path integral is nothing but a multi-dimensional integral, one could imagine that we just compute this integral numerically using computers. However, this multi-dimensional integral cannot be evaluated directly on a computer because

it takes too much time.

Note that those configurations which have large values of action contribute little to the path integral, they are suppressed exponentially. What really contributes the most to the path integral are those configurations which are near the minimum of the action. One only tries to sample the part of the configuration space that makes the most important contributions to the path integral. This is the idea of important sampling.

One way to implement the idea of importance sampling is to use Monte Carlo methods. Note that the expectation value of an observable can be viewed as an average with a probability distribution $\exp(-S)$. Once the probability distribution is correctly generated, one can just take samples from this probability distribution and average over these samples.

The desired probability distribution can be obtained by a Markov process. A Markov process is characterized by a transition probability $T(\{\phi'\}|\{\phi\})$ which means the probability to get $\{\phi'\}$ if starting from $\{\phi\}$, where $\{\phi\}$ denotes a configuration which specifies the value of the field on all lattice points. The probability obeys

$$0 \leq T(\{\phi'\}|\{\phi\}) \leq 1, \quad \sum_{\{\phi'\}} T(\{\phi'\}|\{\phi\}) = 1. \quad (2.36)$$

The inequality simply delimits the range of the probability. The sum states that the total probability to jump from some configuration $\{\phi\}$ to any target configuration $\{\phi'\}$ is equal to 1.

One more important restriction on $T(\{\phi'\}|\{\phi\})$ is

$$\sum_{\{\phi\}} T(\{\phi'\}|\{\phi\})P(\{\phi\}) = \sum_{\{\phi\}} T(\{\phi\}|\{\phi'\})P(\{\phi'\}), \quad (2.37)$$

where $P(\{\phi\})$ is the probability that the system is in the configuration $\{\phi\}$. The left hand side is the total probability to hopping into a configuration $\{\phi'\}$ from all starting configurations $\{\phi\}$. The right hand side the total probability to hopping out of $\{\phi'\}$. This condition expresses the requirement of a system to be in equilibrium.

Note that the sum of the right hand side of Eq. 2.39 can be calculated explicitly using Eq. 2.36. We have

$$\sum_{\{\phi\}} T(\{\phi'\}|\{\phi\})P(\{\phi\}) = P(\{\phi'\}), \quad (2.38)$$

showing that the equilibrium distribution $P(\{\phi\})$ is a fixed point of the Markov process. Once the equilibrium distribution is obtained, the system stays there upon applying T .

A sufficient condition for a solution of the balance equation 2.39 is

$$T(\{\phi'\}|\{\phi\})P(\{\phi\}) = T(\{\phi\}|\{\phi'\})P(\{\phi'\}). \quad (2.39)$$

This equation is called detailed balance condition.

There are two algorithms in common use: the Metropolis algorithm and the heat bath algorithm. Both algorithms satisfy the detailed balance condition.

The Metropolis algorithm consists the following steps:

1. Choose a candidate configuration $\{\phi'\}$ according to a priori selection probability $T_0(\{\phi'\}|\{\phi\})$.
2. Accept the candidate configuration $\{\phi'\}$ as the configuration with the acceptance probability

$$T_A(\{\phi'\}|\{\phi\}) = \min\left(1, \frac{T_0(\{\phi\}|\{\phi'\}) \exp(-S[\{\phi'\}])}{T_0(\{\phi'\}|\{\phi\}) \exp(-S[\{\phi\}])}\right). \quad (2.40)$$

3. Repeat these steps from the beginning.

It is straightforward to show that the total transition probability $T = T_0 T_A$ satisfy the detailed balance condition:

$$\begin{aligned}
& T(\{\phi'\}|\{\phi\}) \exp(-S[\{\phi\}]) \\
= & T_0(\{\phi'\}|\{\phi\}) \min\left(1, \frac{T_0(\{\phi\}|\{\phi'\}) \exp(-S[\{\phi'\}])}{T_0(\{\phi'\}|\{\phi\}) \exp(-S[\{\phi\}])}\right) \exp(-S[\{\phi\}]) \\
= & \min(T_0(\{\phi'\}|\{\phi\}) \exp(-S[\{\phi\}]), T_0(\{\phi\}|\{\phi'\}) \exp(-S[\{\phi'\}])) \\
= & T_0(\{\phi\}|\{\phi'\}) \min\left(1, \frac{T_0(\{\phi'\}|\{\phi\}) \exp(-S[\{\phi\}])}{T_0(\{\phi\}|\{\phi'\}) \exp(-S[\{\phi'\}])}\right) \exp(-S[\{\phi'\}]) \\
= & T(\{\phi\}|\{\phi'\}) \exp(-S[\{\phi'\}]). \tag{2.41}
\end{aligned}$$

We need to address how we choose a trial configuration $\{\phi'\}$ in the Metropolis algorithm. Let's take the pure gauge theory as an example. Choose a link variable at site n and direction μ , the trial configuration can be obtained by replace $U_\mu(n)$ by $U'_\mu(n)$ and keep the other link variables fixed. A convenient way to get $U'_\mu(n)$ is

$$U'_\mu(n) = XU_\mu(n) \tag{2.42}$$

where X is a randomly chosen element of the gauge group close to the unit element. In practical simulation the priori selection probability is usually taken to be symmetry, i. e. $T_0(\{\phi'\}|\{\phi\}) = T_0(\{\phi\}|\{\phi'\})$. To achieve a symmetric T_0 , X and X^{-1} have to be chosen with equal probability. The acceptance rate can be adjusted by tuning the spread of X around unity. A high acceptance rate may be desirable but usually means small change and slow motion in configuration space. Smaller acceptance is costly because many candidates are generated but not accepted. A reasonable acceptance rate has to be chosen to suit practical purpose.

Another parameter on which the Metropolis algorithm has an essential depen-

dence is the number of trial changes attempt on a given link before going on to the next. In most statistical problems this is taken to be one. However, for the gauge theory the interaction is rather complicated and requires considerable computation time. It is beneficial to repeat the updating at one link while the multiplication of the neighboring link variables appearing in the action need not be repeated. As the number of trials goes to infinity, the Metropolis algorithm approaches the heat bath algorithm. When we keep repeating the procedure on one link, this link will ultimately be brought into thermal equilibrium with its temporarily fixed neighbors. This is what the heat bath does in one step. The heat bath algorithms approaches the equilibrium more efficiently than the Metropolis algorithm. But the implementation of it depends on the details of the gauge group and the action, which often causes challenges to the simulation.

2.6 Simulation of fermions

Simulating fermions is more difficult than simulating pure gauge theory because the computer can not manipulate Grassman numbers directly. Fermions have to be integrated out first, yielding the the determinant of the fermion matrix. The fermion matrix is a huge non-local matrix with space-time, color and spin indices, which makes the calculation of its determinant computationally costly. In practice, simulation of fermions is performed by introducing the so-called pseudo-fermions which can be represented by normal numbers on computer.

Write the path integral as

$$Z = \int DUD\psi D\bar{\psi} e^{-\bar{\psi}D[U]\psi - S_g[U]}, \quad (2.43)$$

where $D[U]$ is the fermion matrix. Integrate out the fermion fields, we get

$$Z = \int DU \det D[U] e^{-S_g[U]}, \quad (2.44)$$

where we have used the integration formula for Grassmann number in Eq. 2.18. Introducing the pseudo-fermions ϕ , the path integral becomes

$$Z = \int DU D\phi^\dagger D\phi e^{-S_g[U] - \phi^\dagger D^{-1}[U]\phi}. \quad (2.45)$$

For dynamical simulations, one has to calculate the inverse of the fermion matrix at each updating step. It is this calculation makes the simulation of fermions much slower than the simulation without fermions.

Quenched approximation ignores the fermion contribution in the sea sector, i.e. set $D[U] = 1$ in the process of generating configurations. This approximation significantly reduce the computational cost, however, it produces noticeable systematic errors. Nowadays, with powerful super computers, full LQCD is commonly used.

2.7 Data analysis

Monte Carlo simulations require the statistical analysis of the measured observables. It is important to understand the statistical error of the results of the numerical simulations. The average value which one quotes for an observable only makes sense when the corresponding statistical error is presented. In this section we introduce the methods of analyzing the statistical data.

2.7.1 Statistical analysis for uncorrelated data

Suppose we have calculated the values (x_1, x_2, \dots, x_n) of an observable x for an ensemble of N configurations in equilibrium. The variance are defined as

$$\sigma_x^2 = \langle (x_i - \langle x \rangle)^2 \rangle, \quad (2.46)$$

where $\langle x \rangle$ denotes the expectation value, which is usually estimated as the mean of the measured values: $\bar{x} = \frac{1}{N} \sum_{i=1}^N x_i$. The variance is estimated as

$$\bar{\sigma}_x^2 = \frac{1}{N-1} (x_i - \bar{x})^2. \quad (2.47)$$

The $\bar{\sigma}_x^2$ indicates the statistical error of \bar{x} . However, \bar{x} itself is a random variable because it may have different values for different ensembles. The variance of \bar{x} is

$$\begin{aligned} \sigma_{\bar{x}}^2 &= \langle (\bar{x} - \langle x \rangle)^2 \rangle = \left\langle \left(\frac{1}{N} \sum_{i=1}^N (x_i - \langle x \rangle) \right)^2 \right\rangle \\ &= \frac{1}{N^2} \left\langle \sum_{i,j=1}^N (x_i - \langle x \rangle)(x_j - \langle x \rangle) \right\rangle \\ &= \frac{1}{N} (\langle x^2 \rangle - \langle x \rangle^2) + \frac{1}{N^2} \sum_{i \neq j} \langle x_i x_j \rangle. \end{aligned} \quad (2.48)$$

For uncorrelated x_i , the last term in the last line of the above equation vanishes.

Then we have

$$\sigma_{\bar{x}}^2 = \frac{1}{N} \sigma_x^2. \quad (2.49)$$

The final result based on the N measurements is presented as

$$\bar{x} \pm \sigma \quad \text{with} \quad \sigma = \sqrt{\frac{1}{N(N-1)} \sum_{i=1}^N (x_i - \bar{x})^2}. \quad (2.50)$$

2.7.2 Statistical analysis in the presence of autocorrelation

Since the configurations are generated successively, it is generally not true that the configurations are statistically independent of each other. To quantify the correlation for a measured quantity x we introduce the autocorrelation function:

$$C_x(\tau) = \frac{\langle x_i x_{i+\tau} \rangle - \langle x \rangle^2}{\langle x_i^2 \rangle - \langle x \rangle^2} \quad (2.51)$$

where τ is the computer time.

For the correlated variables x_i the last term in the second line of Eq. 2.48 doesn't vanish. Let's recalculate the variance of mean:

$$\begin{aligned} \sigma_{\bar{x}}^2 &= \langle (\bar{x} - \langle x \rangle)^2 \rangle = \frac{1}{N^2} \sum_{i,j=1}^N (\langle x_i x_j \rangle - \langle x \rangle^2) \\ &= \frac{\langle x_i^2 \rangle - \langle x \rangle^2}{N^2} \sum_{i,j=1}^N \frac{\langle x_i x_j \rangle - \langle x \rangle^2}{\langle x_i^2 \rangle - \langle x \rangle^2} = \frac{\sigma_x^2}{N^2} \sum_{i,j=1}^N C_x(|i-j|) \\ &= \frac{\sigma_x^2}{N^2} \sum_{t=-N}^N (N-|t|) C_x(|t|) = \frac{\sigma_x^2}{N} \sum_{t=-N}^N \left(1 - \frac{|t|}{N}\right) C_x(|t|) \end{aligned} \quad (2.52)$$

Comparing with the variance of mean in the uncorrelated case there is an additional factor $\sum_{t=-N}^N \left(1 - \frac{|t|}{N}\right) C_x(|t|)$, for simplicity we denote this factor as τ_{int} . It means that out of N values there are N/τ_{int} independent data. In other words, in order to get independent measurements one should skip N/τ_{int} updating sweeps between two measurements.

The problem of applying this formula is that $C_x(|t|)$ is hard to measure. In practice it is usually better to handle the autocorrelation by "blocking" the data. The idea is that we average n successive measurements and take the block averages B_i as the new set of data. If the blocks are big enough we can expect that the B_i are

independent. Then we can use the formula of variance for uncorrelated data.

2.7.3 Data blocking methods

There are two widely used data blocking methods: Jackknife and bootstrap. Given a set of N data (x_1, x_2, \dots, x_N) , assume that we are interested in some observable y which is estimated from that set.

Jackknife constructs a subset by removing the i th value of the original set, leaving $N - 1$ values to form the subset. We can estimate the value of the observable y_i for this subset. Do the same thing for every i (running from 1 to N), we get a set of values for y : (y_1, y_2, \dots, y_N) . The variance is given by

$$\sigma_{\hat{y}}^2 = \frac{N-1}{N} \sum_{i=1}^N (y_i - \hat{y})^2 \quad (2.53)$$

where \hat{y} is the value of the observable obtained from the original set.

The jackknife method is also capable of giving an estimate of sampling bias. We may have a situation in which an estimate tends to come out on the high side (or low side) of its true value if a data sample is too small. When this happens, removing a measurement would enhance the bias. The bias can be measured by comparing the mean of the jackknife values y_i , denoted as \bar{y} , with the result of fitting the original data set. If there is a difference, we can correct for the bias using

$$\tilde{y} = \hat{y} - (N-1)(\bar{y} - \hat{y}) \quad (2.54)$$

The final result can be quoted either $\bar{y} \pm \sigma_{\bar{y}}$ or $\tilde{y} \pm \sigma_{\tilde{y}}$.

Bootstrap recreates other samples by choosing randomly N data out of the original set. Suppose we have done this K times and thus have K sets of N data values. For each set we can estimate the value of the observable, resulting a set of K values:

(y_1, y_2, \dots, y_K) . Then one estimate the expectation of y and the variance as

$$\bar{y} = \frac{1}{K} \sum_{i=1}^K y_i, \quad \sigma_y^2 = \frac{1}{K} \sum_{i=1}^K (y_i - \bar{y})^2. \quad (2.55)$$

Jackknife and bootstrap methods can be applied to determine the statistical error for derived quantities without considering the complicate error propagation.

2.7.4 Data fitting

In practical simulation, the observables we are interested are usually not the simple average of the simulated data but the quantities from a fit. For example, to obtain the hadron masses, we need to calculate the two point correlation functions and then fit the correlation functions to exponentials. Here we take it as an example to explain the data fitting methods. The correlation functions are expected to obey some theory:

$$\langle \mathcal{O}(t_i) \mathcal{O}(0) \rangle = f(t_i, \lambda). \quad (2.56)$$

Here λ are a set of parameters $(\lambda_a, \lambda_b, \dots)$. In our example, they are the amplitude and the mass. Our task is to estimate these parameters and find the statistical error on these estimates.

Suppose we have N independent measurements of the correlation function, denote the n th measurement at distance t_i as y_{in} . The average of all measurements at distance t_i is

$$\bar{y}_i = \frac{1}{N} \sum_{n=1}^N y_{in}. \quad (2.57)$$

y_i may be correlated. Define the covariance matrix

$$C_{ij} = \frac{1}{N(N-1)} \sum_{n=1}^N (y_{in} - \bar{y}_i)(y_{jn} - \bar{y}_j). \quad (2.58)$$

The square root of the diagonal elements C_{ii} are the variance of \bar{y}_i . The off diagonal elements $C_{ij}(i \neq j)$ indicate the correlation of \bar{y}_i and \bar{y}_j .

If we repeat the simulation many times, we would get a distribution of the \bar{y} . The distribution probability is

$$P(\bar{y}) = N \exp\left(-\frac{1}{2}(\bar{y}_i - f(t_i, \lambda))C_{ij}^{-1}(\bar{y}_j - f(t_j, \lambda))\right), \quad (2.59)$$

By writing down this, we take two assumptions. One is that the theory is correct, which means $f(t_i, \lambda)$ give the right value of y . The other one is to assume y_i are Gaussian distributed.

Now we need to find the parameters in $f(t_i, \lambda)$ to give the best fit to \bar{y}_i . The most commonly used method is to find the parameters that maximize the distribution probability, or minimize the exponent. Twice the exponent is called χ^2 :

$$\chi^2 = (\bar{y}_i - f_i(\lambda))C_{ij}^{-1}(\bar{y}_j - f_j(\lambda)). \quad (2.60)$$

In general χ^2 is an indicator of the agreement between the observed and expected values.

To minimize χ^2 , we need to solve the equations:

$$\frac{\partial \chi^2}{\partial \lambda_{a,b,\dots}} = 0 \quad (2.61)$$

where a, b, \dots are used to index the parameters. Denote the solutions of these equations as $\bar{\lambda}$. Now we need to answer how would the $\bar{\lambda}$ fluctuate when we repeat the simulations. Notice that the "best fit" defines a mapping from the measurements \bar{y}_i to the parameters $\bar{\lambda}$, therefore we can obtain the distribution probability for the $\bar{\lambda}$ from the distribution probability of the \bar{y}_i .

Define a matrix Δ_{ab} :

$$\Delta_{ab} = \langle (\bar{\lambda}_a - \bar{\bar{\lambda}}_a)(\bar{\lambda}_b - \bar{\bar{\lambda}}_b) \rangle_{P(\bar{y})} = \frac{\int [d\bar{y}] P(\bar{y}) (\bar{\lambda}_a - \bar{\bar{\lambda}}_a)(\bar{\lambda}_b - \bar{\bar{\lambda}}_b)}{\int [d\bar{y}] P(\bar{y})}, \quad (2.62)$$

where $\bar{\bar{\lambda}}$ denotes the expectation of λ . Expand λ around $\bar{\lambda}$:

$$\bar{\lambda}_a(\bar{y}) = \bar{\lambda} + \sum_i \frac{\partial \bar{\lambda}_a}{\partial \bar{y}_i} (\bar{y}_i - \bar{\bar{y}}_i) + \dots \quad (2.63)$$

Ignoring the second and higher order of this expansion and then substitute it into Eq. 2.62, we can simplify Δ_{ab} after some straightforward calculation steps:

$$\Delta_{ab} = 2H_{ab}^{-1}, \quad (2.64)$$

where H_{ab} is called Hessian matrix given by

$$H_{ab} = \left. \frac{\partial^2 \chi^2}{\partial \lambda_a \partial \lambda_b} \right|_{\lambda=\bar{\lambda}}. \quad (2.65)$$

Δ_{ab} describes the covariance of the $\bar{\lambda}_a$, just like C_{ij} describes the covariance of \bar{y}_i . The distribution probability of $\bar{\lambda}$ is

$$P(\bar{\lambda}) = N \exp\left[-\frac{1}{2}(\bar{\lambda}_a - \bar{\bar{\lambda}}_a)\Delta_{ab}^{-1}(\bar{\lambda}_b - \bar{\bar{\lambda}}_b)\right] \quad (2.66)$$

The variance of some parameter λ_a is just the square root of Δ_{aa} . We can quote the final result as $\bar{\lambda}_a \pm \sqrt{\Delta_{aa}}$.

CHAPTER 3

Effective Field Theory

The goal of modern physics is to find a simple and unified theory to describe all observed phenomena in terms of some fundamental dynamics among the basic constituents of the nature. However, even if such a theory is found at some point, a quantitative analysis at the most elementary level is of little use for providing a comprehensive understanding of physics at all scales.

Usually, a physics problem involves widely separated energy scales. We may only be interested in the physics at a certain scale while the details of the physics above this scale are not needed. An effective field theory is an approximate theory to describe low-energy physics, where *low* is defined with respect to some energy scale Λ . Only the relevant degrees of freedom, i.e. those states with energy less than Λ , are presented explicitly in the effective theory, while those states far above Λ are integrated out. In this way we construct the Lagrangian containing a string of interactions among the light states which can be arranged as an expansion in powers of energy/ Λ . The information of the heavier degrees of freedom is then encoded in the coefficients of the low-energy Lagrangian. All the operators in the Lagrangian are required to satisfy all the symmetries of the underlying theory.

If the underlying theory is known, the coefficients of the low-energy Lagrangian can be determined by matching the effective theory to the underlying theory by requiring the physics to be the same at an energy scale in both theories. If the underlying theory is unknown or is not computable at the energy scales of interest, as we encounter in QCD, the coefficients can be obtained by fitting expressions of physical observables computed with the effective theory either to experimental data or to Lattice QCD simulations. Once these coefficients are determined, we are able to make predictions about other physical quantities.

In this chapter we introduce Heavy Quark Effective Theory [35] and Chiral Perturbation theory (χ PT) [36, 37, 38].

3.1 Heavy quark effective theory

The heavy quark effective theory (HQET) is constructed to provide a simplified description of the processes where a heavy quark interacts with light degrees of freedom. Clearly, the heavy quark mass is the high energy scale and Λ_{QCD} is the scale of interest. The content of this section is mainly based on the reference [39, 40].

3.1.1 Derivation of the effective lagrangian

Consider a very heavy quark bound inside a hadron, it moves with the velocity almost equal to the hadron's velocity v and is almost on-shell. We can write its momentum as

$$p = m_Q v + k, \tag{3.1}$$

where m_Q is the heavy quark mass, the residual momentum k determines the amount by which the quark is off-shell due to its interactions. k is of order Λ_{QCD} while m_Q is much larger than Λ_{QCD} .

In the limit $m_Q \rightarrow \infty$, the usual quark propagator becomes

$$\begin{aligned} i \frac{\not{p} + m_Q}{p^2 - m_Q^2 + i\epsilon} &= i \frac{m_Q \not{v} + \not{k} + m_Q}{2m_Q v \cdot k + k^2 + i\epsilon} \\ &\rightarrow i \frac{1 + \not{v}}{2} \frac{1}{v \cdot k + i\epsilon}. \end{aligned} \quad (3.2)$$

The factor $\frac{1+\not{v}}{2}$ is an energy projector, denote as P_+ . Define $P_- = \frac{1-\not{v}}{2}$. P_+ and P_- satisfy the relations :

$$P_{\pm}^2 = P_{\pm}, \quad P_{\pm} P_{\mp} = 0. \quad (3.3)$$

Introduce the new fields by applying the projectors P_{\pm} on the heavy quark field $Q(x)$:

$$h_v(x) = \exp(im_Q v \cdot x) P_+ Q(x), \quad H_v(x) = \exp(im_Q v \cdot x) P_- Q(x), \quad (3.4)$$

so that

$$Q(x) = \exp(-im_Q v \cdot x) (h_v(x) + H_v(x)). \quad (3.5)$$

The new fields satisfy $\not{v} h_v = h_v$, $\not{v} H_v = -H_v$. In the hadron rest frame, $v = (1, \vec{0})$, $P_{\pm} = (1 \pm \gamma_0)/2$, thus $h_v(x)$ and $H_v(x)$ correspond to the upper and lower components of $Q(x)$ respectively. The field $h_v(x)$ annihilates a heavy quark with velocity v , while $H_v(x)$ creates a heavy antiquark with the same velocity. At the energy scale Λ_{QCD} we are interested, heavy antiquark can hardly be created. We will show later that $H_v(x)$ is suppressed by a factor of $1/M_Q$. Thus, in the limit $m_Q \rightarrow \infty$, only $h_v(x)$ remains, the heavy quark Lagrangian $L_{QCD}^{(Q)}(x) = \bar{Q}(x)(i\not{D} - m_Q)Q(x)$ becomes

$$L_{QCD}^{(h)}(x) = \bar{h}_v(x) i(v \cdot D) h_v(x) \quad (3.6)$$

The propagator of this Lagrangian is

$$i \frac{1 + \not{v}}{2} \frac{1}{v \cdot k + i\epsilon}. \quad (3.7)$$

The factor $\frac{1+\not{v}}{2}$ arises because $P_+ h_v = h_v$. The Lagrangian in Eq. 3.6 exactly reproduce the quark propagator in the limit $m_Q \rightarrow \infty$, which is obtained in Eq. 3.2.

The interaction vertex in the full theory is $-ig\gamma_\mu t^a$, while in effective theory the vertex is $-igv_\mu t^a$. The vertex is sandwiched between quark propagators. Each quark propagator is proportional to $(1 + \not{v})/2$, so the vertex $-ig\gamma_\mu t^a$ can be replaced by $-igv_\mu t^a$ because

$$\frac{1 + \not{v}}{2} (-ig\gamma_\mu t^a) \frac{1 + \not{v}}{2} = \frac{1 + \not{v}}{2} (-igv_\mu t^a) \frac{1 + \not{v}}{2}. \quad (3.8)$$

Therefore, the effective Lagrangian in Eq. 3.6 reproduces all the Green's functions in the full theory to leading order in $1/m_Q$.

In order to analyze $1/m_Q$ corrections, we have to consider the small component H_v . With the definition of Eq. 3.5, the heavy quark Lagrangian $L_{QCD}^{(Q)}$ becomes

$$\begin{aligned} L_{QCD}^{(Q)} &= (\bar{h}_v + \bar{H}_v) e^{im_Q v \cdot x} (i\not{D} - m_Q) e^{-im_Q v \cdot x} (h_v + H_v) \\ &= (\bar{h}_v + \bar{H}_v) [i\not{D} - m_Q(1 - \not{v})] (h_v + H_v) \\ &= \bar{h}_v i(v \cdot D) h_v - \bar{H}_v (iv \cdot D + 2m_Q) H_v + \bar{h}_v i\not{D} H_v + \bar{H}_v i\not{D} h_v, \end{aligned} \quad (3.9)$$

where we have used the relations $\not{v} h_v = h_v$, $\not{v} H_v = -H_v$. It is convenient to project four vectors into components parallel and perpendicular to the velocity v . The perpendicular component of the Dirac operator is

$$D_\perp^\mu \equiv D^\mu - v^\mu (v \cdot D). \quad (3.10)$$

The $i\cancel{D}$ in Eq. 3.9 can be replaced by $i\cancel{D}_\perp$ since $\bar{h}_v\cancel{D}H_v = \bar{H}\cancel{D}h_v = 0$.

In Eq. 3.9, h_v describes a massless degree of freedom, H_v corresponds to the fluctuations with mass $2m_Q$, the last two terms describe quark-antiquark creation and annihilation.

At tree level, H_v can be integrated out by solving the equation of motion $(i\cancel{D} - m_Q)Q = 0$, which in terms of h_v and H_v takes the form

$$i\cancel{D}h_v + (i\cancel{D} - 2m_Q)H_v = 0 \quad (3.11)$$

by applying P_\pm on both sides, this equation can be projected into two pieces:

$$iv \cdot Dh_v = -i\cancel{D}_\perp H_v, \quad (iv \cdot D + 2m_Q)H_v = i\cancel{D}_\perp h_v. \quad (3.12)$$

From the second equation we get

$$H_v = \frac{1}{iv \cdot D + 2m_Q - i\epsilon} i\cancel{D}_\perp h_v, \quad (3.13)$$

which explicitly shows that $H_v \sim \mathcal{O}(1/m_Q)$. Substitute it back into Eq. 3.9, one gets

$$L_{eff} = \bar{h}_v i(v \cdot D)h_v + \bar{h}_v i\cancel{D}_\perp \frac{1}{iv \cdot D + 2m_Q - i\epsilon} i\cancel{D}_\perp h_v. \quad (3.14)$$

3.1.2 $1/m_Q$ expansion

Because of the phase factor in Eq. 3.5, the x-dependence of the effective heavy quark field is weak. Derivatives acting on h_c produce powers of the residual momentum k , which is much smaller than m_Q . Therefore, the HQET Lagrangian Eq. 3.9 can be expanded in powers of D/m_Q .

Expand the factor $\frac{1}{iv \cdot D + 2m_Q - i\epsilon}$ in Eq. 3.9, we have

$$L_{eff} = \bar{h}_v(iv \cdot D)h_v + \frac{1}{2m_Q} \bar{h}_v(i\mathcal{D}_\perp)^2 h_v + \mathcal{O}(1/m_Q^2) \quad (3.15)$$

Using the identity

$$\mathcal{D}_\perp \mathcal{D}_\perp = D_\perp^2 - \frac{g}{2} \sigma_{\mu\nu} F^{\mu\nu}, \quad (3.16)$$

where $F_{\mu\nu}$ is the gauge tensor defined in Eq. 1.18, $\sigma_{\mu\nu} = i[\gamma_\mu, \gamma_\nu]/2$. Eq. 3.15 becomes

$$L_{eff} = \bar{h}_v(iv \cdot D)h_v + \frac{1}{2m_Q} \bar{h}_v(iD_\perp)^2 h_v + \frac{g}{4m_Q} \bar{h}_v \sigma_{\mu\nu} F^{\mu\nu} h_v + \mathcal{O}(1/m_Q^2). \quad (3.17)$$

It is more clear to write the Lagrangian as power of corrections:

$$L_{eff} = L_0 + L_1 + L_2 + \dots, \quad (3.18)$$

where $L_0 = \bar{h}_v(iv \cdot D)h_v$ is the leading term, and

$$L_1 = \frac{1}{2m_Q} \bar{h}_v(iD_\perp)^2 h_v + \frac{g}{4m_Q} \bar{h}_v \sigma_{\mu\nu} F^{\mu\nu} h_v \quad (3.19)$$

is the first order correction, and so on.

In the hadron rest frame, $D_\perp = (0, \vec{D})$. It is clear that the first term in L_1 is nothing but the heavy quark kinetic energy $\vec{p}_Q^2/2m_Q$. It breaks the heavy quark flavor symmetry because of the explicit dependence on m_Q , but it doesn't break heavy quark spin symmetry. The second term in L_1 is the chromo-magnetic momentum interaction, it breaks both heavy quark spin and flavor symmetry.

3.1.3 Hadron masses

The hadron masses in the effective theory is $m_H - m_Q$ since the heavy quark mass m_Q has been subtracted from all energies in the field redefinition in Eq. 3.5. At order m_Q , all heavy hadrons containing a single heavy quark have degenerated mass m_Q . At order of unity, the hadron masses get the contribution

$$\bar{\lambda} = \frac{1}{2} \langle H^{(Q)} | \mathcal{H}_0 | H^{(Q)} \rangle, \quad (3.20)$$

where \mathcal{H}_0 is the Hamiltonian obtained from the leading term L_0 in the effective Lagrangian, as well as the terms involving light quarks and gluons. $\bar{\lambda}$ has the same value for all particles in a spin-flavor multiplet due to the heavy quark spin-flavor symmetry at the leading order. In the SU(3) limit, $\bar{\lambda}$ does not depend on the light quark flavor. We will denote the value by λ for the mesons B , B^* , D and D^* , λ^Λ for the baryons Λ_b , Λ_c , Ξ_b and Ξ_c , and λ_Σ for the baryons Σ_b , Σ_c , Ξ'_b , Ξ'_c , Ω_b , Ω_c , Σ_b^* , Σ_c^* , Ξ_b^* , Ξ_c^* , Ω_b^* , Ω_c^* .

At order $1/m_Q$, there is an additional contribution to the hadron masses given by the $1/m_Q$ correction term L_1 in the effective Lagrangian. Define two parameters (λ_1 and λ_2) from the two terms in L_1 :

$$\begin{aligned} -\langle H^{(Q)} | \bar{h}_v D_\perp^2 | H^{(Q)} \rangle &= 2\lambda_1, \\ \langle H^{(Q)} | \bar{h}_v g \sigma_{\mu\nu} F^{\mu\nu} h_v | H^{(Q)} \rangle &= 16(s_Q \cdot s_l) \lambda_2. \end{aligned} \quad (3.21)$$

Here λ_1 is independent of m_Q . λ_2 depends on m_Q through a renormalization factor, here we ignore the dependence since the loop corrections are small. From the definition, it is clear that $\lambda_{1,2} \sim \bar{p}_Q^2 \sim \Lambda_{QCD}^2$. In the hadron rest frame, the term $\bar{h}_v g \sigma_{\mu\nu} F^{\mu\nu} h_v$ reduces to $\bar{h}_v g \vec{S} \cdot \vec{B} h_v$, where \vec{S} is the heavy quark spin and \vec{B} is

the chromomagnetic field. The matrix element of \vec{B} is proportional to the spin of light degrees of freedom. Thus the matrix element of the chromomagnetic operator is defined to be proportional to $s_Q \cdot s_l$.

Now we can derive the mass of a hadron

$$m_H = m_Q + \lambda - \frac{\lambda_1}{2m_Q} + \frac{2(s_Q \cdot s_l)\lambda_2}{m_Q} \quad (3.22)$$

The parameters λ and $\lambda_{1,2}$ are different for the hadrons in different spin-flavor multiplets.

For the B meson, $s_Q = s_l = 1/2$, $J = 0$, $s_Q s_l = (J^2 - s_Q^2 - s_l^2)/2 = -3/4$, thus the mass of B meson is

$$m_B = m_b + \lambda - \frac{\lambda_1}{2m_b} - \frac{3\lambda_2}{2m_b}, \quad (3.23)$$

where m_b is the mass of b -quark. Similarly, the mass of B^* can be obtained

$$m_B^* = m_b + \lambda - \frac{\lambda_1}{2m_b} + \frac{\lambda_2}{2m_b}. \quad (3.24)$$

The mass of D and D^* have the same form as B and B^* respectively except that m_b should be replaced by m_c . From Eq. 3.23 and Eq. 3.24, we can see that the spin average mass of B and B^* , e. g., $(3m_{B^*} + m_B)/4$ dose not depend on λ_2 . The chromo-magnetic interaction is responsible for the hyperfine splittings $m_{B^*} - m_B$ and $m_{D^*} - m_D$.

For the baryons Λ_b , Λ_c , Ξ_b and Ξ_c , $s_Q = 1/2$, $s_l = 0$, $J = 1/2$, so $s_Q s_l = 0$, the masses are

$$\begin{aligned} m_{\Lambda_b} &= m_{\Xi_b} = m_b + \lambda_\Lambda - \frac{\lambda_{1,\Lambda}}{2m_b}, \\ m_{\Lambda_c} &= m_{\Xi_c} = m_c + \lambda_\Lambda - \frac{\lambda_{1,\Lambda}}{2m_c}. \end{aligned} \quad (3.25)$$

For the baryons Σ_b , Σ_c , Ξ'_b , Ξ'_c , Ω_b and Ω_c , $s_Q = 1/2$, $s_l = 1$, $J = 1/2$, so $s_Q s_l = -1$, the masses are

$$\begin{aligned} m_{\Sigma_b} &= m_{\Xi'_b} = m_{\Omega_b} = m_b + \lambda_\Sigma - \frac{\lambda_{1,\Sigma}}{2m_b} - \frac{2\lambda_{2,\Sigma}}{m_b}, \\ m_{\Sigma_c} &= m_{\Xi'_c} = m_{\Omega_c} = m_c + \lambda_\Sigma - \frac{\lambda_{1,\Sigma}}{2m_c} - \frac{2\lambda_{2,\Sigma}}{m_c}. \end{aligned} \quad (3.26)$$

For the baryons Σ_b^* , Σ_c^* , Ξ_b^* , Ξ_c^* , Ω_b^* and Ω_c^* , $s_Q = 1/2$, $s_l = 1$, $J = 3/2$, so $s_Q s_l = 1/2$, the masses are

$$\begin{aligned} m_{\Sigma_b^*} &= m_{\Xi_b^*} = m_{\Omega_b^*} = m_b + \lambda_\Sigma - \frac{\lambda_{1,\Sigma}}{2m_b} + \frac{\lambda_{2,\Sigma}}{m_b}, \\ m_{\Sigma_c^*} &= m_{\Xi_c^*} = m_{\Omega_c^*} = m_c + \lambda_\Sigma - \frac{\lambda_{1,\Sigma}}{2m_c} + \frac{\lambda_{2,\Sigma}}{m_c}. \end{aligned} \quad (3.27)$$

The parameters λ_1 and λ_2 are nonperturbative parameters of QCD and have not been computed from first principles. One can obtain their values by fitting the hadron masses and use them to compute other quantities which can be expressed by these parameters, such as the form factors and decay rates. The mass formulas from HQET also show how the hadron masses depend on the heavy quark mass. In lattice calculation, they are useful tools for analyzing the systematic errors due to discretization effects.

3.2 Chiral perturbation theory

Chiral perturbation theory is the low-energy realization of QCD in the light quark sector. In Lattice QCD simulations the light quark propagators are not calculated at the physical light quark mass because it is computationally costly to simulate light quarks. The observables are calculated for several different quark masses which are higher than the physical quark mass and then extrapolated to the physical point.

Therefore, the light quark mass dependence of the observables has to be investigated systematically.

3.2.1 Chiral symmetry in QCD

Consider the quark content of the QCD Lagrangian, keeping only the three light flavors u, d and s :

$$L_{QCD} = \sum_i^3 \bar{q}_i (i\not{D} - m_i) q_i. \quad (3.28)$$

Define the right-handed quark and left-handed quark by applying the projectors $P_R = (1 + \gamma_5)/2$ and $P_L = (1 - \gamma_5)/2$ on the quark field:

$$q_R = \frac{1 + \gamma_5}{2} q, \quad q_L = \frac{1 - \gamma_5}{2} q. \quad (3.29)$$

The kinetic term can be written in terms of q_L and q_R :

$$\sum_i \bar{q}_i i\not{D} q_i = \sum_i (\bar{q}_{Li} i\not{D} q_{Li} + \bar{q}_{Ri} i\not{D} q_{Ri}). \quad (3.30)$$

This term is invariant under $SU(3)_L \times SU(3)_R$ transformation, where the left-handed quark and right handed quark transform as $SU(3)$ group independently. This symmetry is called ‘‘chiral symmetry’’.

Chiral symmetry is not an exact symmetry of QCD since the quark mass terms explicitly break this symmetry. In terms of q_L and q_R , the quark mass terms may be written as

$$\sum_i m_i \bar{q}_i q_i = \sum_{ij} (\bar{q}_{Li} M_{ij} q_{Rj} + \bar{q}_{Ri} M_{ij}^\dagger q_{Lj}) \quad (3.31)$$

where

$$M = \begin{pmatrix} m_u & & \\ & m_d & \\ & & m_s \end{pmatrix} \quad (3.32)$$

The mass terms couple left- and right-handed quarks, the $SU(3)_L \times SU(3)_R$ symmetry is broken down to the vector subgroup. However, this explicit breaking can be treated perturbatively considering that the u, d, s quark masses are small comparing to Λ_{QCD} .

In the zero quark mass limit, or chiral limit, the QCD Lagrangian exhibits an exact chiral symmetry. However, this chiral symmetry is not seen in the hadron spectrum. The degenerate multiplets with opposite parity do not exist. The observed parity partner of the nucleon is significantly heavier than the nucleon. Moreover, the octet of pseudoscalar mesons happens to be much lighter than all the other hadronic states. This phenomena lead us to postulate that the vacuum of QCD spontaneously breaks the chiral symmetry of the QCD Lagrangian to the vector subgroup. The hypothesis is that the quark condensate in the QCD vacuum is nonzero:

$$\langle 0 | \bar{q}_{Rj} q_{Li} | 0 \rangle = \Lambda^3 \delta_{ij}. \quad (3.33)$$

Here Λ has dimension of mass. Under a chiral transformation

$$\langle 0 | \bar{q}_{Rj} q_{Li} | 0 \rangle \rightarrow \langle 0 | \bar{q}_{Rk} R_{kj}^\dagger L_{il} q_{Ll} | 0 \rangle = \Lambda^3 (LR^\dagger)_{ij}, \quad (3.34)$$

where R and L are $SU(3)$ matrices. If $L = R$, i.e. an $SU(3)_V$ transformation, $(LR^\dagger)_{ij} = \delta_{ij}$ which means that the condensate leaves the $SU(3)_V$ unbroken. But it does break the $SU(3)_L \times SU(3)_R$ symmetry because Σ_{ij} represents a different vacuum from Eq. 3.33 for $L \neq R$. According to Goldstone's theorem, this spontaneous symmetry breaking creates eight pseudoscalar massless bosons, one for each of the

eight broken generators. The quark mass matrix, which explicitly breaks $SU(3)_L \times SU(3)_R$ symmetry, gives rise to the small masses of these boson, which we can identify with the lightest hadronic states (π^+ , π^- , π^0 , K^+ , K^- , K^0 , \bar{K}^0 and η). We will parameterize these states by replacing

$$\Sigma \rightarrow \Sigma(x) \equiv \exp\left(\frac{2i\phi(x)}{f}\right), \quad \text{with} \quad \phi(x) = \sum_{a=1}^8 t_a \phi_a(x), \quad (3.35)$$

where we use the normalization $f \simeq 132MeV$, t^a are the generators of $SU(3)$ group, ϕ_a represent the eight pseudoscalar mesons. Write down ϕ explicitly as

$$\phi = \begin{pmatrix} \frac{\pi^0}{\sqrt{2}} + \frac{\eta}{\sqrt{6}} & \pi^+ & K^+ \\ \pi^- & -\frac{\pi^0}{\sqrt{2}} + \frac{\eta}{\sqrt{6}} & K^0 \\ K^- & \bar{K}^0 & -\frac{2\eta}{\sqrt{6}} \end{pmatrix}. \quad (3.36)$$

3.2.2 Effective chiral Lagrangian

From Eq. 3.34, we can see that the field Σ transforms under the chiral group as

$$\Sigma \rightarrow L\Sigma R^\dagger \quad (3.37)$$

The chiral Lagrangian must exhibit the same approximate symmetry as QCD, which means that it must be invariant under the transformation in Eq. 3.37 in chiral limit.

The lowest dimension operator which preserve chiral symmetry is

$$\frac{f^2}{8} Tr(\partial_\mu \Sigma \partial^\mu \Sigma^\dagger) \quad (3.38)$$

The factor $\frac{f^2}{8}$ is to generate the standard form of the kinetic term $\frac{1}{2} \partial_\mu \phi_a \partial^\mu \phi_a$.

To include the effect of quark masses, the mass matrix M have to be included. From Eq: 3.31 we can see that if M transform as

$$M \rightarrow LMR^\dagger, \quad (3.39)$$

the QCD Lagrangian has chiral symmetry. This property must be preserved in the effective Lagrangian. So the lowest order effective Lagrangian with mass term is

$$L_2 = \frac{f^2}{8} \text{Tr}(\partial_\mu \Sigma \partial^\mu \Sigma^\dagger) + \frac{f^2 B_0}{4} \text{Tr}(\Sigma M^\dagger + M \Sigma^\dagger), \quad (3.40)$$

where B_0 is a low energy coefficient.

Expand L_2 to the second order in ϕ , we get

$$\begin{aligned} L_2 = & \partial_\mu \pi^+ \partial^\mu \pi^- + \frac{1}{2} (\partial_\mu \pi^0)^2 + \partial_\mu K^+ \partial^\mu K^- + (\partial_\mu K^0)^2 + \frac{1}{2} (\partial_\mu \eta)^2 \\ & - B_0(m_u + m_d) \pi^+ \pi^- - \frac{1}{2} B_0(m_u + m_d) \pi^0 \pi^0 - B_0(m_u + m_s) K^+ K^- \\ & - B_0(m_d + m_s) K^0 \bar{K}^0 - \frac{1}{6} B_0(m_u + m_d + 4m_s) \eta^2 \\ & - \frac{1}{\sqrt{3}} B_0(m_u - m_d) \pi^0 \eta. \end{aligned} \quad (3.41)$$

We take isospin-symmetric limit $m_u = m_d = m$, the term with $\pi^0 - \eta$ mixing vanishes. The masses of these pseudoscalar mesons to the lowest order of light quark masses are

$$m_\pi^2 = 2B_0 m, \quad m_K^2 = B_0(m + m_s), \quad m_\eta^2 = \frac{2}{3} B_0(m + 2m_s). \quad (3.42)$$

The masses in Eq. 3.42 satisfy the Gell-Mann-Okuba relation

$$4m_K^2 = 3m_\eta^2 + m_\pi^2. \quad (3.43)$$

Eq. 3.42 shows that $m_{\pi,K,\eta}^2 \simeq M$, for on-shell mesons $p^2 \sim m_{\pi,K,\eta}^2$, it follows that one insertion of the quark mass matrix M is equivalent to two derivatives in the power counting of the effective Lagrangian. Generally the effective Lagrangian is written as

$$L_{eff} = L_2 + L_4 + L_6 + \dots \quad (3.44)$$

The index 2, 4, 6, \dots indicate the power of p of each order of Lagrangian. Two derivatives or one quark mass matrix are inserted to get a higher order Lagrangian.

When we consider the one loop correction from L_2 , we have to include the tree level contribution from L_4 since they are in the same order. Similarly, the two loop correction from L_2 has the same order as the one loop correction from L_4 and the tree level contribution from L_6 , and so on.

The most general Lagrangian L_4 which consist with the symmetries is

$$\begin{aligned} L_4 = & l_1(Tr(\partial_\mu \Sigma^\dagger \partial^\mu \Sigma))^2 + l_2 Tr(\partial_\mu \Sigma^\dagger \partial^\nu \Sigma) Tr(\partial_\mu \Sigma^\dagger \partial^\nu \Sigma) \\ & + l_3 Tr(\partial_\mu \Sigma^\dagger \partial^\mu \Sigma \partial_\nu \Sigma^\dagger \partial^\nu \Sigma) \\ & + 2B_0 l_4 Tr(\partial_\mu \Sigma^\dagger \partial^\mu \Sigma) Tr(M \Sigma^\dagger + \Sigma M^\dagger) \\ & + 2B_0 l_5 Tr((\partial_\mu \Sigma^\dagger \partial^\mu \Sigma)(M \Sigma^\dagger + \Sigma M^\dagger)) \\ & + 4B_0^2 l_6 (Tr(M \Sigma^\dagger + \Sigma M^\dagger))^2 + 4B_0^2 l_7 (Tr(M \Sigma^\dagger - \Sigma M^\dagger))^2 \\ & + 4B_0^2 l_8 Tr(M \Sigma^\dagger M \Sigma^\dagger + \Sigma M^\dagger \Sigma M^\dagger). \end{aligned} \quad (3.45)$$

3.2.3 Heavy baryon chiral perturbation theory (HB χ PT)

When we consider the baryons in chiral perturbation theory, the power counting problem arises. The baryon mass is not small comparing to the chiral symmetry breaking scale Λ_χ . Thus we can not power count loop diagrams or the higher dimen-

sional operators with arbitrary powers of M/Λ_χ as we did for the light pseudoscalar mesons.

This problem can be solved by applying the formalism developed for HQET [41, 42]. In Eq. 3.5, by the redefinition using a velocity dependent phase, the heavy quark field is decomposed into two parts: the large part h_v and the small part H_v which is suppressed by $1/m_Q$. Here we do the same thing for the baryon fields. Define

$$B_v(x) = e^{im_B v \cdot x} \frac{1 + \not{v}}{2} B(x), \quad (3.46)$$

where m_B is the mass of the baryon B and v is the four-velocity of B . The momentum of the baryon is

$$p_\mu = m_B v_\mu + k_\mu, \quad (3.47)$$

where k_μ is the off-shell momentum of the baryon which is supposed to be small.

As we have shown in Sec. 3.1, in the limit $m_Q \rightarrow \infty$, the Dirac Lagrangian $\bar{B}(i\not{\partial} - m_B)B \rightarrow \bar{B}_v i\not{\partial} B_v$. Derivatives acting on $B_v(x)$ produce factors of k , rather than p , so that the higher derivative terms in effective Lagrangian are suppressed by powers of k/Λ_χ which is small. Thus the heavy baryon Lagrangian has a consistent derivative expansion.

The baryon chiral perturbation Lagrangian is written in terms of the octet baryon fields

$$B_v = \begin{pmatrix} \frac{\Sigma_v^0}{\sqrt{2}} + \frac{\Lambda_v}{\sqrt{2}} & \Sigma_v^+ & p_v \\ \Sigma_v^- & -\frac{\Sigma_v^0}{\sqrt{2}} + \frac{\Lambda_v}{\sqrt{6}} & n_v \\ \Sigma_v^- & \Sigma_v^0 & -\frac{2\Lambda_v}{\sqrt{6}} \end{pmatrix} \quad (3.48)$$

and the Goldstone boson fields ϕ defined in Eq. 3.36.

One can define spin operators S_v^μ that act on the baryon fields B_v , with the

properties

$$v \cdot S_v = 0, \quad S_v^2 B_v = -\frac{3}{4} B_v, \quad (3.49)$$

$$\{S_v^\lambda, S_v^\sigma\} = \frac{1}{2}(v^\lambda v^\sigma - g^{\lambda\sigma}), \quad [S_v^\lambda, S_v^\sigma] = i\epsilon^{\lambda\sigma\alpha\beta} v_\alpha S_{v\beta}. \quad (3.50)$$

With this definition, all Lorentz tensors made from spinors can be written in terms of v and S :

$$\bar{B}_v \gamma_5 B_v = 0, \quad \bar{B}_v \gamma_\mu B_v = v_\mu \bar{B}_v B_v, \quad \bar{B}_v \gamma^\mu \gamma_5 B_v = 2\bar{B}_v S_v^\mu B_v, \quad (3.51)$$

$$\bar{B}_v \sigma^{\mu\nu} B_v = 2\epsilon^{\mu\nu\alpha\beta} v_\alpha \bar{B}_v S_{v\beta} B_v, \quad \bar{B}_v \sigma^{\mu\nu} \gamma_5 B_v = 2i(v^\mu \bar{B}_v S_v^\nu B_v - v^\nu \bar{B}_v S_v^\mu B_v). \quad (3.52)$$

Introduce a new matrix $\xi = \Sigma^{1/2}$, which transform under an $SU(3)_L \times SU(3)_R$ as

$$\xi \rightarrow \xi' = L\xi U^\dagger = U\xi R^\dagger, \quad (3.53)$$

where U is a unitary matrix depending on L , R and ϕ . From ξ we can construct a vector field V_μ and axial vector field A_μ :

$$V_\mu = \frac{1}{2}(\xi^\dagger \partial_\mu \xi + \xi \partial_\mu \xi^\dagger), \quad (3.54)$$

$$A_\mu = \frac{i}{2}(\xi^\dagger \partial_\mu \xi - \xi \partial_\mu \xi^\dagger). \quad (3.55)$$

The vector field acts like an gauge field under a chiral transformation

$$V_\mu \rightarrow V'_\mu = UV_\mu U^\dagger + U \partial_\mu U^\dagger, \quad (3.56)$$

while the axial field transforms as an $SU(3)$ octet

$$A_\mu \rightarrow A'_\mu = U A_\mu U^\dagger. \quad (3.57)$$

The most general Lagrangian at lowest order is [43]

$$\begin{aligned} L_v = & Tr(\bar{B}_v i v \cdot D B_v) + 2D Tr(\bar{B}_v S_v^\mu \{A_\mu, B_v\}) + 2F Tr(\bar{B}_v S_v^\mu [A_\mu, B_v]) \\ & + b_D Tr(\bar{B}_v \{M_+, B_v\}) + b_F Tr(\bar{B}_v [M_+, B_v]) \\ & + \sigma Tr(M(\Sigma + \Sigma^\dagger)) Tr(\bar{B}_v B_v) \\ & + \frac{f^2}{8} Tr(\partial_\mu \Sigma \partial^\mu \Sigma^\dagger) + a Tr(M(\Sigma + \Sigma^\dagger)), \end{aligned} \quad (3.58)$$

where $M_+ = \xi^\dagger M \xi^\dagger + \xi M^\dagger \xi$, $D^\mu B_v = \partial^\mu B_v + [V^\mu, B_v]$, in the second term D is a coefficient, not to be confused with the derivative operator D .

The decuplet baryons which have spin $\frac{3}{2}$ can also be included in the effective chiral theory. The decuplet can be described by a Rarita-Schwinger field [44] $(T^\mu)_{abc}$, satisfying the constraint $\gamma^\mu T_\mu = 0$. T_{abc}^μ transforms under chiral group as

$$T_{ijk} \rightarrow U_i^l U_j^m U_k^n T_{lmn}, \quad (3.59)$$

with the normalization

$$\begin{aligned} T_{111} = \Delta^{*++}, \quad T_{112} = \frac{1}{\sqrt{3}} \Delta^{*+}, \quad T_{122} = \frac{1}{\sqrt{3}} \Delta^{*0}, \quad T_{222} = \Delta^{*-}, \\ T_{113} = \frac{1}{\sqrt{3}} \Sigma^{*+}, \quad T_{123} = \frac{1}{\sqrt{6}} \Sigma^{*0}, \quad T_{223} = \frac{1}{\sqrt{3}} \Sigma^{*-}, \\ T_{133} = \frac{1}{\sqrt{3}} \Xi^{*0}, \quad T_{233} = \frac{1}{\sqrt{3}} \Xi^{*-}, \\ T_{333} = \Omega^{*-}. \end{aligned} \quad (3.60)$$

Define the velocity dependent field for T the same way as we define B_v :

$$T_v(x) = e^{im_B v \cdot x} \frac{1 + \not{v}}{2} T(x). \quad (3.61)$$

The lowest order containing the decuplet baryons is

$$\begin{aligned} L_v = & -i\bar{T}_v^\mu (v \cdot D) T_{v\mu} + \Delta m \bar{T}_v^\mu T_{v\mu} + c \bar{T}_v^\mu M_+ T_{v\mu} - \sigma \text{Tr}(M(\Sigma + \Sigma^\dagger)) \bar{T}_v^\mu T_{v\mu} \\ & + \mathcal{C}(\bar{T}_v^\mu A_\mu B_v + \bar{B}_v A_\mu T_v^\mu) + 2\mathcal{H} \bar{T}_v^\mu S_{v\nu} A^\nu T_{v\mu}. \end{aligned} \quad (3.62)$$

The covariant derivative acting on the T field as

$$D^\mu T_{ijk} = \partial^\mu T_{ijk} + (V^\mu)_i^{i'} T_{i'jk} + (V^\mu)_j^{j'} T_{ij'k} + (V^\mu)_k^{k'} T_{ijk'}. \quad (3.63)$$

Notice that there is a mass term $\Delta m \bar{T}_v^\mu T_{v\mu}$ in the decuplet Lagrangian, where Δm is the mass splitting between the decuplet and the octet baryons. This term is introduced by the definition of T_v in Eq. 3.61, where we use m_B instead of m_T in the phase factor. Derivative acting on T_v removes the mass m_B instead of m_T , thus an explicit mass term proportional $m_T - m_B$ remains in the Lagrangian. This definition avoids introducing factors of $e^{i\Delta m v \cdot x}$ into the Lagrangian in terms which contain both decuplet and octet fields.

3.2.4 χ PT for baryons containing a heavy quark

Now let's move on to the chiral perturbation theory for the baryons containing a heavy quark (c or b). In the limit $m_Q \rightarrow \infty$, the heavy quark spin decouples from the light degrees of freedom. Thus we can classify them by the spin of their light degree of freedom, which can be $s_l = 0$ or 1 .

For the baryons with $s_l = 0$, they have spin $\frac{1}{2}$ because there is only one way to

combine the spin of the heavy quark with the spin of the light degrees of freedom. They can be described by an antisymmetric tensor

$$T^{ij} = \begin{pmatrix} 0 & \Lambda_c^+ & \Xi_c^+ \\ -\Lambda_c^+ & 0 & \Xi_c^0 \\ -\Xi_c^+ & -\Xi_c^0 & 0 \end{pmatrix} \quad (3.64)$$

here we specify the baryons to be charmed baryons since one of the goal of this work is to study the charmed baryon spectrum. Notice that in Eq. 3.64 we have suppressed the velocity labels on all charmed baryons. For example, by Λ_c^+ we actually mean $\Lambda_{cv}^+ = e^{im_\Lambda v \cdot x} \frac{1+\not{v}}{2} \Lambda_c^+$. From now on, we will suppress the velocity labels on all heavy hadrons in this chapter.

For the baryons with $s_l = 1$, the total spin the baryons can be $J = \frac{1}{2}$ or $\frac{3}{2}$. In the limit $m_Q \rightarrow \infty$, these two multiplets are degenerate and can be described by one filed S_{ij}^μ

$$S_\mu^{ij} = \frac{1}{\sqrt{3}}(\gamma_\mu + v_\mu)\gamma^5 B^{ij} + B_\mu^{*ij}, \quad (3.65)$$

where

$$B^{ij} = \begin{pmatrix} \Sigma_c^{++} & \frac{1}{\sqrt{2}}\Sigma_c^+ & \frac{1}{\sqrt{2}}\Xi_c'^+ \\ \frac{1}{\sqrt{2}}\Sigma_c^+ & \Sigma_c^0 & \frac{1}{\sqrt{2}}\Xi_c'^0 \\ \frac{1}{\sqrt{2}}\Xi_c'^+ & \frac{1}{\sqrt{2}}\Xi_c'^0 & \Omega_c^0 \end{pmatrix} \quad (3.66)$$

is the $J = \frac{1}{2}$ baryons and B_μ^{*ij} is the $J = \frac{3}{2}$ baryons. B_μ^{*ij} has similar form as B^{ij} .

The field S_{ij}^μ satisfies the constraints $v_\mu S_\mu^{ij} = 0$ and $\not{v} S_\mu^{ij} = S_\mu^{ij}$. It transforms under $SU(3)_L \times SU(3)_R$ as

$$S_\mu^{ij} \rightarrow U_k^i U_l^j S_\mu^{kl}, \quad (3.67)$$

where U is defined in Eq. 3.53.

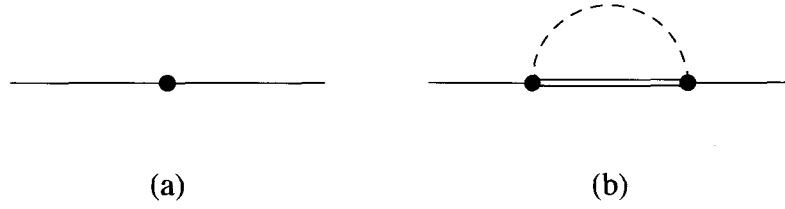


Figure 3.1: Tree level and one-loop diagrams which contribute to the masses of the charmed baryons with $s_l = 0$. The single, double, dashed lines correspond to $s_l = 0$ baryons, $s_l = 1$ baryons and mesons respectively.

The lowest order Lagrangian takes the form

$$\begin{aligned}
L = & -i\bar{S}^\mu v \cdot DS_\mu + \Delta\bar{S}^\mu S_\mu + i\bar{T}v \cdot DT \\
& + \lambda_1\bar{S}^\mu M_+ S_\mu + \lambda_2\bar{S}^\mu S_\mu Tr M_+ + \lambda_3\bar{T}M_+ T + \lambda_4\bar{T}T Tr M_+ \\
& + ig_2\epsilon_{\mu\nu\rho\sigma}(\bar{S}^\mu v^\nu A^\rho S^\sigma) + g_3(\bar{T}A^\mu S_\mu + h.c.).
\end{aligned} \tag{3.68}$$

Fig. 3.1 and Fig. 3.2 show the diagrams which contribute the masses of $s_l = 0$ charmed baryons and $s_l = 1$ charmed baryons to one loop. The single, double, dashed lines correspond to $s_l = 0$ baryons, $s_l = 1$ baryons and mesons respectively. Fig. 3.1 (a) is the tree level contribution to the masses of $s_l = 0$ charmed baryons which comes from the terms with coefficients λ_3 and λ_4 in the Lagrangian in Eq. 3.68. 3.2 (a) comes from the terms with coefficients λ_1 and λ_2 . 3.1 (b) and 3.2 (c) both arise from the axial coupling of T field and S field, i.e. the term with coefficient g_3 . 3.2 (b) arises from the term with coefficient g_2 . Notice that there is no axial coupling of T field and T field, this term is ruled out by parity. Here we are not going to calculate these diagrams. For the detailed calculations, please see reference [45]. We will use the results therein to perform the chiral extrapolation of the charmed baryons masses simulated on lattice.

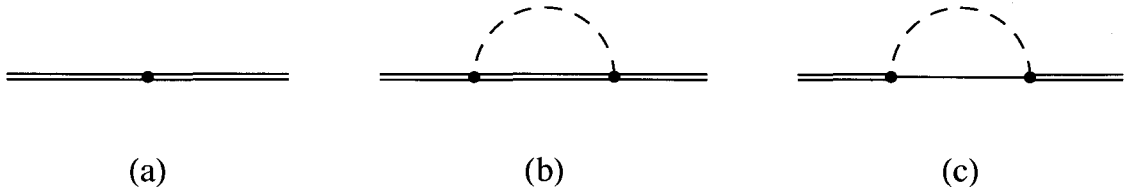


Figure 3.2: Tree level and one-loop diagrams which contribute to the masses of the charmed baryons with $s_l = 1$. The single, double, dashed lines correspond to $s_l = 0$ baryons, $s_l = 1$ baryons and mesons respectively.

3.2.5 χ PT for Heavy mesons

The chiral perturbation theory for heavy mesons is quite similar with the HB χ PT. For the meson with a heavy quark, the spin of the light degree of freedom is $s_l = 1/2$. There are two ways to combine with the heavy quark. The total spin of the meson can be $J = 0$, denote as P , or $J = 1$, denote as P^* . In $m_Q \rightarrow \infty$, P and P^* are degenerate due to the heavy quark spin symmetry. The two fields can be combined into a single field

$$H_i = P_{i\mu}^* \gamma^\mu + iP_i \gamma^5, \quad (3.69)$$

where the velocity labels of the fields have been suppressed. H transforms as an antitriplet matter field under the chiral group

$$H_i \rightarrow H_j U^{(t)j}_i. \quad (3.70)$$

For charmed mesons

$$P = (D^0, D^+, D_s^+), \quad P^* = (D^{0*}, D^{+*}, D_s^{+*}). \quad (3.71)$$

The chiral Lagrangian of H field is constructed by considering the chiral symmetry. The term with zero derivative is the mass term which is removed by the

redefinition of the fields. The terms with one derivative are

$$L = -iTr(\bar{H}_a v \cdot DH_a + g_\pi Tr(\bar{H}^a H_b (A)_a^b \gamma^5)). \quad (3.72)$$

The covariant derivative acting on H as

$$D^\mu H_a = \partial^\mu H_a - H_b (V^\mu)_a^b. \quad (3.73)$$

Expanding V and A in terms of M gives the interactions between the fields P , P^* and the Goldstone bosons. The explicit calculation of the T-matrices of the interacting processes is out of the scope of this work. We refer the interested readers to the references [46, 47].

CHAPTER 4

Lattice Setup and Computational Techniques

In this work we study the charmed hadron spectrum and interactions. The method of extracting the mass of the hadrons from lattice simulation is introduced in section 4.2. Although we are not going to study excited states in this work, it is worth to mention the variational method which is used to extract multiple energy levels from a correlation matrix. To extract the hadronic interactions from lattice QCD, one need to utilize Lüscher’s finite volume technic, which is presented in section 4.3. The condition to form a bound state by weakly attractive interaction is discussed. First of all, we present the lattice we use in the calculations.

4.1 Lattice Setup

4.1.1 Light-Quark Action

In this work we employ the “coarse” ($a \simeq 0.125$ fm) gauge configurations generated by the MILC Collaboration [48] using the one-loop tadpole-improved gauge action [49], where both $\mathcal{O}(a^2)$ and $\mathcal{O}(g^2 a^2)$ errors are removed. For the fermions in the vacuum, the asqtad-improved Kogut-Susskind action [50, 51, 52, 53, 54, 55] is used. This is the Naik action [56] ($\mathcal{O}(a^2)$ improved Kogut-Susskind action) with smeared

links for the one-link terms so that couplings to gluons with any of their momentum components equal to π/a are set to zero.

For the valence light quarks (up, down and strange) we use the five-dimensional Shamir [33, 34] domain-wall fermion propagators [31] calculated by the NPLQCD Collaboration [57]. The domain-wall fermion action introduces a fifth dimension of extent L_5 and a mass parameter M_5 ; in our case the values $L_5 = 16$ and $M_5 = 1.7$ were chosen. The physical quark fields, $q(\vec{x}, t)$, reside on the 4-dimensional boundaries of the fifth coordinate. The left and right chiral components are separated on the corresponding boundaries, resulting in an action with chiral symmetry at finite lattice spacing as $L_5 \rightarrow \infty$. We use hypercubic-smeared gauge links [58, 59, 60, 61] to minimize the residual chiral symmetry breaking, and the bare quark-mass parameter $(am)_q^{\text{dwf}}$ is introduced as a direct coupling of the boundary chiral components.

The calculation we have performed, because the valence and sea quark actions are different, is inherently partially quenched and therefore violates unitarity. Unlike conventional partially quenched calculations, to restore unitarity, one must take the continuum limit in addition to tuning the valence and sea quark masses to be degenerate. This process is aided with the use of mixed-action chiral perturbation theory [62, 63, 64, 65, 66, 67]. Given the situation, there is an ambiguity in the choice of the valence light-quark masses. One appealing choice is to tune the masses such that the valence pion mass is degenerate with one of the staggered pion masses. In the continuum limit, the $N_f = 2$ staggered action has an $SU(8)_L \otimes SU(8)_R \otimes U(1)_V$ chiral symmetry due to the four-fold taste degeneracy of each flavor, and each pion has 15 degenerate partners. At finite lattice spacing this symmetry is broken and the taste multiplets are no longer degenerate, but have splittings that are $\mathcal{O}(\alpha_s^2 a^2)$ [50, 51, 52, 55, 68]. The propagators used in this work were tuned to give valence pions that match the Goldstone Kogut-Susskind pion. This is the only pion that becomes massless in the

Ensemble	β	am_l	am_s	am_l^{dwf}	am_s^{dwf}	N_{cfgs}	N_{props}
m007	6.76	0.007	0.050	0.0081	0.081	461	2766
m010	6.76	0.010	0.050	0.0138	0.081	636	3816
m020	6.79	0.020	0.050	0.0313	0.081	480	1920
m030	6.81	0.030	0.050	0.0478	0.081	563	1689

Table 4.1: The parameters of the configurations and domain-wall propagators used in this work. The subscript l denotes light quark, and s denotes the strange quark. The superscript “dwf” denotes domain-wall fermion.

chiral limit at finite lattice spacing. As a result of this choice, the valence pions are as light as possible, while being tuned to one of the staggered pion masses, providing better convergence in the χ PT needed to extrapolate the lattice results to the physical quark-mass point. This set of parameters, listed in Table 4.1, was first used by LHPC [69, 70] and recently to compute the spectroscopy hadrons composed of up, down and strange quarks [1].

4.1.2 Heavy-Quark Action

For the charm quark we use the Fermilab action [71], which controls discretization errors of $\mathcal{O}((am_Q)^n)$. Following the Symanzik improvement [72], an effective continuum action is constructed using operators that are invariant under discrete rotations, parity-reversal and charge-conjugation transformations, representing the long-distance limit of our lattice theory, including leading finite- a errors. Using only the Dirac operator and the gluon field tensor (and distinguishing between the time and space components of each), we enumerate seven operators with dimension up to five. By applying the isospectral transformations [73], the redundant operators are identified and their coefficients are set to appropriate convenient values. The lattice action then takes the form

$$S = S_0 + S_B + S_E, \quad (4.1)$$

with

$$S_0 = \sum_x \bar{Q}(x) \left[m_0 + \left(\gamma_0 \nabla_0 - \frac{a}{2} \Delta_0 \right) + \nu \sum_i \left(\gamma_i \nabla_i - \frac{a}{2} \Delta_i \right) \right] Q(x), \quad (4.2)$$

$$S_B = -\frac{a}{2} c_B \sum_x \bar{Q}(x) \left(\sum_{i<j} \sigma_{ij} F_{ij} \right) Q(x), \quad (4.3)$$

$$S_E = -\frac{a}{2} c_E \sum_x \bar{Q}(x) \left(\sum_i \sigma_{0i} F_{0i} \right) Q(x), \quad (4.4)$$

where a is the lattice spacing, ∇_0 and ∇_i are first-order lattice derivatives in the time and space directions, Δ_0 and Δ_i are second-order lattice derivatives, and $F_{\mu\nu}$ is the gauge field strength tensor. The spectrum of heavy-quark bound states can be determined accurately through $|\vec{p}|a$ and $(am_Q)^n$ for arbitrary exponent n by using a lattice action containing m_0 , ν , c_B and c_E , which are functions of am_Q .

The coefficients c_B and c_E are different due to the broken space-time interchange symmetry, which can be computed in perturbation theory by requiring elimination of the heavy-quark discretization errors at a given order in the strong coupling constant α_s . We use the tree-level tadpole-improved results obtained by using field transformation (as in Ref. [73]):

$$c_B = \frac{\nu}{u_0^3}, \quad c_E = \frac{1}{2}(1 + \nu) \frac{1}{u_0^3}, \quad (4.5)$$

where u_0 is the tadpole factor

$$u_0 = \left\langle \frac{1}{3} \sum_p \text{Tr}(U_p) \right\rangle^{1/4}, \quad (4.6)$$

and U_p is the product of gauge links around the fundamental lattice plaquette p . The remaining two parameters m_0 and ν are determined nonperturbatively. The bare

Ensemble	c^2			
	η_c	J/Ψ	D	D_s
m007	0.991(4)	0.985(5)	1.021(15)	1.018(9)
m010	0.989(3)	0.958(3)	1.016(10)	0.992(6)
m020	0.997(4)	0.993(5)	1.019(20)	1.004(14)
m030	0.963(5)	0.947(6)	1.029(12)	1.015(10)

Table 4.2: Speed of light for charmed mesons.

charm-quark mass m_0 is tuned so that the experimentally observed spin average of the J/Ψ and η_c masses

$$M_{\text{avg}} = \frac{1}{4}M_{\eta_c} + \frac{3}{4}M_{J/\Psi} \quad (4.7)$$

is reproduced; see Sec. 5.3.2 for further details. The value of ν must be tuned to restore the dispersion relation $E_h^2 = m_h^2 + c^2 p^2$ such that $c^2 = 1$. Since the values of ν and m_0 are coupled, one needs to iterate the tuning process in order to achieve a consistent pair of values. To do this, we calculate the single-particle energy of η_c , J/Ψ , D_s and D at the six lowest momenta (with unit of a^{-1}): $\frac{2\pi}{L}(0, 0, 0)$, $\frac{2\pi}{L}(1, 0, 0)$, $\frac{2\pi}{L}(1, 1, 0)$, $\frac{2\pi}{L}(1, 1, 1)$, $\frac{2\pi}{L}(2, 0, 0)$, $\frac{2\pi}{L}(2, 1, 0)$. For each ensemble, the energy levels are calculated at two charm-quark masses (denoted $m_1 = 0.2034$ and $m_2 = 0.2100$) and extrapolated to the physical charm-quark mass (as described below). The values of c^2 are obtained by fitting the extrapolated energy levels to the dispersion relation. We tune ν using the dispersion relation of η_c . As one can see from Table 4.2, the dispersion relations for either the charmonium J/Ψ or the charm-light mesons (D and D_s) are generally consistent with $c^2 = 1$ to within 1-2%.

4.2 Extracting Baryon Masses from Correlation Functions

4.2.1 Spectral representation of correlation functions

The two point correlation function is defined by

$$\langle \mathcal{O}(t)\bar{\mathcal{O}}(0) \rangle = \frac{1}{Z} \int D\phi \mathcal{O}(t)\bar{\mathcal{O}}(0)e^{-S[\phi]}. \quad (4.8)$$

where $Z = \int D\phi e^{-S[\phi]}$, ϕ represents all field variables in the system. We already know how to calculate the path integral on the right-hand side of this equation using Monte Carlo simulations on lattice. In this section we will show how this quantity is related to the hadron spectrum. To do this we need to connect the path integral to the Hamiltonian approach.

For simplicity, we consider a real scalar field theory with Lagrangian density L given by

$$L = \frac{1}{2}(\partial_\mu \phi(x))^2 - \frac{m^2}{2}\phi^2(x) - V(\phi(x)). \quad (4.9)$$

The Hamiltonian operator can be obtained by the Legendre transform:

$$\hat{H} = \int d^3x \left(\frac{1}{2}\hat{\pi}^2(t, \mathbf{x}) + \frac{1}{2}(\nabla \hat{\phi}(t, \mathbf{x}))^2 + \frac{m^2}{2}\hat{\phi}^2(t, \mathbf{x}) + V(\hat{\phi}(t, \mathbf{x})) \right) \quad (4.10)$$

where $\hat{\pi}$ is the canonical momentum operator. Here we use a hat to denote operators, to be distinguished with the ordinary numbers. Using the discretization method introduced in Chapter 2,

$$\mathbf{x} \rightarrow a\mathbf{n}, \quad n_i = 0, 1, \dots, N-1 \quad \text{for } i = 1, 2, 3, \quad (4.11)$$

we obtain a lattice version of the Hamiltonian operator

$$\hat{H} = a^3 \sum_{\mathbf{n} \in \Lambda_3} \left(\frac{1}{2} \hat{\pi}^2(\mathbf{n}) + \frac{1}{2} \sum_{j=1}^3 \left(\frac{\hat{\phi}(\mathbf{n} + \hat{j}) - \hat{\phi}(\mathbf{n} - \hat{j})}{2a} \right)^2 + \frac{m^2}{2} \hat{\phi}^2(\mathbf{n}) + V(\hat{\phi}(\mathbf{n})) \right). \quad (4.12)$$

The operators $\hat{\pi}(\mathbf{n})$ and $\hat{\phi}(\mathbf{n})$ obey the canonical equal time commutation relations:

$$\left[\hat{\phi}(\mathbf{m}), \hat{\pi}(\mathbf{n}) \right] = ia^{-3} \delta_{\mathbf{m}, \mathbf{n}}, \quad \left[\hat{\phi}(\mathbf{m}), \hat{\phi}(\mathbf{n}) \right] = 0, \quad \left[\hat{\pi}(\mathbf{m}), \hat{\pi}(\mathbf{n}) \right] = 0. \quad (4.13)$$

Introduce a set of eigenstates of the field operator:

$$\hat{\phi}(\mathbf{n})|\phi\rangle = \phi(\mathbf{n})|\phi\rangle. \quad (4.14)$$

The states $|\phi\rangle$ are orthogonal and complete:

$$\begin{aligned} \langle \phi' | \phi \rangle &= \delta(\phi' - \phi) \equiv \prod_{\mathbf{n} \in \Lambda_3} \delta(\phi'(\mathbf{n}) - \phi(\mathbf{n})), \\ \int_{-\infty}^{+\infty} \mathcal{D}\phi |\phi\rangle \langle \phi| &= 1 \quad \text{with} \quad \mathcal{D} = \prod_{\mathbf{n} \in \Lambda_3} d\phi(\mathbf{n}). \end{aligned} \quad (4.15)$$

Now we are ready to prove that the trace of the time evolution operator $e^{-T\hat{H}}$

$$Tr(e^{-T\hat{H}}) = \int \mathcal{D}\phi \langle \phi | e^{-T\hat{H}} | \phi \rangle \quad (4.16)$$

is equivalent to the path integral $Z = \int D\phi e^{-S[\phi]}$.

Rewrite the Hamiltonian operator as

$$\hat{H} = \hat{H}_0 + \hat{U}, \quad (4.17)$$

$$\hat{H}_0 = a^3 \sum_{\mathbf{n} \in \Lambda_3} \frac{1}{2} \hat{\pi}^2(\mathbf{n}),$$

$$\hat{U} = a^3 \sum_{\mathbf{n} \in \Lambda_3} \left(\frac{1}{2} \sum_{j=1}^3 \left(\frac{\hat{\phi}(\mathbf{n} + \hat{j}) - \hat{\phi}(\mathbf{n} - \hat{j})}{2a} \right)^2 + \frac{m^2}{2} \hat{\phi}^2(\mathbf{n}) + V(\hat{\phi}(\mathbf{n})) \right), \quad (4.18)$$

\hat{H}_0 is the free part and \hat{U} is the interaction part.

For small time intervals ϵ , the evolution operator

$$e^{-\epsilon \hat{H}} = \hat{W}_\epsilon + \mathcal{O}(\epsilon^3), \quad (4.19)$$

where $\hat{W}_\epsilon = \exp(-\epsilon \hat{U}/2) \exp(-\hat{H}_0 \epsilon) \exp(-\epsilon \hat{U}/2)$. The matrix elements of \hat{W}_ϵ is explicitly known:

$$\begin{aligned} \langle \phi' | \hat{W}_\epsilon | \phi \rangle &= \langle \phi' | \exp(-\epsilon \hat{U}/2) \exp(-\hat{H}_0 \epsilon) \exp(-\epsilon \hat{U}/2) | \phi \rangle \\ &= \left(\frac{a^3}{2\pi\epsilon} \right)^{N^3/2} \exp \left\{ -\frac{\epsilon}{2} (U[\phi'] + U[\phi]) - \frac{a^3}{2\epsilon} \sum_{\mathbf{n} \in \Lambda_3} (\phi'(\mathbf{n}) - \phi(\mathbf{n}))^2 \right\}, \end{aligned} \quad (4.20)$$

where $U[\phi]$ is the eigenvalue of the operator \hat{U} .

In Eq. 4.20 we have used the matrix element for the free Hamiltonian \hat{H}_0 :

$$\langle \phi' | e^{-\epsilon \hat{H}_0} | \phi \rangle = \left(\frac{a^3}{2\pi\epsilon} \right)^{N^3/2} \exp \left\{ -\frac{a^3}{2\epsilon} \sum_{\mathbf{n} \in \Lambda_3} (\phi'(\mathbf{n}) - \phi(\mathbf{n}))^2 \right\}. \quad (4.21)$$

This expression can be obtained easily by inserting a complete set of eigenstates of $\hat{\pi}$.

We can build a finite time interval T from infinitesimal steps ϵ (see e.g. [74] for

a proof)

$$e^{-T\hat{H}} = \lim_{N_T \rightarrow \infty} \hat{W}_\epsilon^{N_T} \quad \text{with} \quad \epsilon = \frac{T}{N_T}. \quad (4.22)$$

Therefore

$$\begin{aligned} \text{Tr}(e^{-T\hat{H}}) &= \int \mathcal{D}\phi_0 \langle \phi_0 | \hat{W}_\epsilon^{N_T} | \phi_0 \rangle \\ &= \int \mathcal{D}\phi_0 \mathcal{D}\phi_1 \cdots \mathcal{D}\phi_{N_T-1} \langle \phi_0 | \hat{W}_\epsilon | \phi_{N_T-1} \rangle \langle \phi_{N_T-1} | \hat{W}_\epsilon | \phi_{N_T-2} \rangle \cdots \langle \phi_1 | \hat{W}_\epsilon | \phi_0 \rangle \\ &= C^{N^3 N_T} \int \mathcal{D}\phi_0 \cdots \mathcal{D}\phi_{N_T-1} e^{-S[\phi]}. \end{aligned} \quad (4.23)$$

where $C = \sqrt{a^3/2\pi\epsilon}$. With periodic boundary condition, $S[\phi]$ reads

$$S[\phi] = \epsilon a^3 \sum_{j=0}^{N_T-1} \sum_{\mathbf{n} \in \Lambda_2} \frac{1}{2} \left(\frac{\phi(\mathbf{n})_{j+1} - \phi(\mathbf{n})_j}{\epsilon} \right)^2 + \epsilon \sum_{j=0}^{N_T-1} U[\phi_j]. \quad (4.24)$$

This expression is equivalent to the discretized Euclidean action of the Klein-Gordan field.

Here we only gave a simple proof for scalar field, for a rigorous treatment of fermions and bosons, see reference [75]. The situation is similar when the operators are included in the path integral.

The two point correlation function becomes

$$\begin{aligned}
\langle \mathcal{O}(t)\bar{\mathcal{O}}(0) \rangle &= \frac{1}{Z} \int D\phi \mathcal{O}(t)\bar{\mathcal{O}}(0)e^{-S[\phi]} \\
&= \frac{\text{Tr}(e^{-(T-t)H}\mathcal{O}e^{-tH}\bar{\mathcal{O}})}{\text{Tr}(e^{-TH})} \\
&= \frac{\sum_n \langle n|e^{-(T-t)H}\mathcal{O}e^{-tH}\bar{\mathcal{O}}|n \rangle}{\sum_m \langle m|e^{-TH}|m \rangle} \\
&= \frac{\sum_n e^{-TE_n} \langle n|e^{tH}\mathcal{O}e^{-tH}\bar{\mathcal{O}}|n \rangle}{\sum_m e^{-TE_m}} \\
&\xrightarrow{T \rightarrow \infty} \langle 0|e^{tH}\mathcal{O}e^{-tH}\bar{\mathcal{O}}|0 \rangle \\
&= \sum_{k=0}^{\infty} \langle 0|\mathcal{O}e^{-tH}|k \rangle \langle k|\bar{\mathcal{O}}|0 \rangle \\
&= \sum_{k=1}^{\infty} |\langle k|\bar{\mathcal{O}}|0 \rangle|^2 e^{-tE_k}. \tag{4.25}
\end{aligned}$$

One can fit the correlation function to exponentials to get the energies. The contribution from the excited states decreases quickly as t increases. Thus at large t

$$\langle \mathcal{O}(t)\bar{\mathcal{O}}(0) \rangle \simeq Ae^{-tE_1}. \tag{4.26}$$

The ground state energy E_1 can be obtained by fitting the correlation function to a single exponential. In this work we use this method to fit the charmed hadron masses. The data fitting method has been introduced in Sec. 2.7.4.

4.2.2 Effective mass

The effective mass is defined by

$$a_t m_{eff}(t) = \ln \frac{C(t)}{C(t+a_t)}, \tag{4.27}$$

where a_t is the lattice spacing at time direction, $C(t)$ is the correlation function: $C(t) = \langle \mathcal{O}(t)\bar{\mathcal{O}}(0) \rangle$.

The effective mass can be expanded as

$$\begin{aligned} m_{eff}(t) &= \ln \frac{A_1 e^{-tE_1} + A_2 e^{-tE_2} + \dots}{A_1 e^{-(t+1)E_1} + A_2 e^{-(t+1)E_2} + \dots} \\ &= E_1 \left(1 + \mathcal{O}\left(\frac{A_2}{A_1} e^{-t(E_2-E_1)}\right) \right), \end{aligned} \quad (4.28)$$

here we have set the lattice spacing to 1. When t is sufficiently large, $m_{eff}(t)$ approaches a plateau of E_1 . Effective mass plots can be used as a visualization tool to choose appropriate fitting range.

4.2.3 Extracting excited states

In order to extract the excited states, one can try to fit the correlation function to multiple exponentials. In practice, this method is usually ineffective due to the rapid decay of signal and the uncertainties of the statistical data.

Lüscher and Wolff suggested a method, called variational method, to extracting multiple excited states [76]. In this approach one construct a set of interpolating operators $\{\mathcal{O}_1, \mathcal{O}_2, \dots, \mathcal{O}_n\}$ for a state we are interested and calculate the correlation matrix

$$C_{ij}(t) = \langle \mathcal{O}_i(t)\bar{\mathcal{O}}_j(0) \rangle. \quad (4.29)$$

Follow the same procedure in 4.25, one can get

$$C_{ij}(t) = \sum_{a=1}^{\infty} v_i^{a*} v_j^a e^{-tE_a}, \quad (4.30)$$

$$v_i^a = \langle a | \mathcal{O}_i | 0 \rangle, \quad H|a\rangle = E_a|a\rangle. \quad (4.31)$$

We will assume that the spectrum has no degeneracy $E_1 < E_2 < \dots < E_n$ and that

the n -component vectors v_i^a ($a = 1, 2, \dots, n$) are linearly independent.

We present an important lemma which provides a basis for the calculation of the energy spectrum given the correlation matrix:

Lemma 4.2.1. *For every $t \geq 0$, let $\lambda_a(t)$ be the eigenvalues of the correlation matrix $C(t)$ ordered such that $\lambda_1 \geq \lambda_2 \geq \dots \geq \lambda_n$, Then, for all $a = 1, 2, \dots$ we have*

$$\lambda_a(t) \xrightarrow{t \rightarrow \infty} c_a e^{-tE_a} [1 + \mathcal{O}(e^{-t\Delta E_a})], \quad (4.32)$$

where $c_a > 0$, and ΔE_a is the distance of E_a from the other energy values.

For the proof of this lemma, see reference [76].

The application of this lemma starts from the generalized eigenvalue problem

$$C(t)\phi_a = \lambda_a(t, t_0)C(t_0)\phi_a \quad (4.33)$$

where t_0 is fixed. If the operators \mathcal{O}_i we choose are linearly independent, $C(0)$ will be non-singular. Thus there are n independent solutions of Eq. 4.33 and the corresponding eigenvalues $\lambda_a(t, t_0)$ satisfy Eq. 4.32. However, the amplitude c_a and the coefficients of the subleading exponentials are different. More precisely, one expects that $c_a \simeq e^{t_0 E_a}$ and the coefficients of $\mathcal{O}(e^{-t\Delta E_a})$ terms are suppressed.

In practice, it may happen that the energy levels are close-by and thus the terms $\sim e^{-t\Delta E_a}$ are not small. A recent study on the generalized eigenvalue problem [77] has shown that the corrections from the energy gaps for λ_a is actually $\sim e^{-t(E_{n+1}-E_a)}$, with the condition $t_0 < t < 2t_0$.

In the right hand side of Eq. 4.30, those terms with large value of E_a die out

quickly. Thus we can expect that the truncated sum

$$C_{ij}^0(t) = \sum_{a=1}^n v_i^{a*} v_j^a e^{-tE_a} \quad (4.34)$$

approximate the correlation matrix $C(t)$ very well. It is easy to show that the eigenvalues of the generalized eigenvalue problem

$$C^0(t)\phi_a = \lambda_a^0(t, t_0)C^0(t_0)\phi_a \quad (4.35)$$

are exactly given by

$$\lambda_a^0(t, t_0) = e^{-(t-t_0)E_a}, \quad a = 1, 2, 3, \dots, n. \quad (4.36)$$

The generalized eigenvalue problem can be turned into a regular eigenvalue problem

$$[C(t_0)^{-1/2}C(t)C(t_0)^{-1/2}]\phi_a = \lambda_a(t, t_0)\phi_a \quad (4.37)$$

To sum up, the energies E_a can be extracted from the eigenvalues $\lambda_a(t, t_0)$ of $C(t_0)^{-1/2}C(t)C(t_0)^{-1/2}$ by

$$E_a = \ln\left(\frac{\lambda_a(t, t_0)}{\lambda_a(t+1, t_0)}\right). \quad (4.38)$$

4.3 Extracting Scattering Length Using Lüscher's Finite Volume Technique

Extracting hadronic interactions from Lattice QCD calculations is not straightforward due to the Maiani-Testa theorem [78], which states that the S-matrix can not be extracted from infinite-volume Euclidean-space Green functions except at kinematic

thresholds. However, this problem can be evaded by computing the correlation functions at finite volume. Lüscher has shown that one can obtain the elastic scattering amplitude from the energy of two particles in finite volume [79, 80]. We use Lüscher's finite volume technique to calculate the scattering lengths.

The scattering phase shift is related to the energy shift ΔE which is the deviation of the total energy of two interacting hadrons from the rest mass of the two hadrons. The energy shift ΔE can be related to the center-of-mass momentum p by

$$\Delta E = \sqrt{p^2 + m_{h_1}^2} + \sqrt{p^2 + m_{h_2}^2} - m_{h_1} - m_{h_2}, \quad (4.39)$$

where m_{h_1} and m_{h_2} are the masses of the two hadrons h_1 and h_2 respectively.

If the interaction range is small compared to the box size L , the s-wave phase shift $\delta(p)$ can be written as [79, 80]

$$\frac{2\mathcal{Z}_{00}(1, q)}{L\pi^{1/2}} = p \cot \delta_0(p) = \frac{1}{a} + \mathcal{O}(p^2), \quad (4.40)$$

where $q = pL/(2\pi)$ takes a non-integer value due to the interaction, a denotes the s-wave scattering length, the function $\mathcal{Z}_{00}(1, q)$ is an analytic continuation of the generalized zeta-function which is defined by

$$\mathcal{Z}_{00}(s, q) = \frac{1}{4\pi} \sum_{\mathbf{n}} (\mathbf{n}^2 - q^2)^{-s}. \quad (4.41)$$

The sign convention for the scattering length is the same with which Lüscher used in [79, 80].

In the limit $L \gg |a|$, one can expand Eq. 4.40 about zero momentum and get the energy shift of the lowest scattering state [79, 80]

$$\Delta E_0 = -\frac{2\pi a_0}{\mu L^3} \left(1 + c_1 \frac{a_0}{L} + c_2 \left(\frac{a_0}{L} \right)^2 \right) + \mathcal{O}(L^6) \quad (4.42)$$

where $c_1 = -2.837297$, $c_2 = 6.375183$, μ denotes the reduced mass of the two hadrons $\mu = m_{h_1} m_{h_2} / (m_{h_1} + m_{h_2})$.

For the second lowest states, one can expand the phase-shift formula Eq. 4.40 around $q^2 = 1$ and obtain the solution

$$\Delta E_1 = \frac{4\pi^2}{\mu L} - \frac{6 \tan \delta_0}{\mu L^2} \left(1 + c'_1 \tan \delta_0 + c'_2 \tan^2 \delta_0 \right) + \mathcal{O}(L^{-6}), \quad (4.43)$$

where $c'_1 = -0.061367$, $c'_2 = -0.354256$.

The scattering length can be obtained by solving either Eq. 4.42 or the full expression Eq. 4.40. In our work, we adopt an alternative form of Eq. 4.40 [81]

$$p \cot \delta_0(p) = \frac{1}{\pi L} \mathbf{S} \left(\left(\frac{pL}{2\pi} \right)^2 \right), \quad (4.44)$$

with

$$\mathbf{S}(\eta) \equiv \sum_j^{\Lambda_j} \frac{1}{|\mathbf{j}|^2 - \eta} - 4\pi \Lambda_j. \quad (4.45)$$

The sum is over all three-vectors of interger \mathbf{j} such that $|\mathbf{j}| < \Lambda_j$ and the limit $\Lambda_j \rightarrow \infty$ is implicit.

Fig. 4.1 shows the plot of S-function $\mathbf{S}(\eta)$. This function has poles for $\eta \geq 0$ and does not have poles for $\eta \leq 0$.

For weakly attractive interaction, the scattering length $a_0 > 0$, the lowest energy level of the elastic scattering state appears below threshold. An important question to ask is how can we distinguish a near-threshold bound state with a scattering state. In scattering theory, poles of the S-matrix correspond to bound states [82]. The appearance of the S-wave bound states are accompanied by an abrupt sign change of the

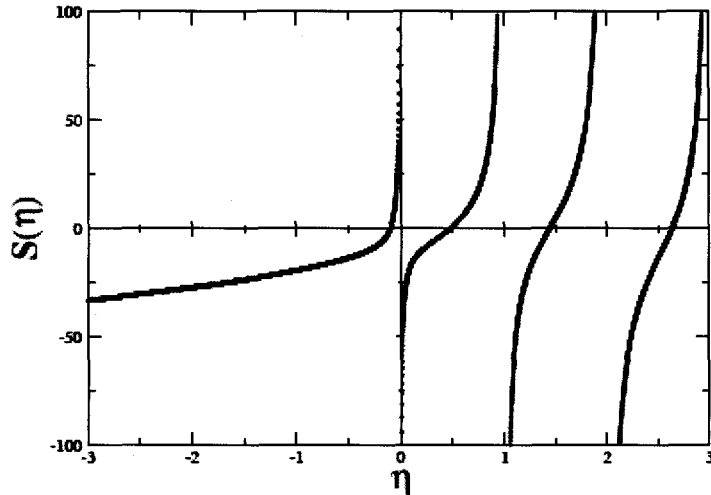


Figure 4.1: S-function plot.

S-wave scattering length. Now the question is: can we use this formation condition of the bound states in Lüscher's finite volume method? It is quite straightforward and reasonable to guess that this condition should be modified by finite volume corrections. This question is studied theoretically and numerically in reference [83]. It is found that the finite volume corrections to the bound state pole condition is exponentially suppressed by the spatial extent L . It is also confirmed by numerical simulations that the appearance of the S-wave bound state is accompanied by an abrupt sign change of the S-wave scattering length even in finite volume [83].

The solution of Eq. 4.40 for bound state have been explicitly derived [81]:

$$\Delta E_{-1} = -\frac{\gamma^2}{2\mu} \left(1 + \frac{12}{\gamma L} \frac{1}{1 - 2\gamma(p \cot \delta_0)'} e^{-\gamma L} + \dots \right), \quad (4.46)$$

where $(p \cot \delta_0)' = \frac{d}{dp^2} p \cot \delta|_{p^2 = -\gamma^2}$. The L -independent term $-\frac{\gamma^2}{2\mu}$ corresponds to the binding energy in the infinite volume limit. The volume dependence $e^{-\gamma L}$ is consistent with the claim that the bound state pole condition is exponentially suppressed by the

spatial extent L . Notice that the energy of the scattering state in Eq. 4.42 is expanded in powers of $1/L$. We can expect to distinguish a bound state from a scattering state by calculating the energy in multiple volumes and checking the volume dependence law.

Numerically, the total energy of two interacting hadrons (h_1 and h_2) is obtained from the four-point correlation function:

$$G^{h_1-h_2}(t) = \langle \mathcal{O}_{h_1 h_2}(t) \bar{\mathcal{O}}_{h_1 h_2}(0) \rangle, \quad (4.47)$$

where $\mathcal{O}_{h_1 h_2}$ is the interpolating operator of the two particle state.

To extract the energy shift ΔE , we define a ratio $R^{h_1-h_2}(t)$:

$$R^{h_1-h_2}(t) = \frac{G^{h_1-h_2}(t)}{G^{h_1}(t)G^{h_2}(t)} \longrightarrow A \exp(-\Delta E \cdot t), \quad (4.48)$$

where $G^{h_1}(t, 0)$ and $G^{h_2}(t, 0)$ are two-point functions. ΔE is obtained by fitting $R^{h_1-h_2}(t)$ to a single exponential in a region where the effective mass exhibits a plateau. The center-of-mass momentum p can be solved from Eq. 4.39 given ΔE .

Assuming $\mathcal{O}(p^2)$ effects are negligible, the scattering length is given by

$$a = \frac{\pi L}{\mathbf{S}\left(\left(\frac{pL}{2\pi}\right)^2\right)}, \quad (4.49)$$

where the function \mathbf{S} is defined in Eq. 4.45 and can be calculated numerically.

CHAPTER 5

Charmed Baryon Spectrum

5.1 Introduction

Experimental and theoretical studies of charmed and bottom hadrons have been the focus of vigorous research over the last several years [84, 85, 86, 87]. In particular, singly and doubly heavy baryon spectroscopy has received significant attention, mainly due to the recent experimental discoveries of both new charmed (SELEX) [88, 89] and bottom baryons by D0 [87] and CDF [90]. In addition to these discoveries, there are still many states of heavy and doubly heavy baryons remaining to be discovered. The new Beijing Spectrometer (BES-III), a detector at the recently upgraded Beijing Electron Positron Collider (BEPCII), has great potential for accumulating large numbers of events to help us understand more about charmed hadrons. The antiProton ANnihilation at DArmstadt (PANDA) experiment, a GSI future project, and the LHCb are also expected to provide new results to help experimentally map out the heavy-baryon sector. For these reasons, lattice quantum chromodynamic (QCD) calculations of the spectrum of heavy baryons are now very timely and will play a significant role in providing theoretical first-principles input to

the experimental program.

Lattice QCD is now a mature field capable of providing accurate results that can be directly compared to experiment, with calculations in the light-quark sector being well established. Although the study of heavy quarks requires careful treatment of discretization errors, significant advances have been made in this sector as well. Lattice heavy quarks have $\mathcal{O}((m_Q a)^n)$ errors, where m_Q is the mass of the heavy quark and a is the lattice spacing. Lattice spacings for typical, currently accessible dynamical ensembles are still too coarse ($a^{-1} \approx 2$ GeV) to make such systematic errors small. To assert better control over the discretization errors for heavy quarks on the lattice, several heavy-quark approaches have proven useful. For example, non-relativistic QCD (NRQCD) [91], which is an expansion of the lattice quark action in powers of $\frac{1}{am_Q}$, is commonly applied to bottom quarks. However, the charm-quark mass is not heavy enough to justify the use of NRQCD. Relativistic heavy-quark actions [71, 92, 93, 94] systematically remove $\mathcal{O}((m_Q a)^n)$ terms and are better suited to charm-quark calculations. Recent updates on the state of heavy-quark physics on the lattice can be found in several reviews [95, 96, 97, 98, 99, 100] and references therein.

Up to now, there have been a few lattice charmed-baryon calculations using the quenched approximation. In some cases an $\mathcal{O}(a)$ -improved light-quark action is used on isotropic or anisotropic lattices with a single lattice spacing: Bowler et al. [101] used a tree-level clover action for both light and heavy quarks to calculate the singly charmed baryons spectrum of spin 1/2 and 3/2. Later, Flynn et al. [102] updated this project with nonperturbative clover action and extended the calculation to doubly charmed baryons. Chiu et al. [103] used a chiral fermion action for the charm quarks and calculated both the positive and negative parity spectrum for singly and doubly charmed baryons. Such calculations using light-quark actions to simulate

heavy quarks introduce large systematic errors proportional to $(am_Q)^2$, which must be carefully addressed. One calculation has used a higher-order improved fermion action: Lewis et al. [104] performed a calculation on both doubly and singly charmed baryons using D234-type fermion action (which would leave a leading error of $\mathcal{O}(a^3)$) for both light and heavy quarks but on a coarse anisotropic ensemble (with anisotropy $\xi = 2$). Finally, heavy-quark effective theory was applied to charm calculation: Mathur et al. [105] continued to use anisotropic lattices, adding two more lattice spacings, but changed the heavy-quark action to NRQCD, which reduces the lattice-spacing discretization effects. For all of these calculations, the quenched approximation remains a significant source of systematic error that is difficult to estimate.

Given the progress on the experimental side, it is time to revisit these charmed baryon calculations using dynamical gauge ensembles and improve the calculations with the current available computational resources. Although more dynamical ensembles are available these days, not many charmed baryon calculations have been published so far, only a few proceedings [106, 3, 107].

In this work, we extend our previous calculation [107] to higher statistics and compute the ground-state spectrum of the spin-1/2 singly and doubly charmed baryons. We use the Fermilab action [71] for the charm quarks and domain-wall fermions for the light valence quarks on gauge configurations with 2+1-flavor Kogut-Susskind fermions and a range of quark masses resulting in pion masses as light as 290 MeV. We nonperturbatively tune the fermion anisotropy and two input bare masses for charm quarks, setting the remaining parameters to tree-level tadpole improved coefficients. Our results are extrapolated to the physical light-quark masses using both heavy-hadron chiral perturbation theory (HH χ PT) as well as HH χ PT-inspired polynomial extrapolations.

5.2 Charmed Hadron Spectrum: Numerical Results

The interpolating operators we use for the $J = 1/2$ singly and doubly charmed baryons are

$$\begin{aligned}
\Lambda_c &: \epsilon^{ijk} (q_u^{iT} C \gamma_5 q_d^j) Q_c^k, \\
\Xi_c &: \epsilon^{ijk} (q_u^{iT} C \gamma_5 q_s^j) Q_c^k, \\
\Sigma_c &: \epsilon^{ijk} (q_u^{iT} C \gamma_5 Q_c^j) q_u^k, \\
\Xi'_c &: \frac{1}{\sqrt{2}} \epsilon^{ijk} [(q_u^{iT} C \gamma_5 Q_c^j) q_s^k + (q_s^{iT} C \gamma_5 Q_c^j) q_u^k], \\
\Omega_c &: \epsilon^{ijk} (q_s^{iT} C \gamma_5 Q_c^j) q_s^k, \\
\Xi_{cc} &: \epsilon^{ijk} (Q_c^{iT} C \gamma_5 q_u^j) Q_c^k, \\
\Omega_{cc} &: \epsilon^{ijk} (Q_c^{iT} C \gamma_5 q_s^j) Q_c^k,
\end{aligned} \tag{5.1}$$

where $q_{u,d}$ are the up and down quark fields, q_s is strange quark field and Q_c is charm quark field.

Using these interpolating fields, we construct the two-point functions

$$C_h(t, t_0) = \sum_{\mathbf{x}} \langle \mathcal{O}_h(\mathbf{x}, t) \mathcal{O}_h(\mathbf{x}, t_0)^\dagger \rangle,$$

where \mathcal{O}_h is an interpolating operator of the hadron h . The correlation functions are calculated with gauge-invariant Gaussian-smearred sources and point sinks. The smearing parameters were optimized so that excited-state contamination to the correlators is minimized. The domain-wall valence propagators were computed with Dirichlet boundary conditions in the time direction, reducing the original lattices to half their temporal size. Similar to baryons, the signal for the charmed correlation functions quickly drops, and thus we do not expect the temporal reduction to reduce

the number of useful time points for our analysis. The sources were located away from the Dirichlet boundary to minimize contamination from the boundary effects. In order to enhance our statistical precision, several valence propagators are taken from each configuration with varying source location. The resulting correlation functions are then source averaged on each configuration to produce one correlator per configuration for each interpolating operator. The masses of the hadrons are obtained by fitting the correlation functions to a single exponential

$$C_h(t) = Ae^{-E_0t} \quad (5.2)$$

in a region where the effective mass is observed to exhibit a plateau. The fitting range is varied by one or two time slices on either end to estimate the systematics from the choice of fitting window. In Tables 5.1 and 5.2, we list the value associated with the listed fitting window. The first uncertainty is statistical and the second uncertainty comes from the varied fitting windows. For most fits, the resulting χ^2 per degree of freedom is about one. In Figure 5.1 we display representative effective mass plots and their fitted masses for both good and poor fits. The results from charmonium are shown in Table 5.2.

5.3 Heavy- and Light-Quark Mass Extrapolation

In order to make contact with experiment, we must extrapolate our results to infinite volume, continuum limit and to the physical value of the light- and heavy-quark masses. Optimally, the extrapolations can be performed in terms of dimensionless ratios of observable quantities, so as to minimize contamination from a particular scale-setting method. In this work, we have chosen to scale our masses by the calculated value of the pion decay constant on each ensemble, forming the dimensionless

Hadron	m_0	m007	m010	m020	m030
Ω_{cc}	m_1	2.3578(18)(8)[8–18]	2.3620(14)(9)[10–18]	2.3456(33)(17)[12–18]	2.3333(23)(6)[11–18]
	m_2	2.3663(18)(8)[8–18]	2.3705(14)(9)[10–18]	2.3542(33)(16)[12–18]	2.3419(23)(7)[11–18]
Ξ_{cc}	m_1	2.3018(27)(0)[7–13]	2.3120(23)(23)[9–17]	2.3087(33)(3)[8–18]	2.3056(28)(33)[11–18]
	m_2	2.3104(27)(0)[7–13]	2.3205(23)(23)[9–17]	2.3173(33)(3)[8–18]	2.3142(28)(33)[11–18]
Ω_c	m_1	1.7216(24)(1)[9–15]	1.7240(24)(5)[12–18]	1.7101(52)(77)[12–16]	1.7160(39)(13)[12–18]
	m_2	1.7261(24)(1)[9–15]	1.7285(24)(5)[12–18]	1.7146(52)(76)[12–16]	1.7205(39)(13)[12–18]
Ξ'_c	m_1	1.6754(26)(32)[6–18]	1.6799(29)(43)[9–16]	1.6875(52)(57)[9–16]	1.6881(43)(2)[11–18]
	m_2	1.6799(26)(32)[6–18]	1.6844(29)(43)[9–16]	1.6920(52)(58)[9–16]	1.6927(43)(2)[11–18]
Ξ_c	m_1	1.6076(82)(86)[12–18]	1.6078(48)(54)[12–18]	1.6167(40)(9)[8–18]	1.6120(41)(47)[12–17]
	m_2	1.6121(82)(87)[12–18]	1.6123(48)(55)[12–18]	1.6211(40)(9)[8–18]	1.6163(41)(48)[12–17]
Σ_c	m_1	1.6157(50)(38)[7–17]	1.6252(55(0))[9–15]	1.6446(56)(0)[8–16]	1.6661(43)(70)[10–18]
	m_2	1.6203(50)(38)[7–17]	1.6298(55)(0)[9–15]	1.6491(56)(0)[8–16]	1.6706(43)(69)[10–18]
Λ_c	m_1	1.4974(71)(47)[6–13]	1.523(16)(3)[12–18]	1.5571(55)(22)[8–18]	1.572(5)(18)[12–17]
	m_2	1.5018(71)(48)[6–13]	1.527(16)(3)[12–18]	1.5615(55)(22)[8–18]	1.577(5)(18)[12–17]

Table 5.1: Charmed baryon masses in lattice units with 2 values of m_0 (indicated as $m_1 = 0.2034$ and $m_2 = 0.2100$) in Eq. (4.2). The first uncertainty is statistical and the second is systematic from the different choice of fitting ranges (presented in square brackets). The m007, m010, m020, m030 indicate the four ensembles listed in Table 4.1.

Hadron	m_0	m007	m010	m020	m030
η_c	m_1	1.8783(4)(0)[14–19]	1.8804(3)(0)[12–19]	1.8687(4)(1)[12–19]	1.8598(3)(2)[8–15]
	m_2	1.8866(4)(1)[14–19]	1.8887(3)(1)[12–19]	1.8771(4)(1)[12–19]	1.8683(5)(0)[8–15]
J/Ψ	m_1	1.9390(7)(0)[14–18]	1.9421(4)(0)[10–19]	1.9296(6)(1)[12–19]	1.9198(6)(2)[11–19]
	m_2	1.9470(7)(0)[14–18]	1.9501(4)(1)[10–19]	1.9376(6)(1)[12–19]	1.9278(6)(3)[11–19]
χ_{c0}	m_1	2.1660(54)(21)[9–16]	2.1803(33)(6)[6–17]	2.1652(55)(50)[6–18]	2.1626(54)(2)[6–18]
	m_2	2.1741(54)(20)[9–16]	2.1883(35)(6)[6–17]	2.1733(55)(49)[6–18]	2.1705(54)(2)[6–18]
χ_{c1}	m_1	2.2092(69)(24)[9–18]	2.2234(52)(35)[9–16]	2.2123(40)(8)[4–17]	2.2004(44)(25)[4–17]
	m_2	2.2171(69)(24)[9–18]	2.2312(52)(35)[9–16]	2.2199(40)(9)[4–17]	2.2081(44)(25)[4–17]
h_c	m_1	2.2224(64)(86)[6–18]	2.2386(32)(24)[4–18]	2.2205(45)(21)[4–17]	2.2151(63)(26)[5–18]
	m_2	2.2301(65)(85)[6–18]	2.2463(32)(25)[4–18]	2.2282(46)(19)[4–17]	2.2226(63)(25)[5–18]

Table 5.2: Charmonium masses in lattice units with $m_1 = 0.2034$ and $m_2 = 0.2100$.

ratios M_h/f_π , where M_h is the mass of a given hadron. We take the values of f_π (and m_π) from Ref. [1]; they are collected in Table 5.3. As can be seen, af_π varies by $\approx 15\%$ over the range of pion masses used in this work, adding additional chiral curvature. However, the light-quark mass dependence of f_π is well understood [37, 108], and so this variation can be accounted for.

Ultimately, one would like to use heavy-hadron chiral perturbation theory (HH χ PT) [109, 110, 111, 112, 113, 114, 115] to perform both the charm-quark mass extrapolation and the chiral extrapolation of the charmed hadron masses, allowing a lattice determina-

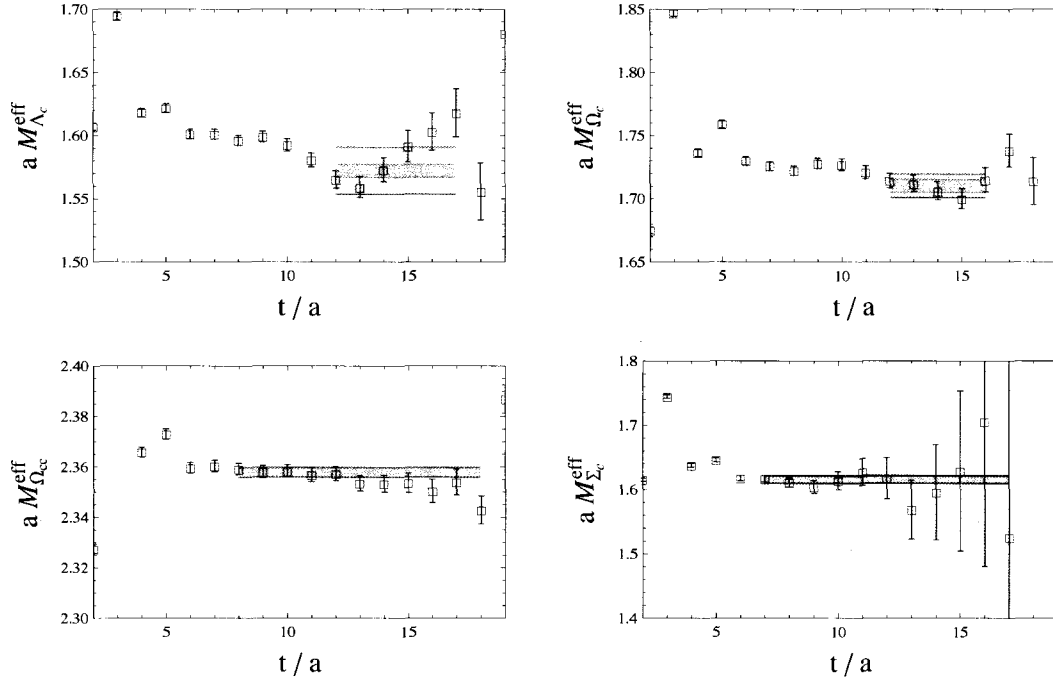


Figure 5.1: Sample effective-mass plots and corresponding fits to the correlation functions. The smaller error bands are statistical and the larger error bands are statistical and systematic (determined by varying fit range) added in quadrature.

ensemble:	β	6.76	6.76	6.79	6.81
	am_l	0.007	0.010	0.020	0.030
	am_π	0.1842	0.2238	0.3113	0.3752
	af_π	0.0929	0.0963	0.1026	0.1076
	m_π/f_π	1.983	2.325	3.035	3.489

Table 5.3: Values of m_π and f_π calculated in Ref. [1]. For all ensembles the staggered strange-quark mass is $am_s = 0.050$ while the domain-wall strange-quark mass is $am_s^{\text{dwf}} = 0.081$.

tion of not just the spectrum but also the low-energy constants entering the effective field theory. There are several reasons we cannot perform a thorough extrapolation in this manner. First, we only have results at four independent values of the light-quark mass, and at only one value of the strange mass. Second, in this work, we only have results for the $J = 1/2$ baryons, and a proper chiral extrapolation requires also the spectrum of $J = 3/2$ charmed baryons; the states are related by the heavy-quark symmetry, and therefore the mass splittings are small (similarly, the extrapolation of the heavy meson masses requires the $J = 1$ states as well as $J = 0$). Third, our calculation is mixed-action, thus requiring either a continuum extrapolation or the use of mixed-action χ PT [62, 63, 64, 65, 66, 67]. The mixed-action effective field theory can be trivially constructed from the partially quenched theories for heavy hadrons [116, 45, 117] by following the prescription in Ref. [66]. However, this work only utilizes one lattice spacing, and so one can not perform the full mixed-action analysis. With these caveats in mind, we proceed with our analysis.

5.3.1 Scale setting with f_π

The light-quark mass expansion of a heavy-hadron mass is given by¹

$$M_h = M_0 + \frac{c_h^{(2)}}{4\pi} \frac{2Bm_l}{f_0} + \dots \quad (5.3)$$

At this order, we are free to make the replacements $f_0 \rightarrow f_\pi$ and $2Bm_l \rightarrow m_\pi^2$, with corrections appearing at $\mathcal{O}(m_\pi^4)$. The dots represent terms of higher order in the chiral expansion, with the first non-analytic (in the quark mass) corrections appearing as corrections which scale as $\sim m_\pi^3$. As stated above, we are scaling our masses with f_π

¹Here we are presenting an $SU(2)$ extrapolation formula with the operator normalization of Ref. [118] such that the coefficient $c_h^{(2)}$ is dimensionless.

range	m007–m010	m007–m020	m007–m030
$l_4(\mu = f_\pi)$	0.0307(27)	0.0293(6)	0.0302(4)

Table 5.4: Values of l_4 needed for chiral extrapolations of M_h/f_π . The different values of l_4 are determined through the different choices of fitting range, also listed.

to form dimensionless ratios for extrapolation,

$$\frac{M_h}{f_\pi} = \frac{M_0}{f_\pi} + \frac{c_h^{(2)}}{4\pi} \frac{m_\pi^2}{f_\pi^2} + \dots \quad (5.4)$$

When performing an extrapolation in this manner, it is important to realize we cannot approximate M_0/f_π as a constant, since the chiral corrections to f_π are $\mathcal{O}(m_\pi^2)$ and thus are the same order as the term with coefficient $c_h^{(2)}$. Rather, the chiral expansion of f_π is given by [37] (with the normalization $f_0 \sim 130$ MeV)

$$\begin{aligned} f_\pi &= f_0 \left[1 - \frac{2m_\pi^2}{(4\pi f_\pi)^2} \ln \left(\frac{m_\pi^2}{\mu^2} \right) + 2l_4(\mu) \frac{m_\pi^2}{f_\pi^2} \right] + \dots \\ &\equiv f_0 \left[1 + \delta f(m_\pi/f_\pi) \right] + \dots \end{aligned} \quad (5.5)$$

In this expression, we have made use of perturbation theory to replace all terms appearing at next-to-leading order with their (lattice) physical values. Similarly, we have rescaled the renormalization scale $\mu \rightarrow \tilde{\mu} f_\pi$ to express the chiral corrections as purely a function of m_π/f_π . Again, the corrections to this rescaling first appear at next-to-next-to-leading order. In order to perform our chiral extrapolations using Eq. (5.4), we must determine l_4 , which captures the chiral corrections of f_π . The mixed-action formula for f_π is known [62], but again, only useful if one has data for at least two lattice spacings. Since we currently only have results at one lattice spacing, we perform a continuum chiral extrapolation analysis of the af_π in Table 5.3. The results are collected in Table 5.4.

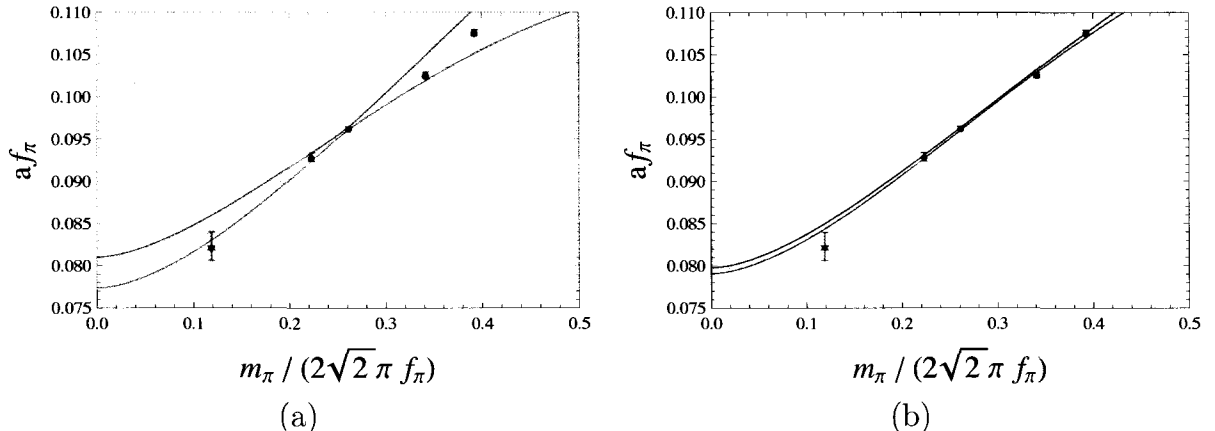


Figure 5.2: The (blue) filled circles represent the lattice data and the (red) star is the physical point, converted to lattice units using $a^{-1} = 1588$ MeV with a 2% error bar added for the scale setting. The error bands are the 68% confidence intervals in the resulting chiral extrapolation from the lightest two points (a) and a fit to all four lattice points (b).

The resulting extrapolations are plotted in Figure 5.2. In this figure, the (blue) filled circles are the lattice data, and the error bands represent the 68% confidence intervals. The (red) star denotes the physical value converted to lattice units using $a^{-1} = 1588$ MeV [119]. We assign an additional 2% error to this point to estimate the uncertainty in the scale setting method. In Figure 5.2(a) we display the fit to the lightest two points and in (b) the fit to all four points. Note that the extrapolation describes the values of f_π very well. Additionally, one sees that using f_π or r_1 to set the scale results in agreement in the extrapolated values, as first observed in Ref. [120].²

5.3.2 Charm-Quark Mass Extrapolation

To tune the charm-quark mass we use the spin-averaged J/Ψ - η_c mass. We use the lattice spacing determined by MILC ($a^{-1} = 1588$ MeV [119]) on the m007 ensemble to estimate the two charm-quark masses used for our charm quark propagator

²The scale of r_1 is determined through the static-quark potential by solving for $r_1^2 F(r_1) = 1$; the values of r_1/a can be found in Ref. [121].

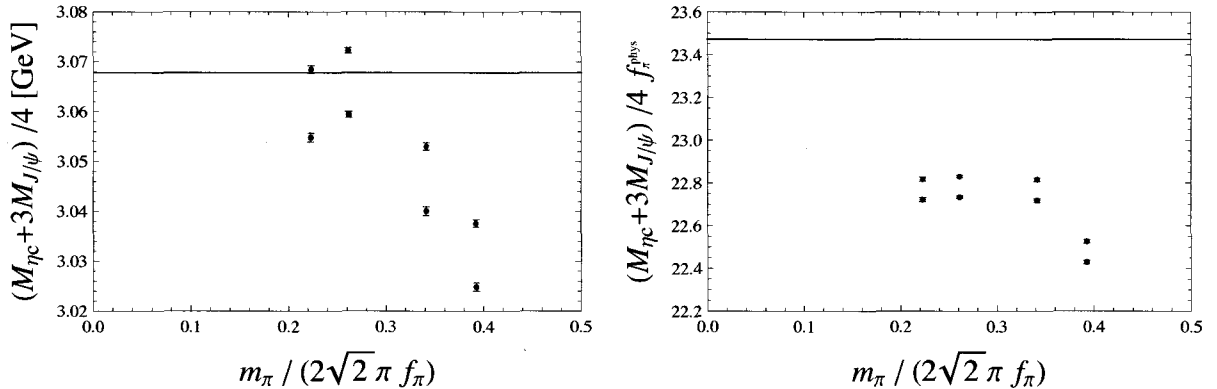


Figure 5.3: Spin-averaged mass of η_c and J/Ψ on the different ensembles. The blue points and purple points indicate the masses at m_1 and m_2 respectively. The red line indicates the experimental value. The left panel displays the results from the lattice spacing $a^{-1} = 1588$ MeV used on all ensembles. This method was used to tune the charm-quark mass on the m007 ensemble. The right panel displays the masses scaled by f_π on the lattice and extrapolated to f_π^{phys} , as discussed in the text.

calculations.³ These same two charm quark masses, m_1 and m_2 , were used on all ensembles. On the MILC ensembles, the value of β was slightly varied for the different light-quark masses. Therefore, the corresponding value of the critical mass changes from ensemble to ensemble, leading to a slightly different charm-quark mass tuning. This can be clearly seen in the left panel of Fig. 5.3, where we display the spin-averaged J/Ψ - η_c mass as a function of the light-quark mass, determined with the $a^{-1} = 1588$ MeV scale setting. Ensembles m007 and m010 share the same value of β and therefore the difference in these points (the left-most two sets of masses) is due entirely to light-quark contributions, whereas the m020 and m030 ensembles each have a different value of β , so that the variation of the spin-averaged mass is due both to light-quark effects as well as a shifted value of the critical mass.

³At the time this work was almost completed we became aware of an updated value for the lattice spacing determined by MILC [121]. As a result the tuned charm quark mass is reduced, consequently the charmed hadron masses in lattice units will be reduced. However, the reduced lattice spacing will compensate this effect by an increase of the masses in physical units. The overall effect of mass shifting in the final baryon masses is estimated to be less than 1%, well within our systematics. Further, in our final analysis, the MILC scale setting is only used as a check on our systematics.

In the right panel of Fig. 5.3, we display our preferred method of determining the charm-quark mass using f_π to set the scale. On each ensemble, we take the spin-averaged J/Ψ - η_c mass and divide by the corresponding value of f_π^{latt} calculated on that ensemble. We then use the value of l_4 determined in Sec. 5.3.1 to scale these values to determine the ratio with f_π^{phys} ,

$$\frac{M_{\eta_c} + 3M_{J/\Psi}}{4f_\pi^{\text{phys}}} = \frac{1 + \delta f(m_\pi^{\text{latt}}/f_\pi^{\text{latt}})}{1 + \delta f(m_\pi^{\text{phys}}/f_\pi^{\text{phys}})} \frac{M_{\eta_c} + 3M_{J/\Psi}}{4f_\pi^{\text{latt}}}. \quad (5.6)$$

It is these scaled values that are plotted in the right panel of Fig. 5.3 and which we use to extrapolate our spectrum calculation to the physical charm-quark mass point, which we take to be

$$\frac{M_{\eta_c}^{\text{phys}} + 3M_{J/\Psi}^{\text{phys}}}{4f_\pi^{\text{phys}}} = 23.47, \quad (5.7)$$

$$\text{with } \frac{m_\pi^{\text{phys}}}{f_\pi^{\text{phys}}} = 1.056. \quad (5.8)$$

Here, m_π^{phys} is taken to be the isospin-averaged pion mass, while f_π^{phys} is taken to be the charged-pion decay constant [2]. On each ensemble, we linearly extrapolate the spin-averaged J/Ψ - η_c mass (scaled by f_π^{phys}) to the experimental value to determine the parameter $m_0 = m_c^{\text{phys}}$ (the masses of all hadrons are then extrapolated linearly to this charm-quark mass on each ensemble). The uncertainties of the extrapolated hadron masses are evaluated using the jackknife method. As a check of systematics, we perform the same procedure using the lattice spacing $a^{-1} = 1588$ MeV to perform the linear charm-quark mass extrapolation. Using this second approach, the resulting charmed baryon spectrum is consistent with that of our preferred charm-quark mass-tuning method.

To test the viability of our choice of mixed-action and to gauge the discretization

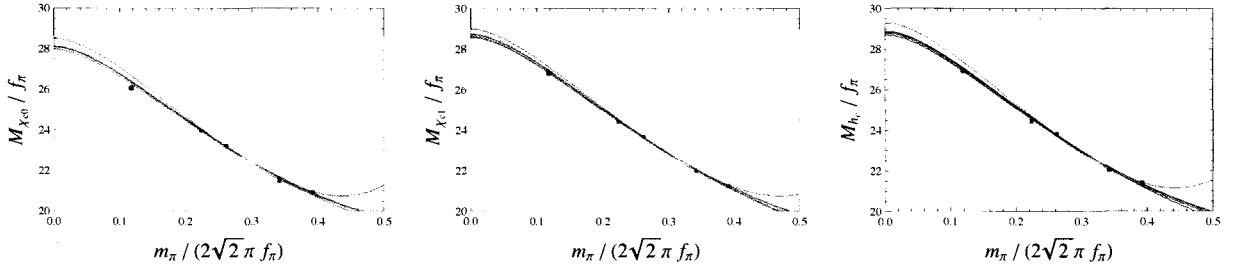


Figure 5.4: The masses of χ_{c0} , χ_{c1} and h_c as functions of m_π/f_π . The blue points are our numerical values. The pink shaded regions show the standard deviation allowed regions of quadratic fit. The blue shaded regions show the standard deviation allowed regions of quartic fit. The red points are experimental values.

errors, we compute both the J/Ψ - η_c hyperfine mass splitting as well as the low-lying charmonium spectrum of the χ_{c0} , χ_{c1} and h_c . The interpolating fields used for these charmonium states are⁴

$$\chi_{c0} = \bar{Q}_c Q_c, \quad (5.9)$$

$$\chi_{c1}^i = \bar{Q}_c \gamma^i \gamma_5 Q_c, \quad (5.10)$$

$$h_c^i = \sum_{j=1}^3 \sum_{k=j}^3 \epsilon_{ijk} \bar{Q}_c \gamma^j \gamma^k Q_c, \quad (5.11)$$

To extrapolate these charmonium masses to the physical light-quark mass values, we use Eq. (5.4) both in quadratic (in m_π) as well quartic form, i.e.

$$\frac{M_h}{f_\pi} = \frac{M_0}{f_\pi} + \frac{c_h^{(2)}}{4\pi} \frac{m_\pi^2}{f_\pi^2} + \frac{c_h^{(4)}}{(4\pi)^2} \frac{m_\pi^4}{f_\pi^4}. \quad (5.12)$$

The results of the extrapolation are displayed in Fig. 5.4, and tabulated in Tab. 5.5.

In the table, the first uncertainty is statistical and the second is an extrapolation systematic from the two extrapolation functions used.

A more stringent test of discretization errors is the calculation of the hyperfine

⁴One can also use improved interpolating operators to extract charmonium states in lattice calculations, especially for the excited states χ_{c0} , χ_{c1} and h_c ; see, for example, Ref. [122].

	$M_{\chi_{c0}}$ (MeV)	$M_{\chi_{c1}}$ (MeV)	M_{h_c} (MeV)
Extrapolated Values	3465(20)(13)	3525(20)(6)	3553(25)(14)
Experimental Values	3415	3511	3526

Table 5.5: Low-lying charmonium spectrum of χ_{c0} , χ_{c1} and h_c . The experimental values are taken from the Particle Data Group [2].

splitting. The hyperfine splitting is obtained by fitting the ratio of the two-point correlation functions of J/Ψ and η_c

$$\mathcal{R} = \frac{C_{J/\Psi}(t)}{C_{\eta_c}(t)} \quad (5.13)$$

to a single exponential

$$\mathcal{R} = Ae^{-\Delta_m t}, \quad (5.14)$$

where Δ_m is the mass splitting between the J/Ψ and η_c . The splittings are first extrapolated to the physical charm-quark mass for each ensemble and then extrapolated to the physical light-quark mass. As with the charmonium spectrum, we perform a light-quark mass extrapolation using both a quadratic and quartic form of Eq. (5.4). In Fig. 5.5 we display this extrapolation, finding $M_{J/\Psi} - M_{\eta_c} = 93(1)(7)$ MeV. The first uncertainty is statistical while the second is a systematic from the chiral extrapolation.

It is well known that the lattice computations of the charmonium hyperfine splitting (experimentally measured to be 117 MeV) are sensitive to the lattice spacing. Qualitatively, one can understand this by performing a Symanzik expansion of the heavy quark action, revealing dimension five operators arising from discretization effects, which are otherwise identical to the heavy quark effective theory (HQET) [123,

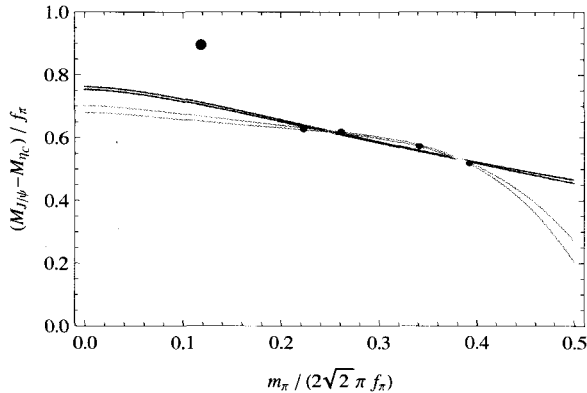


Figure 5.5: Extrapolation of the hyperfine splitting. The blue points are the lattice data. The red point is the experimental value. The blue band is the quadratic fit with Eq. 5.4, while the pink band is the quartic fit with Eq. 5.4.

35, 124] operator responsible for the hyperfine splitting⁵

$$\begin{aligned}
 \mathcal{L}_{HQET} &\supset -g \bar{h}_c^{(+)} \frac{\sigma \cdot \mathbf{B}}{2m_c} h_c^{(+)} \\
 \longrightarrow \mathcal{L}_{\text{latt}} &\supset -g \bar{h}_c^{(+)} \frac{\sigma \cdot \mathbf{B}}{2m_c} h_c^{(+)} + a c(am_c) \bar{h}_c^{(+)} \sigma \cdot \mathbf{B} h_c^{(+)} ,
 \end{aligned} \tag{5.15}$$

where $h_c^{(+)}$ is the heavy quark field. In the heavy quark action we are using, the coefficients of the operators S_B (4.3) and S_E (4.4) have been given their tree-level, tadpole improved values in order to mitigate the effects of this unwanted discretization effect. It is known the operator S_B (4.3) has a significant effect on the hyperfine splitting [71, 93, 94]. A nonperturbative tuning of the coefficient c_B can improve the hyperfine splitting in a fixed-lattice spacing calculation; see Ref. [125], in particular Fig. 3. However, the qualitative aspects of this effect remain even after tuning the coefficients. Previous quenched calculations of the hyperfine splitting have generally been low, being about 80 MeV, and showed a strong lattice-spacing dependence. Further, a recent direct calculation of the disconnected diagrams has ruled out these (or

⁵A proper treatment of heavy quark discretization effects is more involved and can be found in Ref. [71].

their lack thereof) being the cause of the discrepancy [126]. Our results are consistent with those of the Fermilab/MILC Collaboration, which utilized a similar heavy quark action, the same dynamical ensembles and staggered light quarks [127]. The Fermilab/MILC Collaboration also performed calculations on different lattice spacings, finding similar lattice-spacing dependence to Ref. [127]. Therefore, the discrepancy of our calculated hyperfine splitting with the experimental value is expected.

5.3.3 Light-Quark Mass Extrapolation

Heavy-Hadron χ PT Extrapolation

To perform the light-quark mass extrapolation, we begin with a continuum HH χ PT extrapolation of the baryon masses. The mass formula for these baryons containing a heavy quark was first determined in Ref. [114] and later extended to partially quenched theories in Ref. [45]. For doubly heavy baryons, the χ PT was formulated in Ref. [115] and later extended to partially quenched theories in Ref. [117]. In this work, we perform $SU(2)$ chiral extrapolations of the baryon masses, inspired by Ref. [118].⁶ To perform the extrapolations, we treat the $J = 1/2$ and $J = 3/2$ baryons as degenerate, which is valid at this order in HQET/HH χ PT.⁷ The baryons are grouped into their respective $SU(2)$ multiplets allowing for a simultaneous two-flavor chiral extrapolation of all masses in related multiplets. This allows us, with only four gauge ensembles, to determine all the relevant LECs for a given pair of multiplets in a global fit. The first pair of multiplets contains the Λ_c and Σ_c baryons. Their $SU(2)$ chiral

⁶For further discussion on $SU(2)$ chiral extrapolations of hadron states with strange valence quarks, see Refs. [128, 129, 130].

⁷It would be more desirable to use the lattice-calculated masses of the $J = 3/2$ baryons, but we do not have them for this work, and so we use this approximation for now.

extrapolation functions are given at next-to-leading order (NLO) by

$$\frac{M_{\Lambda_c}}{f_\pi} = \frac{M_0}{f_0} \frac{1}{1 + \delta f(m_\pi/f_\pi)} - \frac{c_\Lambda^r(\mu)}{4\pi} \frac{m_\pi^2}{f_\pi^2} - \frac{6g_3^2}{(4\pi)^2} \frac{\mathcal{F}(m_\pi, \Delta_{\Sigma\Lambda}, \mu)}{f_\pi^3}, \quad (5.16)$$

$$\begin{aligned} \frac{M_{\Sigma_c}}{f_\pi} = & \frac{M_0 + \Delta_{\Sigma\Lambda}^{(0)}}{f_0} \frac{1}{1 + \delta f(m_\pi/f_\pi)} - \frac{c_\Sigma^r(\mu)}{4\pi} \frac{m_\pi^2}{f_\pi^2} \\ & - \frac{2}{3} \frac{g_3^2}{(4\pi)^2} \frac{\mathcal{F}(m_\pi, -\Delta_{\Sigma\Lambda}, \mu)}{f_\pi^3} + \frac{4}{3} \frac{g_2^2}{(4\pi)^2} \frac{\mathcal{F}(m_\pi, 0, \mu)}{f_\pi^3}, \end{aligned} \quad (5.17)$$

where $\Delta_{\Sigma\Lambda}^{(0)}$ is the mass difference of Σ_c and Λ_c in chiral limit, $\Delta_{\Sigma\Lambda}$ is the mass difference of Σ_c and Λ_c calculated on lattice. The chiral functions are

$$\mathcal{F}(m, \Delta, \mu) = (\Delta^2 - m^2 + i\epsilon)^{3/2} \ln \left(\frac{\Delta + \sqrt{\Delta^2 - m^2 + i\epsilon}}{\Delta - \sqrt{\Delta^2 - m^2 + i\epsilon}} \right) - \frac{3}{2} \Delta m^2 \ln \left(\frac{m^2}{\mu^2} \right) - \Delta^3 \ln \left(\frac{4\Delta^2}{m^2} \right). \quad (5.18)$$

with

$$\mathcal{F}(m, 0, \mu) = \pi m^3, \quad (5.19)$$

and

$$\mathcal{F}(m, -\Delta, \Lambda) = \begin{cases} -\mathcal{F}(m, \Delta, \Lambda) + 2i\pi(\Delta^2 - m^2)^{3/2}, & m < |\Delta| \\ -\mathcal{F}(m, \Delta, \Lambda) + 2\pi(m^2 - \Delta^2)^{3/2}, & m > |\Delta| \end{cases}. \quad (5.20)$$

To stabilize the fits, we first fit $M_{\Sigma_c} - M_{\Lambda_c}$ to a quadratic in m_π/f_π , and feed this into a fit of the masses, yielding the results in Table 5.6 and extrapolations displayed in Figure 5.6. One observes that the continuum HH χ PT fits describe the lattice data very well. However, only the leading term, M_0 is well determined,⁸ while the rest of the LECs, most notably the axial couplings, $g_{\Sigma\Sigma\pi}$ and $g_{\Sigma\Lambda\pi}$ are consistent with zero. This phenomenon is not unique to the charmed baryons. In Ref. [1],

⁸To determine M_0/f_π^{phys} we take our results for M_0/f_0 and scale them by $[1 + \delta f(m_\pi^{\text{phys}}/f_\pi^{\text{phys}})]^{-1}$.

Fit Range	$\Delta_{\Sigma\Lambda}/f_\pi^{\text{phys}}$	M_0/f_π^{phys}	$c_\Lambda^r(f_\pi)$	$c_\Sigma^r(f_\pi)$	g_2^2	g_3^2	χ^2	dof	Q
m007–m030	1.46(10)	17.9(2)	-0.8(5)	0.2(1.2)	0.8(1.0)	-0.1(1)	0.32	3	0.95

Table 5.6: Fit to Λ_c and Σ_c masses with NLO continuum formulae.

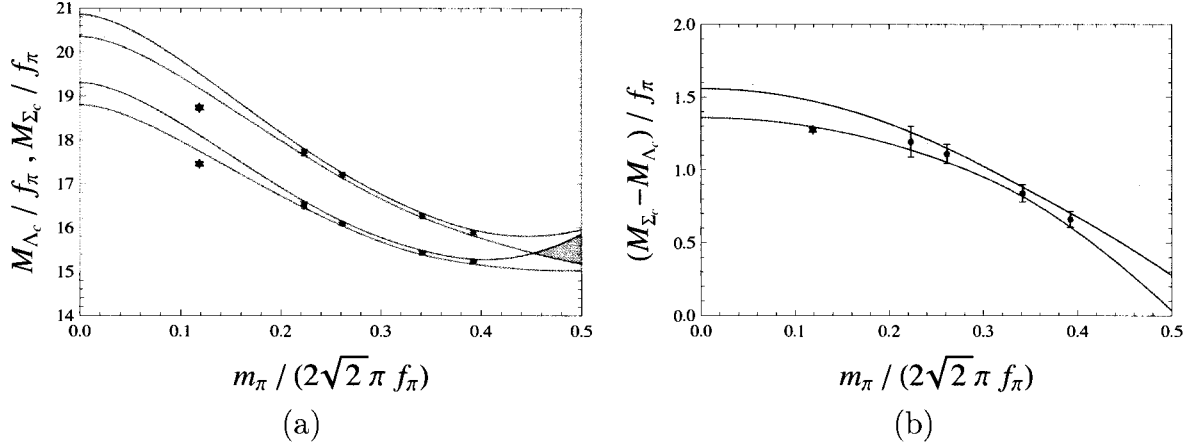


Figure 5.6: NLO HH χ PT extrapolation of M_{Λ_c} and M_{Σ_c} (a) as well as $M_{\Sigma_c} - M_{\Lambda_c}$ (b).

chiral extrapolations on the nucleon mass in which the nucleon axial coupling, $g_{\pi NN}$ (commonly denoted as g_A in baryon χ PT) was left as a free parameter, returned values which were inconsistent with experiment and phenomenology. In fact, given the lattice results for the nucleon mass as a function of m_π , it was found that the nucleon mass scales linearly in m_π . Such behavior signals a delicate cancelation between different orders, a trend which is found in all $2 + 1$ dynamical lattice computations of the nucleon mass [131]. Therefore, our findings for the axial couplings of the charmed baryons are not surprising in this light. To improve the situation, a simultaneous fit of the axial charges themselves, along with the masses will most likely be necessary.

We perform a similar analysis for the $J = 1/2$ $\Xi_c - \Xi'_c$ isospin doublets, the results of which are collected in Table 5.7 and displayed in Figure 5.7. The extrapolation formulae for $M_{\Xi'_c}$ and M_{Ξ_c} are similar to those for M_{Σ_c} and M_{Λ_c} . They can be deduced

Fit Range	$\Delta_{\Xi'/\Xi}/f_\pi^{\text{phys}}$	M_0/f_π^{phys}	$c_{\Xi}^r(f_\pi)$	$c_{\Xi'}^r(f_\pi)$	g_2^2	g_3^2	χ^2	dof	Q
m007–m030	0.85(6)	19.4(2)	0.6(6)	1.3(1.2)	5.9(3.9)	-1.0(6)	0.04	3	1.00

Table 5.7: Fit to Ξ_c and Ξ'_c masses with NLO continuum formulae.

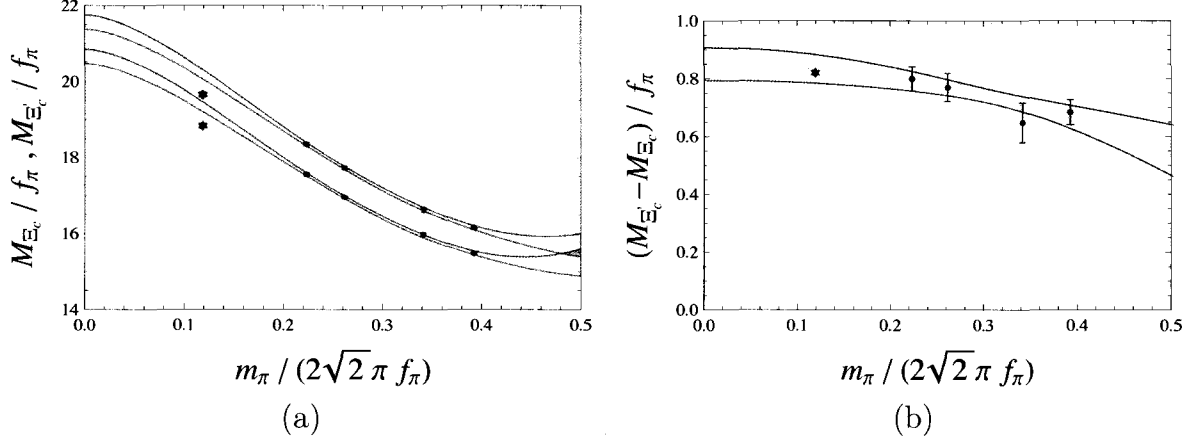


Figure 5.7: NLO HH χ PT extrapolation of M_{Ξ_c} and $M_{\Xi'_c}$ (a) as well as $M_{\Xi'_c} - M_{\Xi_c}$ (b).

by comparing Eqs. (5.16) and (5.17) to Ref. [45],⁹

$$\frac{M_{\Xi_c}}{f_\pi} = \frac{M_0}{f_0} \frac{1}{1 + \delta f(m_\pi/f_\pi)} - \frac{c_{\Xi}^r(\mu) m_\pi^2}{4\pi f_\pi^2} - \frac{3}{2} \frac{g_3^2}{(4\pi)^2} \frac{\mathcal{F}(m_\pi, \Delta_{\Xi'/\Xi}, \mu)}{f_\pi^3}, \quad (5.21)$$

$$\begin{aligned} \frac{M_{\Xi'_c}}{f_\pi} = & \frac{M_0 + \Delta_{\Xi'/\Xi}^{(0)}}{f_0} \frac{1}{1 + \delta f(m_\pi/f_\pi)} - \frac{c_{\Xi'}^r(\mu) m_\pi^2}{4\pi f_\pi^2} \\ & - \frac{1}{2} \frac{g_3^2}{(4\pi)^2} \frac{\mathcal{F}(m_\pi, -\Delta_{\Xi'/\Xi}, \mu)}{f_\pi^3} + \frac{1}{2} \frac{g_2^2}{(4\pi)^2} \frac{\mathcal{F}(m_\pi, 0, \mu)}{f_\pi^3}, \end{aligned} \quad (5.22)$$

where $\Delta_{\Xi'/\Xi}^{(0)}$ is the mass difference of Ξ'_c and Ξ_c in chiral limit, $\Delta_{\Xi'/\Xi}$ is the mass difference of Ξ'_c and Ξ_c calculated on lattice.

The masses of the remaining $J = 1/2$ charmed baryons, $M_{\Xi_{cc}}$, M_{Ω_c} and $M_{\Omega_{cc}}$, can be treated independently. The extrapolation formula for $M_{\Xi_{cc}}$ is similar to that of M_{Σ_c} . There is an axial coupling $g_{\Xi_{cc}\Xi_{cc}\pi}$ as well as $g_{\Xi_{cc}^*\Xi_{cc}\pi}$ where the second coupling is the axial transition coupling of the $J = 3/2$ to the $J = 1/2$ - π state. The heavy

⁹In $SU(3)$ HH χ PT, the axial couplings for the Ξ_c - Ξ'_c system are the same as those for the Λ_c - Σ_c system, $g_2 = g_{\Sigma\Sigma\pi} = g_{\Xi'\Xi'\pi}$ and $g_3 = g_{\Sigma\Lambda\pi} = g_{\Xi'\Xi\pi}$. However, in the $SU(2)$ theories, they differ by $SU(3)$ breaking corrections.

Fit Range	M_0/f_π^{phys}	$c_{\Xi_{cc}}^r(f_\pi)$	g^2	χ^2	dof	Q
m007–m030	28.1(2)	1.4(1.0)	-1.7(1.0)	3.0	1	0.08

Table 5.8: Fit to $J = 1/2$ Ξ_{cc} mass with the NLO continuum heavy-hadron formula.

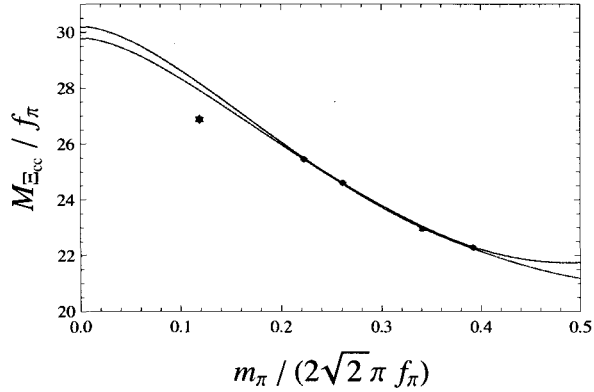


Figure 5.8: NLO HH χ PT extrapolation of $M_{\Xi_{cc}}$.

quark symmetry also requires these couplings to be the same in the heavy quark limit. At this order, we can treat the $J = 3/2$ Ξ_{cc}^* as degenerate with the Ξ_{cc} . The results are collected in Table 5.8 and displayed in Figure 5.8, with the extrapolation formula [117]

$$\frac{M_{\Xi_{cc}}}{f_\pi} = \frac{M_0}{f_0} \frac{1}{1 + \delta f(m_\pi/f_\pi)} - \frac{c_{\Xi_{cc}}^r(\mu) m_\pi^2}{4\pi f_\pi^2} - \frac{g^2}{(4\pi)^2} \frac{\mathcal{F}(m_\pi, 0, \mu)}{f_\pi^3}, \quad (5.23)$$

where we have set $\Delta_{\Xi^*\Xi} = 0$ in this analysis, valid at this order in the heavy-quark expansion. One feature which is more pronounced in this fit is $g^2 < 0$. Taken at face value, this would suggest the Lagrangian was non-Hermitian, and the theory not sensible. Therefore, even though these fits reproduce the lattice data well and predict a mass within a few percent of the physical value, they must be taken with caution. Most likely, as with the nucleon mass [131], there is a delicate cancelation of terms at different orders, and therefore one does not have confidence in these determinations of the LECs.

Ω	Fit Range	M_0/f_π^{phys}	$c_{\Omega_c}^r(f_\pi)$	$\alpha_\Omega^{(4)}$	$\beta_\Omega^{(4)}$	χ^2	dof	Q
Ω_c	m007–m030	20.4(6)	-3.0(4.6)	46(61)	-164(227)	0.00	0	-
Ω_{cc}	m007–m030	27.7(4)	-7.3(3.0)	109(40)	-392(149)	0.00	0	-

Table 5.9: Fit to $J = 1/2$ Ω_c and Ω_{cc} masses with NLO continuum heavy-hadron formulae.

Similar to the $s = -3$ Ω , the $J = 1/2$ Ω_c and Ω_{cc} do not have mass corrections which scale as m_π^3 . This is because these baryons do not contain any valence up or down quarks, and therefore, the leading $SU(2)$ axial coupling vanishes [132, 118]. The $SU(2)$ chiral extrapolation formula for these baryon masses is then expected to be as convergent as that for pions. The mass extrapolation formula for the Ω_c and Ω_{cc} are both given by

$$\frac{M_\Omega}{f_\pi} = \frac{M_0}{f_0} \frac{1}{1 + \delta f(m_\pi/f_\pi)} - \frac{c_{\Xi_{cc}}^r}{4\pi} \frac{m_\pi^2}{f_\pi^2} + \frac{m_\pi^4}{(4\pi)^3 f_\pi^4} \left[\alpha_\Omega^{(4)} \ln \left(\frac{m_\pi^2}{\mu^2} \right) + \beta_\Omega^{(4)(\mu)} \right]. \quad (5.24)$$

At this order, the two-loop corrections from f_π should be included as corrections to $\alpha_\Omega^{(4)}$ and $\beta_\Omega^{(4)}$. Further, there is a $\ln^2(m_\pi)$ correction with fixed coefficient. However, since we only have four mass points, we cannot judge the quality of the fit anyway, so we ignore these corrections. The results are collected in Table 5.9 and displayed in Figure 5.9. Performing a fit with $\alpha_\Omega = 0$ and $\beta_\Omega = 0$ returns consistent mass predictions with smaller uncertainties. We take the zero-degree-of-freedom fit as our central result as it provides a more conservative uncertainty.

Polynomial Extrapolation

Given the issues of performing the heavy-hadron chiral extrapolations as discussed above, we also perform polynomial extrapolations in m_π^2 . We use the difference between the polynomial extrapolations and the heavy-hadron chiral extrapolations as an additional estimate of systematic extrapolation uncertainty. We use up to three

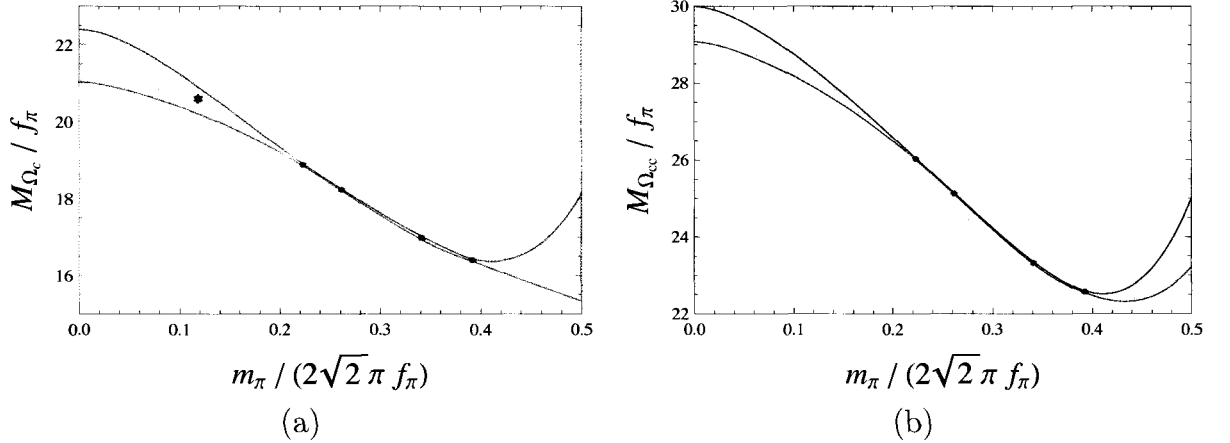


Figure 5.9: NLO HH χ PT extrapolation of M_{Ω_c} (a) and $M_{\Omega_{cc}}$ (b).

different polynomial fit functions for each of the charmed hadron masses:

$$\frac{M_2}{f_\pi} = \frac{M_0}{f_0} \frac{1}{1 + \delta f(m_\pi/f_\pi)} + c_2 \frac{m_\pi^2}{f_\pi^2}, \quad (5.25)$$

$$\frac{M_3}{f_\pi} = \frac{M_0}{f_0} \frac{1}{1 + \delta f(m_\pi/f_\pi)} + c_2 \frac{m_\pi^2}{f_\pi^2} + c_3 \frac{m_\pi^3}{f_\pi^3}, \quad (5.26)$$

$$\frac{M_4}{f_\pi} = \frac{M_0}{f_0} \frac{1}{1 + \delta f(m_\pi/f_\pi)} + c_2 \frac{m_\pi^2}{f_\pi^2} + c_4 \frac{m_\pi^4}{f_\pi^4}. \quad (5.27)$$

In Figure 5.10, we display the results of these fits as well the heavy-hadron χ PT fits as ratios with respect to the experimental masses. The experimental values for the baryon masses are taken from the Particle Data Group [2]. As it can be seen, there is very little variation in the results of the extrapolated masses. In all cases, the different extrapolations are consistent within one sigma.

In Table 5.10, we provide the extrapolated baryon masses, taking the central value from the HH χ PT extrapolations. The first uncertainty is statistical and the second uncertainty is a comprehensive systematic uncertainty. This systematic uncertainty is derived by comparing the polynomial light quark mass extrapolations to the HH χ PT extrapolation. Further, it includes the uncertainty associated with the choice of fitting window for the correlators as well. Except for the Ω_c , the extrapolated masses are

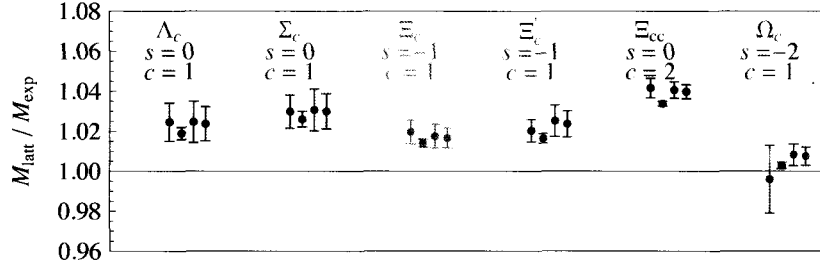


Figure 5.10: Ratio of extrapolated masses to experimentally measured masses. The first point represents the HH χ PT fit, the second point is a fit with Eq. (5.25), the third with Eq. (5.26) and the fourth with Eq. (5.27).

State ($J = 1/2$)	M_{Λ_c} [MeV]	M_{Ξ_c} [MeV]	M_{Σ_c} [MeV]	$M_{\Xi'_c}$ [MeV]	M_{Ω_c} [MeV]	$M_{\Xi_{cc}}$ [MeV]	$M_{\Omega_{cc}}$ [MeV]
Prediction	2342(22)(11)	2527(17)(13)	2527(20)(08)	2638(17)(10)	2687(46)(16)	3665(17)(14)	3680(31)(38)
Exp. Mass	2286	2468	2454	2576	2698	3519	-

Table 5.10: Direct light/heavy quark mass extrapolation of the $J = 1/2$ charmed baryon spectrum.

systematically high, indicative of a discretization error.

5.3.4 Discretization Errors and Mass Splittings

In this work, we have performed calculations at only a single value of the lattice spacing, with $a \sim 0.125$ fm, prohibiting us from performing a continuum extrapolation. However, we can take advantage of various symmetries and power counting to make a reasonable estimate of the discretization errors present in our calculation.¹⁰ In these heavy-light systems, the discretization errors arise both from the light and heavy quark actions. The corrections from both generically scale as $\mathcal{O}(a^2)$ for each of the charmed baryon masses. If we consider $SU(3)$ symmetry, then the leading discretization errors for all baryons in a given $SU(3)$ multiplet must be the same, with corrections scaling as $\mathcal{O}(a^2(m_s - m_u))$. Further, if one considers the combined large- N_c , $SU(3)$ and heavy-quark symmetries [133], then all the singly charmed baryon

¹⁰With a single lattice spacing, we can not disentangle both the discretization errors and the tuning of the charm quark mass. The effects we discuss here as discretization errors are really a combination of the two.

masses we calculate in this work share a common discretization correction to their masses, with sub-leading corrections scaling as $\mathcal{O}(a^2/N_c)$ as well as the $SU(3)$ breaking corrections. Therefore, all the singly charmed baryon masses we compute in this work, $\{\Lambda_c, \Xi_c, \Sigma_c, \Xi'_c, \Omega_c\}$ share a common discretization correction, which happens to be the dominant discretization error. The same analysis holds for the doubly charmed baryons as well, $\{\Xi_{cc}, \Omega_{cc}\}$ with a common error, albeit different from the singly charmed correction.¹¹ It is therefore advantageous to consider extrapolations of baryon mass splittings, as these mass splittings exactly cancel the leading discretization errors.

Before proceeding with the analysis of the mass splittings, we first use power counting arguments to estimate the discretization errors. The leading discretization corrections from the light and heavy quark actions can be estimated as [95]

$$\begin{aligned}\delta_q &= \frac{1}{2}(ap)^2\Lambda_{QCD}, \\ \delta_Q &= \frac{\alpha_s(m_c)(ap)}{2(1+am_c)}\Lambda_{QCD},\end{aligned}\tag{5.28}$$

where p is a typical momentum scale, of the order of Λ_{QCD} , the characteristic hadronic scale. To be conservative, we can take $\Lambda_{QCD} = 700$ MeV which leads to the estimates

$$\begin{aligned}\delta_q &= 68 \text{ MeV}, \\ \delta_Q &= 19 \text{ MeV}.\end{aligned}\tag{5.29}$$

When considering mass splittings amongst a given $SU(3)$ multiplet, these leading

¹¹With the full $J = 3/2$ and $J = 1/2$ heavy baryon mass spectrum, one could perform an analysis of the large- N_c baryon mass relations [134, 135] as has recently been performed for the light quark octet and decuplet baryons [136].

errors become further suppressed by $m_s - m_u$ effects,

$$\begin{aligned}\delta\Delta M_q &= \frac{1}{2}(ap)^2\Lambda_{QCD}\frac{m_K^2 - m_\pi^2}{\Lambda_\chi^2}, \\ \delta\Delta M_Q &= \frac{\alpha_s(m_c)(ap)}{2(1 + am_c)}\Lambda_{QCD}\frac{m_K^2 - m_\pi^2}{\Lambda_\chi^2}.\end{aligned}\tag{5.30}$$

Mass splittings between the two singly charmed $SU(3)$ multiplets, $\Delta M^{6,\bar{3}}$, would receive similar discretization corrections, with the extra suppression of $1/N_c$. Combining these estimates in quadrature,¹² we estimate the discretization errors for the baryon masses, and various mass splittings (using $\Lambda_\chi = 2\sqrt{2}\pi f_\pi$ and the physical kaon and pion masses)

$$\begin{aligned}\delta M_{h_c} &= 71 \text{ MeV}, \\ \delta M_{h_{cc}} &= 78 \text{ MeV}, \\ \delta\Delta M_{h_c} &= 12 \text{ MeV}, \\ \delta\Delta M_{h_{cc}} &= 13 \text{ MeV}, \\ \delta\Delta M_{h_c}^{6,\bar{3}} &= 24 \text{ MeV}, \\ \delta\Delta M_{h_{cc}}^{6,\bar{3}} &= 26 \text{ MeV}.\end{aligned}\tag{5.31}$$

Given our limited number of light-quark mass values, we are not able to perform the (mixed-action) HH χ PT analysis of the mass splittings. We therefore perform our fits using the polynomial fit functions, Eqs. (5.25)–(5.27), with M_0 replaced by $\Delta_{h_2h_1}^{(0)}$. We perform the extrapolations of the mass splittings, $M_{\Xi_c} - M_{\Lambda_c}$, $\{M_{\Xi_c'}, M_{\Omega_c}\} - M_{\Sigma_c}$, $M_{\Sigma_c} - M_{\Lambda_c}$ and $M_{\Omega_{cc}} - M_{\Xi_{cc}}$. In Figure 5.11 we display the extrapolation of these mass splittings using Eq. (5.27) and in Figure 5.12 we show the ratio of these fits to

¹²For the doubly charmed baryon masses, we double the estimated heavy quark discretization error. As mentioned above, this uncertainty also includes any miss-tuning of the charm quark mass, and thus a double charmed baryon will be miss-tuned twice as much.

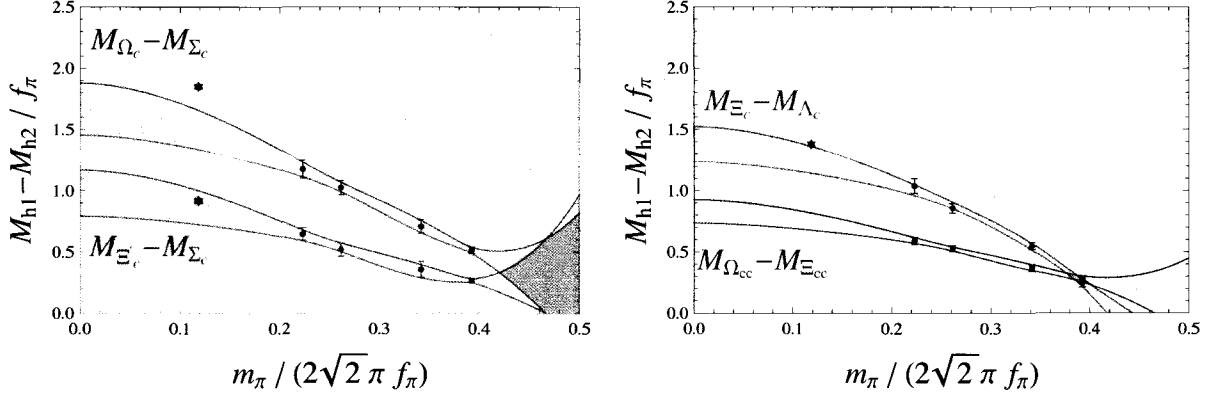


Figure 5.11: Polynomial extrapolations of of $J = 1/2$ mass splittings amongst heavy-quark- $SU(3)$ multiplets with Eq. (5.27).

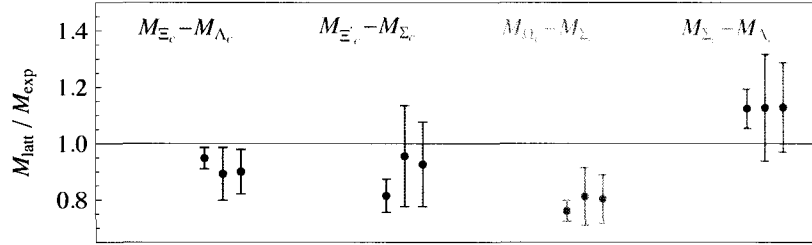


Figure 5.12: Ratio of extrapolated mass splittings to experiment [2]. The first point is a fit with Eq. (5.25), the second with Eq. (5.26) and the third with Eq. (5.27).

the experimental values. Our final predicted splittings are determined by using the quartic fit function as the central value with the differences from the quadratic and cubic fits to estimate light quark mass extrapolation errors (in addition to those from the quartic fit).

As discussed earlier in this section, the dominant discretization error in the mass calculations is common to all baryons, given the various symmetries. Therefore, this correction will shift all the baryon masses in one direction. We can determine the sign of this correction in the following manner. First, we can determine the singly charmed baryon spectrum by taking our extrapolated mass splittings, column (a) of Table 5.11, and using $M_{\Lambda_c}^{\text{phys}}$ and $M_{\Sigma_c}^{\text{phys}}$ as reference scales, $M_{hc}^{\text{split}} = M_{\Lambda_c, \Sigma_c}^{\text{phys}} + \Delta M_{hc-\Lambda_c, \Sigma_c}$, resulting in the predicted masses, Table 5.11 (b). We then compare these to our direct mass

extrapolations $M_{h_c}^{\text{direct}}$, given in Table 5.10. The first method is free of the leading discretization errors while the second is not. We can then construct the quantity,

$$\delta M_c = \frac{1}{N_{h_c}} \sum_{h_c} \left(M_{h_c}^{\text{direct}} - M_{h_c}^{\text{split}} \right), \quad (5.32)$$

which is a measure of these discretization errors. The sum runs over all four singly charmed baryons h_c for which we have both methods to determine the masses ($N_{h_c} = 4$). The first thing to note is that every element contributing to the sum is a positive quantity, suggesting the discretization errors increase the baryon masses. It is also interesting to note that in our calculation, $\delta M_c(a^2) = 59$ MeV, comparable to our estimated leading discretization effects, Eq. (5.31). We can then refine our estimate of the leading discretization errors to be

$$\begin{aligned} \delta M_{h_c} &= {}^{+0}_{-71} \text{ MeV}, \\ \delta M_{h_{cc}} &= {}^{+0}_{-78} \text{ MeV}, \end{aligned} \quad (5.33)$$

where we have also assumed that the doubly charmed discretization errors do not change sign relative to the singly charmed baryon corrections. Our final numbers, collected in Table 5.11, include these discretization error estimates in the quoted uncertainties.

5.4 Discussion and Conclusions

The central results of this work are the predicted mass splittings, displayed in the left panel of Table 5.11. The first uncertainty is statistical and the second uncertainty is a comprehensive systematic as discussed in the text. The third uncertainty is an estimate of discretization errors, which must scale as $\mathcal{O}(a^2(m_s - m_u))$ for members of

State	Latt. Pred. [MeV]	Exp. [MeV]	State	Mass Split. [MeV]	Direct Mass [MeV]	Exp. Mass [MeV]
$M_{\Xi_c} - M_{\Lambda_c}$	$164 \pm 14 \pm 23 \pm 12$	182	M_{Λ_c}		$2342 \pm 22 \pm 11^{+0}_{-71}$	2286
$M_{\Sigma_c} - M_{\Lambda_c}$	$190 \pm 27 \pm 18 \pm 27$	168	M_{Ξ_c}	$2450 \pm 14 \pm 23 \pm 12$	$2527 \pm 17 \pm 13^{+0}_{-71}$	2468
$M_{\Xi'_c} - M_{\Sigma_c}$	$113 \pm 18 \pm 8 \pm 12$	122	M_{Σ_c}	$2476 \pm 27 \pm 18 \pm 27$	$2527 \pm 20 \pm 8^{+0}_{-71}$	2454
$M_{\Omega_c} - M_{\Sigma_c}$	$195 \pm 21 \pm 7 \pm 12$	244	$M_{\Xi'_c}$	$2567 \pm 18 \pm 8 \pm 12$	$2638 \pm 17 \pm 10^{+0}_{-71}$	2576
			M_{Ω_c}	$2649 \pm 21 \pm 7 \pm 12$	$2687 \pm 46 \pm 16^{+0}_{-71}$	2698
			$M_{\Xi_{cc}}$		$3665 \pm 17 \pm 14^{+0}_{-78}$	3519
$M_{\Omega_{cc}} - M_{\Xi_{cc}}$	$98 \pm 9 \pm 22 \pm 13$	-	$M_{\Omega_{cc}}$	$3763 \pm 19 \pm 26^{+13}_{-79}$	$3680 \pm 31 \pm 38^{+0}_{-78}$	-
	(a)			(b)	(c)	

Table 5.11: Resulting charmed spectrum, extrapolated in the light-quark mass to the physical $m_\pi^{\text{phys}}/f_\pi^{\text{phys}}$ point. In (a) we display the mass splittings of the baryons related by $SU(3)$ and large N_c symmetry. As discussed in detail in the text, the first uncertainty is statistical, the second is systematic and the third is our estimate of discretization errors. These are the central results of this work. In (b), we display our resulting baryon spectrum determined using the experimental values of $M_{\Lambda_c}^{\text{exp}}$ and $M_{\Sigma_c}^{\text{exp}}$, combined with our splittings in (a). For the Ω_{cc} , we use our extrapolated value of $M_{\Xi_{cc}}$ given the present uncertainty in the experimental value. In (c), we present the results of our direct mass extrapolations, including our estimated discretization errors. The results from the two methods are consistent at the one-sigma level.

the same $SU(3)$ multiplet or $\mathcal{O}(a^2/N_c) + \mathcal{O}(a^2(m_s - m_u))$ otherwise, as dictated by the approximate symmetries. These results have been extrapolated to the physical charm quark mass and the physical light quark mass defined respectively by

$$\frac{M_{\eta_c}^{\text{phys}} + 3M_{J/\Psi}^{\text{phys}}}{4f_\pi^{\text{phys}}} = 23.47,$$

$$\frac{m_\pi^{\text{phys}}}{f_\pi^{\text{phys}}} = 1.056.$$

To perform these extrapolations, we first formed the dimensionless ratios $(M_{h_1}^{\text{latt}} - M_{h_2}^{\text{latt}})/f_\pi^{\text{latt}}$, taking into account the known light-quark mass dependence of f_π . The mass splittings in MeV are then determined with $f_\pi = 130.7$ MeV. These physical values are all taken from the PDG [2]. In Fig. 5.13, we compare some of our mass splitting results with those of Gottlieb and Na [106, 3], the only other dynamical calculation of the charmed baryon spectrum. They used the same MILC gauge en-

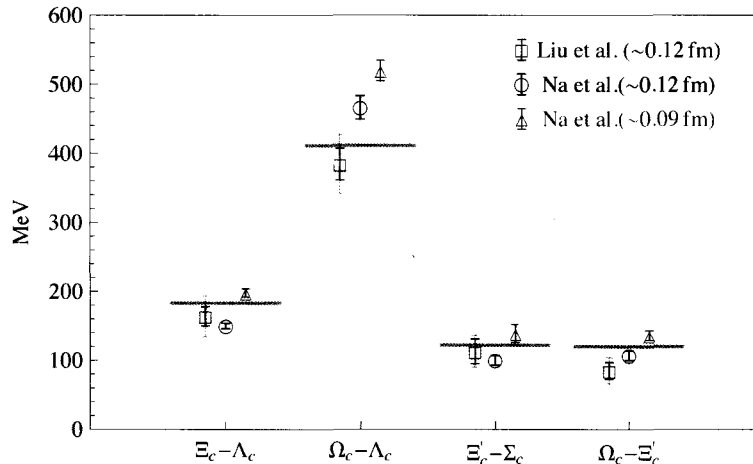


Figure 5.13: Comparison among charmed baryon mass splittings of dynamical lattice calculations. The results of Na et al. are taken from Ref. [3].

sembles, as well as the fine $a \sim 0.09$ fm lattices. For the light quark propagators, they used staggered fermions, and for the heavy quark, an interpretation of the Fermilab action was used, defining the charm mass with the kinetic mass instead of the rest mass. Their work is still somewhat preliminary and does not yet provide a systematic uncertainty. However, our results are consistent with theirs, especially those on the same ensembles with $a \sim 0.125$ fm.

We additionally use these mass splittings, combined with the experimental value of $M_{\Lambda_c}^{\text{exp}}$ and $M_{\Sigma_c}^{\text{exp}}$ to determine the $J = 1/2$ baryon masses. Aside from the Ξ_{cc} state,¹³ the masses determined in this way are consistent with our direct mass extrapolation results, Table 5.11 (c), after including our estimated discretization errors. We used power counting arguments [139, 95] to estimate the size of these corrections and we compared our two methods of determining the baryon masses to determine the expected sign of the leading discretization corrections. In Fig. 5.14, we display our resulting mass calculations using the results from both the mass splitting method (Liu

¹³Because the Ξ_{cc} has not been verified by multiple experimental groups [88, 89, 137, 138, 2], we chose to use our extrapolated value of $M_{\Xi_{cc}}$, combined with our extrapolated value of $M_{\Omega_{cc}} - M_{\Xi_{cc}}$ to make a prediction for the Ω_{cc} mass.

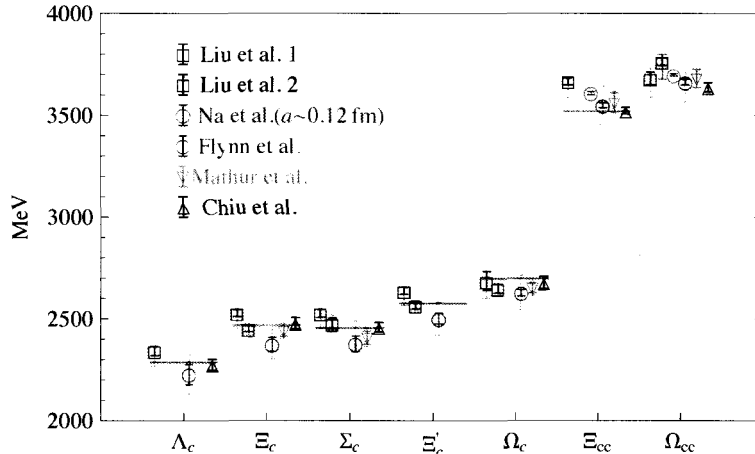


Figure 5.14: A summary of charmed baryon masses in MeV calculated using LQCD. We show both of our methods for obtaining the spectrum, the direct mass extrapolation (Liu et al. 1) and also using the extrapolated mass splittings, combined with $M_{\Lambda_c}^{\text{exp}}$ and $M_{\Sigma_c}^{\text{exp}}$ (Liu et al. 2). These results are taken from Table 5.11. The other results, displayed for comparison, are taken from Table 5.12.

et al. 2) as well as the direct extrapolation of the masses (Liu et al. 1). Additionally, we compare these with results from previous calculations, found in the Refs. of Table 5.12 (for those calculations with more than one lattice spacing, we show only the results from the ensemble with lattice spacing closest to the one used in this work).

Finally, we compare the doubly charmed baryons with the predictions of theo-

Group	N_f	S_H	a_t^{-1} (GeV)	L (fm)
Bowler et al. [101]	0	tree clover [140]	2.9	1.63
Lewis et al. [104]	0	D234 [141]	1.8, 2.2, 2.6	1.97
Mathur et al. [105]	0	NRQCD [140]	1.8, 2.2	2.64, 2.1
Flynn et al. [102]	0	NP clover	2.6	1.82
Chiu et al. [103]	0	ODWF [142]	2.23	1.77
Na et al. [106, 3]	2 + 1	Fermilab [71]	2.2, 1.6, 1.3	2.5
This work	2 + 1	Fermilab	1.6	2.5

Table 5.12: Summary of existing charmed baryon published calculations from lattice QCD. Please refer to the above references and references within for more details.

retical models, as shown in Fig. 5.15. Although the SELEX Collaboration has reported the first observation of doubly charmed baryons, searches by the BaBar [137], Belle [138] and Focus [143] Collaborations have not confirmed their results. This makes it interesting to look back to the theory to see where the various predictions lie. We compare with a selection of other theoretical results, such as a recent quark-model calculation [4], relativistic three-quark model [5], the relativistic quark model [6], the heavy quark effective theory [7], potential model [8], sum rules of non-relativistic QCD [9] and the Feynman-Hellmann theorem [10]. We compute the mass of Ξ_{cc} to be $3665 \pm 17 \pm 14^{+0}_{-78}$ MeV, which is higher than what SELEX observed, although less than two sigma with our estimated discretization errors; most theoretical results suggest that the Ξ_{cc} that is about 100–200 MeV higher than the SELEX experimental value. To improve this situation, we need results at multiple lattice spacings to reduce this systematic uncertainty. The Ω_{cc} mass prediction made by this work is $3763 \pm 19 \pm 26^{+13}_{-79}$ MeV, and the overall theoretical expectation is for the Ω_{cc} to be 3650–3850 MeV. We hope that upcoming experiments will be able to resolve these mysteries of doubly charmed baryons.

Our largest uncertainty presently arises from the lack of a continuum extrapolation. Therefore, in the future we plan to extend these calculations to a second lattice spacing. This will hopefully allow us to significantly reduce the size of our discretization errors. Additionally, we are extending our calculation to include the spin-3/2 spectroscopy.

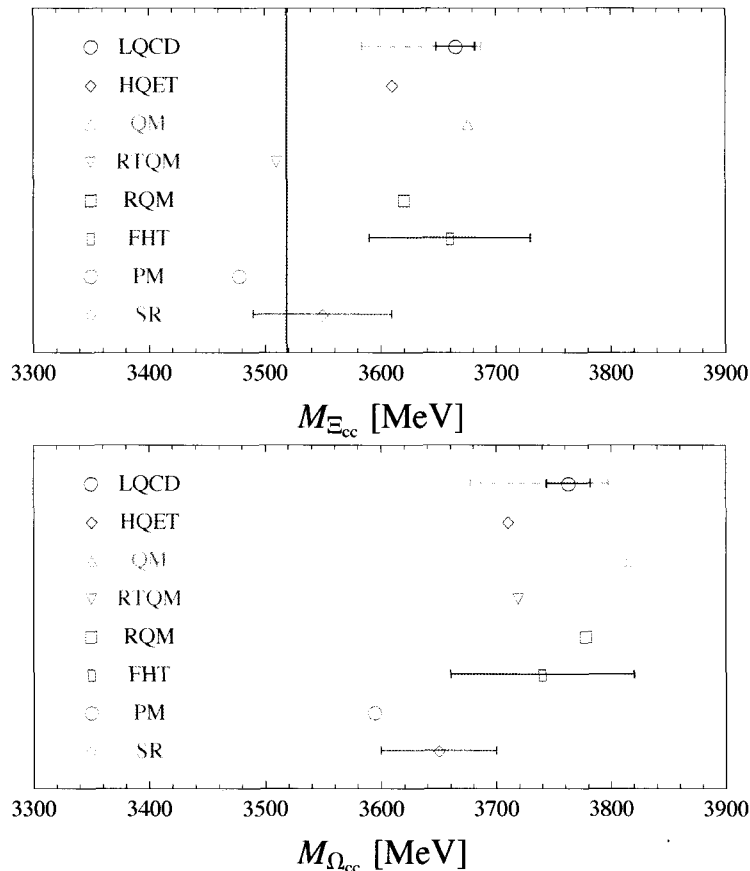


Figure 5.15: Comparison of theoretical predictions for doubly charmed baryons of spin 1/2. “LQCD” is the lattice QCD calculation done in this work with solid error bars for the statistical error and dashed bars for the total error including the estimated systematic; “QM” is taken from a recent quark-model calculation [4]; “RTQM” is the result of relativistic three-quark model [5]; “RQM” and “HQET” are from the relativistic quark model [6] and the heavy-quark effective theory [7] respectively; “PM” is the result of a potential model [8]; note that there is no error estimation done in these calculations. “SR” and “FHT” are based on the sum rules of nonrelativistic QCD [9] and the Feynman-Hellmann theorem [10] respectively, where rough uncertainties are estimated.

CHAPTER 6

Charmed Hadron Interaction

6.1 Introduction

Lattice QCD calculations of the properties of hadronic interactions such as elastic scattering phases shifts and scattering lengths have recently started to develop. Precision results have been obtained in the light meson sector for certain processes such as pion-pion, kaon-kaon and pion-kaon scattering and preliminary results for baryon-baryon scattering lengths have been presented. A review of these calculations can be found in [57]. In the heavy meson sector, only a few quenched calculations have been done [144, 145]. In this work we study scattering processes where one or both hadrons contain charm quarks in full lattice QCD.

In 2003 BaBar Collaboration discovered a positive-parity scalar charm strange meson $D_{sJ}(2317)$ with a very narrow width. CLEO Collaboration confirmed this state later. The discovery of this state has inspired heated discussion in the past several years. The key point is to understand the low mass of this state. There are several interpretations of its structure, such as being, a DK molecule, the chiral partner of D_s , a conventional $c\bar{s}$ state, coupled-channel effects between the $c\bar{s}$ state

and DK continuum etc. See reference [146] for a detailed review. The study of DK interaction is very important in understand the structure of $D_{sJ}(2317)$.

The study of the interaction of charmonium and nucleon is also very interesting. As it has been pointed out in the literature [147, 148, 149], such interaction has a direct relation to possible charmonium-nucleus bound states with binding energy of a few MeV. Unlike the traditional nuclear force that binds nucleons, in this case, there are no quark exchange diagrams, and only gluons are responsible for the binding. In other words, the charmonium nucleon force is purely a gluonic van der Waals force.

6.2 Scattering of charmed mesons (D, D_s) with light pseudoscalar mesons (π, K)

In this section, we calculate the scattering lengths of the scattering processes of charmed mesons with light pseudoscalar mesons. We need to construct the correlations functions which involve pion, kaon and charmed mesons. The operators to create these particles are

$$D^+(\mathbf{x}, t) = -\bar{d}(\mathbf{x}, t)\gamma_5 c(\mathbf{x}, t), \quad D^-(\mathbf{x}, t) = \bar{c}(\mathbf{x}, t)\gamma_5 d(\mathbf{x}, t), \quad (6.1)$$

$$D^0(\mathbf{x}, t) = -\bar{u}(\mathbf{x}, t)\gamma_5 c(\mathbf{x}, t), \quad \bar{D}^0(\mathbf{x}, t) = \bar{c}(\mathbf{x}, t)\gamma_5 u(\mathbf{x}, t), \quad (6.2)$$

$$D_s^+(\mathbf{x}, t) = -\bar{s}(\mathbf{x}, t)\gamma_5 c(\mathbf{x}, t), \quad D_s^-(\mathbf{x}, t) = \bar{c}(\mathbf{x}, t)\gamma_5 s(\mathbf{x}, t), \quad (6.3)$$

$$K^+(\mathbf{x}, t) = -\bar{s}(\mathbf{x}, t)\gamma_5 u(\mathbf{x}, t), \quad K^-(\mathbf{x}, t) = \bar{u}(\mathbf{x}, t)\gamma_5 s(\mathbf{x}, t), \quad (6.4)$$

$$K^0(\mathbf{x}, t) = -\bar{s}(\mathbf{x}, t)\gamma_5 d(\mathbf{x}, t), \quad \bar{K}^0(\mathbf{x}, t) = \bar{d}(\mathbf{x}, t)\gamma_5 s(\mathbf{x}, t), \quad (6.5)$$

$$\pi^+(\mathbf{x}, t) = -\bar{d}(\mathbf{x}, t)\gamma_5 u(\mathbf{x}, t) \quad \pi^-(\mathbf{x}, t) = \bar{u}(\mathbf{x}, t)\gamma_5 d(\mathbf{x}, t). \quad (6.6)$$

The interpolating operators for two-particle states are constructed from these single particle operators. We calculate the following five channels:

$$\mathcal{O}_{D\pi}^{I=3/2}(t) = D^+(t)\pi^+(t), \quad \mathcal{O}_{D_s\pi}(t) = D_s^+(t)\pi^+(t), \quad (6.7)$$

$$\mathcal{O}_{D\bar{K}}^{I=1}(t) = D^+(t)\bar{K}^0(t), \quad \mathcal{O}_{D\bar{K}}^{I=0}(t) = D^+(t)K^-(t) - D^0(t)\bar{K}^0(t), \quad (6.8)$$

$$\mathcal{O}_{D_sK}(t) = D_s^+(t)K^+(t), \quad (6.9)$$

where the subscripts π , K , \bar{K} and D represent the isospin triplet and doublets (π^+, π^0, π^-) , (K^+, K^0) , (\bar{K}^0, K^-) and (D^+, D^0) respectively, $D^+(t)$ is the operator $D^+(\mathbf{x}, t)$ projecting on the zero momentum, i.e.

$$D^+(t) = \frac{1}{L^{3/2}} \sum_{\mathbf{x}} D^+(\mathbf{x}, t), \quad (6.10)$$

so are $\pi^+(t)$, $K^+(t)$, $K^-(t)$, $\bar{K}^0(t)$, $D^0(t)$ and $D_s^+(t)$.

The total energy of two interacting hadrons (h_1 and h_2) is obtained from the four-point correlation function:

$$C_{h_1h_2}(t) = \langle \mathcal{O}_{h_1h_2}(t)^\dagger \mathcal{O}_{h_1h_2}(0) \rangle. \quad (6.11)$$

To be explicit, the four point correlation function for the $D\pi(I = 3/2)$ channel is

$$C_{D\pi}^{I=3/2} = \langle D^-(t)\pi^-(t)D^+(0)\pi^+(0) \rangle. \quad (6.12)$$

The correlation functions for the other channels have similar form.

To extract the energy shift ΔE , we define a ratio $R_{h_1h_2}(t)$:

$$R_{h_1h_2}(t) = \frac{C_{h_1h_2}(t)}{C_{h_1}(t)C_{h_2}(t)} \longrightarrow A \exp(-\Delta E \cdot t), \quad (6.13)$$

where $C^{h_1}(t)$ and $C^{h_2}(t)$ are two-point functions. ΔE is obtained by fitting $R^{h_1-h_2}(t)$ to a single exponential in a region where the effective energy shift exhibits a plateau.

6.2.1 Numerical results

For each channel, we calculate the ratio $R_{h_1 h_2}$ at two different charm quark masses and four different light valence quark masses. Fig. 6.1 shows the effective energy shifts of each channel with the lowest light quark mass and the input charm quark mass $m_0 = 0.2034$. The fitted energy shifts and the fitting ranges are indicated by the grey bars in these plots. The height of the grey bars show the statistical errors. The effective energy shift plots for other ensembles are similar.

The energy shifts are extrapolated to the physical charm quark mass using the same method as we used for the charmed baryon spectrum, which is explained in section 5.3.2. The scattering lengths are then calculated for each ensemble using Lüscher's finite volume method introduced in section 4.3.

The scattering lengths have to be extrapolated to the physical light quark mass to make contact with experiment. The scattering lengths of heavy mesons and light pseudoscalar mesons have been studied using heavy meson chiral perturbation theory in references [46, 47]. The χ PT formulas of the scattering lengths of the five channels we study to $\mathcal{O}(p^3)$ are [47]

$$\begin{aligned}
8\pi\left(1 + \frac{m_K}{m_D}\right)a_{D\bar{K}}^{I=1} &= -\frac{2m_K}{f_K^2} + C_1 \frac{m_K^2}{f_K^2} + \frac{m_K^2}{4\pi^2 f_K^4} \left\{ -m_K \left(3 - \ln \frac{m_\pi}{\lambda} - 2 \ln \frac{m_K}{\lambda} - 3 \ln \frac{m_\eta}{\lambda} \right) \right. \\
&\quad + \sqrt{m_K^2 - m_\pi^2} \ln \frac{m_K + \sqrt{m_K^2 - m_\pi^2}}{m_\pi} - 3 \sqrt{m_\eta^2 - m_K^2} \arccos \frac{m_K}{m_\eta} \\
&\quad \left. + \frac{1}{3} g^2 \pi \left(3m_\eta + \frac{2m_\pi^2}{m_\eta + m_\pi} \right) \right\} - 8\kappa \frac{m_K^3}{f_K^2}, \tag{6.14}
\end{aligned}$$

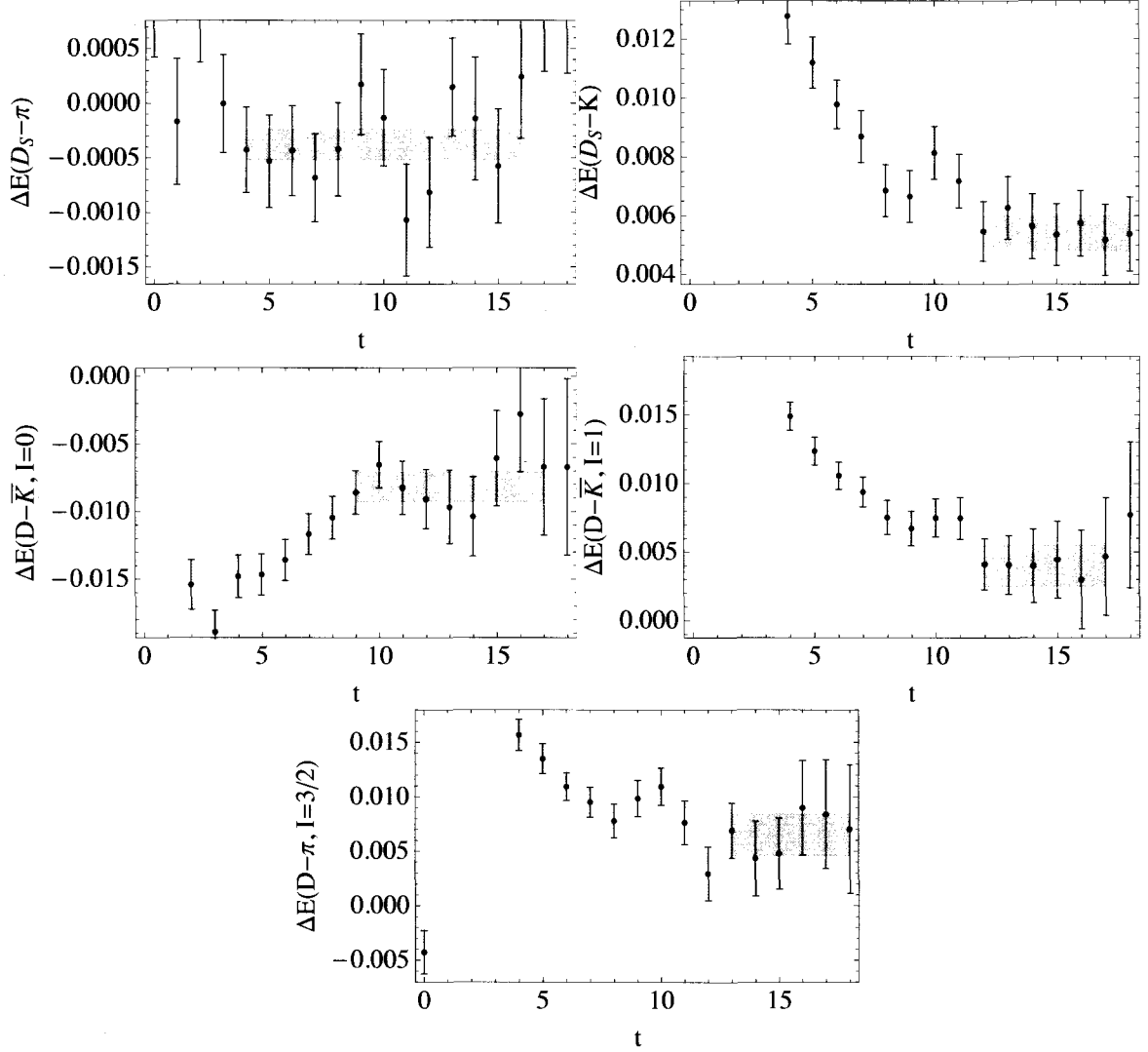


Figure 6.1: Effective energy shifts plots of the scattering channels $D_s - \pi$, $D_s - K$, $D - \bar{K}(I = 0)$, $D - \bar{K}(I = 1)$, $D - \pi(I = 3/2)$. All plots are for ensemble m007. The grey bars show the fitted energy shifts and the fitting ranges. The height of the grey bars show the statistical errors.

$$\begin{aligned}
8\pi\left(1 + \frac{m_K}{m_D}\right)a_{DK}^{I=0} &= \frac{2m_K}{f_K^2} + C_0 \frac{m_K^2}{f_K^2} + \frac{m_K^2}{4\pi^2 f_K^4} \left\{ 3m_K \left(1 + \ln \frac{m_\pi}{\lambda} - 2 \ln \frac{m_K}{\lambda} - \ln \frac{m_\eta}{\lambda}\right) \right. \\
&+ 3\sqrt{m_K^2 - m_\pi^2} \ln \frac{m_K + \sqrt{m_K^2 - m_\pi^2}}{m_\pi} + 3\sqrt{m_\eta^2 - m_K^2} \arccos \frac{m_K}{m_\eta} \\
&\left. - \frac{1}{3}g^2\pi\left(5m_\eta + \frac{6m_\pi^2}{m_\eta + m_\pi}\right) \right\} + 8\kappa \frac{m_K^3}{f_K^2}, \tag{6.15}
\end{aligned}$$

$$\begin{aligned}
8\pi\left(1 + \frac{m_K}{m_{D_s}}\right)a_{D_s K} &= -\frac{2m_K}{f_K^2} + C_1 \frac{m_K^2}{f_K^2} + \frac{3m_K^2}{4\pi^2 f_K^4} \left\{ -m_K \left(1 - \ln \frac{m_\pi}{\lambda} - \ln \frac{m_\eta}{\lambda}\right) \right. \\
&+ \sqrt{m_K^2 - m_\pi^2} \ln \frac{m_K + \sqrt{m_K^2 - m_\pi^2}}{m_\pi} - \sqrt{m_\eta^2 - m_K^2} \arccos \frac{m_K}{m_\eta} \\
&\left. + \frac{4}{9}g^2\pi m_\eta \right\} - 8\kappa \frac{m_K^3}{f_K^2}, \tag{6.16}
\end{aligned}$$

$$\begin{aligned}
8\pi\left(1 + \frac{m_\pi}{m_D}\right)a_{D\pi}^{I=3/2} &= -\frac{2m_\pi}{f_\pi^2} + C_1 \frac{m_\pi^2}{f_\pi^2} + \frac{m_\pi^2}{2\pi^2 f_\pi^4} \left\{ -m_\pi \left(\frac{3}{2} - 2 \ln \frac{m_\pi}{\lambda} - \ln \frac{m_K}{\lambda}\right) \right. \\
&- \sqrt{m_K^2 - m_\pi^2} \arccos \frac{m_K}{m_\pi} + \frac{1}{12}g^2\pi(9m_\pi - m_\eta) \left. \right\} \\
&- 8\kappa \frac{m_\pi^3}{f_\pi^2}, \tag{6.17}
\end{aligned}$$

$$8\pi\left(1 + \frac{m_\pi}{m_{D_s}}\right)a_{D_s \pi} = (C_1 + C_0) \frac{m_\pi^2}{2f_\pi^2} + \frac{m_\pi^2}{6\pi^2 f_\pi^4} \left\{ -3\sqrt{m_K^2 - m_\pi^2} - g^2 m_\eta \right\}. \tag{6.18}$$

where λ is the renormalization scale, the coefficients C_0 , C_1 , g^2 and κ are to be determined from the fits. C_0 , C_1 and κ are dimensionful. To minimize the contamination from a particular scale-setting method, it is preferable to perform dimensionless ex-

trapolations. To do this, we rewrite the scattering length formulas in dimensionless form:

$$\begin{aligned}
8\pi m_K \left(1 + \frac{m_K}{m_D}\right) a_{D\bar{K}}^{I=1} &= -\frac{2m_K^2}{f_K^2} + C_1 f_0 \frac{m_K^3}{f_K^2 f_\pi} \\
&+ \frac{m_K^3}{4\pi^2 f_K^4} \left\{ -m_K \left(3 - \ln \frac{m_\pi}{f_\pi} - 2 \ln \frac{m_K}{f_\pi} - 3 \ln \frac{m_\eta}{f_\pi}\right) \right. \\
&+ \sqrt{m_K^2 - m_\pi^2} \ln \frac{m_K + \sqrt{m_K^2 - m_\pi^2}}{m_\pi} - 3 \sqrt{m_\eta^2 - m_K^2} \arccos \frac{m_K}{m_\eta} \\
&\left. + \frac{1}{3} g^2 \pi \left(3m_\eta + \frac{2m_\pi^2}{m_\eta + m_\pi}\right) \right\} - 8\kappa f_0^2 \frac{m_K^4}{f_K f_\pi^2}, \tag{6.19}
\end{aligned}$$

$$\begin{aligned}
8\pi m_K \left(1 + \frac{m_K}{m_D}\right) a_{D\bar{K}}^{I=0} &= \frac{2m_K^2}{f_K^2} + C_0 f_0 \frac{m_K^3}{f_K^2 f_\pi} + \frac{m_K^3}{4\pi^2 f_K^4} \left\{ 3m_K \left(1 + \ln \frac{m_\pi}{f_\pi} - 2 \ln \frac{m_K}{f_\pi} - \ln \frac{m_\eta}{f_\pi}\right) \right. \\
&+ 3 \sqrt{m_K^2 - m_\pi^2} \ln \frac{m_K + \sqrt{m_K^2 - m_\pi^2}}{m_\pi} + 3 \sqrt{m_\eta^2 - m_K^2} \arccos \frac{m_K}{m_\eta} \\
&\left. - \frac{1}{3} g^2 \pi \left(5m_\eta + \frac{6m_\pi^2}{m_\eta + m_\pi}\right) \right\} + 8\kappa f_0^2 \frac{m_K^4}{f_K f_\pi^2}, \tag{6.20}
\end{aligned}$$

$$\begin{aligned}
8\pi m_K \left(1 + \frac{m_K}{m_{D_s}}\right) a_{D_s K} &= -\frac{2m_K^2}{f_K^2} + C_1 f_0 \frac{m_K^3}{f_K^2 f_\pi} + \frac{3m_K^3}{4\pi^2 f_K^4} \left\{ -m_K \left(1 - \ln \frac{m_\pi}{f_\pi} - \ln \frac{m_\eta}{f_\pi}\right) \right. \\
&+ \sqrt{m_K^2 - m_\pi^2} \ln \frac{m_K + \sqrt{m_K^2 - m_\pi^2}}{m_\pi} - \sqrt{m_\eta^2 - m_K^2} \arccos \frac{m_K}{m_\eta} \\
&\left. + \frac{4}{9} g^2 \pi m_\eta \right\} - 8\kappa f_0^2 \frac{m_K^4}{f_K f_\pi^2}, \tag{6.21}
\end{aligned}$$

$$\begin{aligned}
8\pi m_\pi \left(1 + \frac{m_\pi}{m_D}\right) a_{D\pi}^{I=3/2} &= -\frac{2m_\pi^2}{f_\pi^2} + C_1 f_0 \frac{m_\pi^3}{f_\pi^3} + \frac{m_\pi^3}{2\pi^2 f_\pi^4} \left\{ -m_\pi \left(\frac{3}{2} - 2 \ln \frac{m_\pi}{f_\pi} - \ln \frac{m_K}{f_\pi} \right) \right. \\
&\quad \left. - \sqrt{m_K^2 - m_\pi^2} \arccos \frac{m_K}{m_\pi} + \frac{1}{12} g^2 \pi (9m_\pi - m_\eta) \right\} \\
&\quad - 8\kappa f_0^2 \frac{m_\pi^4}{f_\pi^4}, \tag{6.22}
\end{aligned}$$

$$8\pi m_\pi \left(1 + \frac{m_\pi}{m_{D_s}}\right) a_{D_s\pi} = (C_1 + C_0) f_0 \frac{m_\pi^3}{2f_\pi^3} + \frac{m_\pi^3}{6\pi^2 f_\pi^4} \left\{ -3\sqrt{m_K^2 - m_\pi^2} - g^2 m_\eta \right\}. \tag{6.23}$$

The coefficients $C_0 f_0$, $C_1 f_0$, g^2 and κf_0^2 are dimensionless. Here we have used the chiral expansion of f_π

$$f_\pi = f_0 (1 + \mathcal{O}(m_\pi^2)). \tag{6.24}$$

The $\mathcal{O}(m_\pi^2)$ corrections can be ignored at the order we are considering. We choose the renormalization scale λ to be the physical value of f_π . The differences between the physical f_π and the values evaluated on each ensemble are higher order in chiral expansion and thus are ignored.

There are four dimensionless coefficients $C_0 f_0$, $C_1 f_0$, g^2 and κf_0^2 to be determined. By fitting the five channels simultaneously, we have 20 data points totally. To ensure the convergence of the chiral expansion, it is desirable to fit the data at the light values of the quark masses. We have four different light quark masses in our data set, corresponding to the four ensembles (m007, m010, m020 and m030) with pion masses approximately 290MeV, 350MeV, 490MeV and 590MeV respectively. We perform three fits by choosing three different fitting ranges of light quark mass. In ‘‘Fit1’’, we fit the data from all four ensembles. In ‘‘Fit2’’, we fit the data from the lightest three

Ensemble	m007	m010	m020	m030
m_π	0.1842	0.2238	0.3113	0.3752
m_K	0.3682	0.3791	0.4058	0.4311
m_η	0.4827	0.4846	0.4816	0.4805
f_π	0.09273	0.09597	0.10179	0.10759
f_K	0.1079	0.1087	0.1103	0.1122
m_D	1.2081	1.2083	1.2226	1.2320
m_{D_s}	1.2637	1.2635	1.2614	1.2599

Table 6.1: The values of m_π , m_K , m_η , f_π , f_K , m_D and m_{D_s} in lattice units.

Fitting Range	$C_0 f_0$	$C_1 f_0$	g^2	κf_0^2	χ^2	dof	Q
m007-m030	0.25(7)	0.73(7)	0.00(1)	0.034(2)	89.4	16	0.00
m007-m020	0.26(7)	0.80(8)	-0.00(3)	0.036(2)	40.5	11	0.00
m007-m010	0.33(8)	0.78(8)	-0.02(4)	0.035(2)	9.5	6	0.15

Table 6.2: The results of fitting the scattering lengths to the χ PT formulas.

ensembles (m007, m010 and m020). In ‘‘Fit3’’, we fit the data from the lightest two ensembles (m007 and m010). The values of m_π , m_K , m_η , f_π and f_K for each ensemble, which are needed for the fits, have been calculated in Ref. [1], m_D and m_{D_s} are from our calculation in this work. The numbers are collected in Table 6.1. Table 6.2 shows the fitting results of the three fits. It is not surprising that the χ^2 reduces rapidly when we constrain the fit to the light ensembles. Note that the axial coupling g^2 turns out to be consistent with zero. We encountered the same phenomenon in the fitting of charmed baryon masses. The extrapolated scattering lengths are presented in Table 6.3. Since the χ^2 of ‘‘Fit1’’ and ‘‘Fit2’’ are too large to be considered as reliable fits, we choose to trust the results from ‘‘Fit3’’.

In this work we didn’t calculate the scattering lengths of the channels $DK(I = 0)$, $DK(I = 1)$, $D\pi(I = 1/2)$ and $D_s K$ due to the simulation difficulties. However, once we have determined the coefficients in the chiral perturbation theory, we can predict the scattering lengths of these channels. The χ PT formulas for these channels are

Channels	a(fm) Fit1	a(fm) Fit2	a(fm) Fit3
$DK(I = 1)$	-0.227(7)	-0.22(1)	-0.22(1)
$D\bar{K}(I = 0)$	0.74(1)	0.76(1)	0.80(1)
$D_s K$	-0.194(7)	-0.182(8)	-0.181(8)
$D\pi(I = 3/2)$	-0.106(3)	-0.102(4)	-0.103(4)
$D_s \pi$	-0.0056(5)	-0.0033(6)	-0.0011(8)

Table 6.3: The scattering lengths extrapolated to the physical light quark masses. “Fit1” fits all four ensembles. “Fit2” fits the lightest three ensembles. “Fit3” fits the lightest two ensembles. The uncertainty presented in the parentheses is statistical.

[47] :

$$\begin{aligned}
8\pi m_K \left(1 + \frac{m_K}{m_D}\right) a_{DK}^{I=0} &= \frac{4m_K^2}{f_K^2} + C_1 f_0 \frac{m_K^3}{f_K^2 f_\pi} + \frac{m_K^3}{2\pi^2 f_K^4} \left\{ 3m_K \left(1 - \ln \frac{m_K}{f_\pi} - \ln \frac{m_\eta}{f_\pi}\right) \right. \\
&\quad \left. - 3\sqrt{m_\eta^2 - m_K^2} \arccos \frac{-m_K}{m_\eta} \right. \\
&\quad \left. + \frac{1}{6} g^2 \pi \left(7m_\eta + \frac{6m_\pi^2}{m_\eta + m_\pi}\right) \right\} + 16\kappa f_0^2 \frac{m_K^4}{f_K^2 f_\pi^2}, \quad (6.25)
\end{aligned}$$

$$\begin{aligned}
8\pi m_K \left(1 + \frac{m_K}{m_D}\right) a_{DK}^{I=1} &= (C_1 + C_0) f_0 \frac{m_K^3}{2f_K^2 f_\pi} + \frac{m_K^3}{2\pi^2 f_K^4} \left\{ -m_K \left(\ln \frac{m_\pi}{f_\pi} - \ln \frac{m_K}{f_\pi}\right) \right. \\
&\quad \left. + \sqrt{m_K^2 - m_\pi^2} \left(i\pi - \ln \frac{m_K + \sqrt{m_K^2 - m_\pi^2}}{m_\pi}\right) \right. \\
&\quad \left. - \frac{1}{6} g^2 \pi \left(m_\eta + \frac{2m_\pi^2}{m_\eta + m_\pi}\right) \right\}, \quad (6.26)
\end{aligned}$$

Channels	$D\pi(I = 1/2)$	$DK(I = 0)$	$DK(I = 1)$	D_sK
a(fm)	0.298(8)	1.3(1)	0.217(6) + 0.176i	0.77(7) + 0.268i

Table 6.4: Scattering lengths of $D\pi(I = 1/2)$, $DK(I = 0)$, $DK(I = 1)$ and D_sK predicted from chiral fits. Statistical errors are presented in the parentheses.

$$\begin{aligned}
8\pi m_K \left(1 + \frac{m_K}{m_{D_s}}\right) a_{D_s\bar{K}} &= \frac{2m_K^2}{f_K^2} + C_1 f_0 \frac{m_K^3}{f_K^2 f_\pi} + \frac{3m_K^3}{4\pi^2 f_K^4} \left\{ m_K \left(1 - \ln \frac{m_\pi}{f_\pi} - \ln \frac{m_\eta}{f_\pi}\right) \right. \\
&\quad \left. + \sqrt{m_K^2 - m_\pi^2} \left(i\pi - \ln \frac{m_K + \sqrt{m_K^2 - m_\pi^2}}{m_\pi}\right) \right. \\
&\quad \left. - \sqrt{m_\eta^2 - m_K^2} \arccos \frac{-m_K}{m_\eta} + \frac{4}{9} g^2 \pi m_\eta \right\} \\
&\quad + 8\kappa f_0^2 \frac{m_K^4}{f_K^2 f_\pi^2}, \tag{6.27}
\end{aligned}$$

$$\begin{aligned}
8\pi m_\pi \left(1 + \frac{m_\pi}{m_D}\right) a_{D\pi}^{I=1/2} &= \frac{4m_\pi^2}{f_\pi^2} + C_1 f_0 \frac{m_\pi^3}{f_\pi^3} + \frac{m_\pi^3}{2\pi^2 f_\pi^4} \left\{ m_\pi \left(3 - 4 \ln \frac{m_\pi}{f_\pi} - 2 \ln \frac{m_K}{f_\pi}\right) \right. \\
&\quad \left. - \sqrt{m_K^2 - m_\pi^2} \left(\frac{3}{2}\pi - 2 \arccos \frac{m_\pi}{m_K}\right) + \frac{1}{12} g^2 \pi (9m_\pi - m_\eta) \right\} \\
&\quad + 16\kappa f_0^2 \frac{m_\pi^4}{f_\pi^4}. \tag{6.28}
\end{aligned}$$

Substitute the values of $C_1 f_0$, $C_0 f_0$, g^2 and κf_0^2 obtained from ‘‘Fit3’’ into the Eq. 6.25 – 6.28, we get the scattering lengths of $DK(I = 0)$, $DK(I = 1)$, $D\pi(I = 1/2)$ and D_sK , which are presented in Table 6.4.

6.2.2 Discussion

The positive sign of $a_{DK}^{I=0}$, $a_{DK}^{I=0}$, $a_{DK}^{I=1}$, $a_{D_s\bar{K}}$ and $a_{D\pi}^{I=1/2}$ indicates that the interactions in these channels are all attractive. The attraction in the $DK(I = 0)$ channel is quite strong. However, we are not able to tell whether it is strong enough to form

a bound state such as a DK molecular state. It is interesting that the $DK(I = 1)$ also have relatively strong interaction since there is no quark pair annihilation in this channel. The possibility to form a four-quark resonance is not excluded. The $D\bar{K}(I = 1)$, $D_s K$, $D\pi(I = 3/2)$ and $D_s\pi$ channels have repulsive interactions. The interaction of $D_s\pi$ is very weak, which is expected. The $D_s\pi$ and $DK(I = 1)$ channels are mixed since they have the same quantum numbers. To perform more reliable analysis of these two channels, we need to construct the correlation matrix and use the variational method to extract the energies of the two channels.

6.3 Scattering of charmonium with light hadrons

In this section we calculate the scattering lengths of the scattering processes of charmonium (η_c and J/Ψ) with the light hadrons (ρ , N). The interpolating operators for these particles are:

$$\begin{aligned}\eta_c(\mathbf{x}, t) &= \bar{c}(\mathbf{x}, t)\gamma_5 c(\mathbf{x}, t), & J/\Psi_i(\mathbf{x}, t) &= \bar{c}(\mathbf{x}, t)\gamma_i c(\mathbf{x}, t), \\ \rho_i(\mathbf{x}, t) &= \bar{d}(\mathbf{x}, t)\gamma_i u(\mathbf{x}, t), & N(\mathbf{x}, t) &= \epsilon_{abc}[u_a^T(\mathbf{x}, t)C\gamma_5 d_b(\mathbf{x}, t)]u_c(\mathbf{x}, t).\end{aligned}\quad (6.29)$$

where C is the charge conjugation matrix, $C = \gamma_4\gamma_2$.

The four point correlation functions are given by

$$C_{ij}^{\eta_c-\rho}(t) = \langle \eta_c^\dagger(t)\rho_i^\dagger(t)\eta_c(0)\rho_j(0) \rangle \quad (6.30)$$

$$C^{\eta_c-N}(t) = \langle \eta_c^\dagger(t)N^\dagger(t)\eta_c(0)N(0) \rangle \quad (6.31)$$

$$C_{ij,kl}^{J/\Psi-\rho} = \langle J/\Psi_i^\dagger(t)\rho_j^\dagger(t)J/\Psi_k(0)\rho_l(0) \rangle \quad (6.32)$$

$$C_{ij}^{J/\Psi-N} = \langle J/\Psi_i^\dagger(t)N^\dagger(t)J/\Psi_j(0)N(0) \rangle \quad (6.33)$$

For s-wave $\eta_c - \rho$ scattering, the total spin is 1, we simply take the average of the

diagonal correlation matrix $\frac{1}{3} \sum_{i=1}^3 C_{ii}^{\eta_c - \rho}(t)$. For the s-wave $J\Psi - \rho$ scattering, the spin can take three different values: $s=0$, $s=1$, $s=2$. We need to disentangle each spin contribution from the four point correlation function. The four point correlation function can be expressed by

$$C_{ij,kl}^{J/\psi-\rho}(t) = C_{J/\Psi-\rho}^0(t)P_{ij,kl}^0 + C_{J/\Psi-\rho}^1(t)P_{ij,kl}^1 + C_{J/\Psi-\rho}^2(t)P_{ij,kl}^2, \quad (6.34)$$

where P^0 , P^1 and P^2 are spin projector to $s=0$, $s=1$ and $s=2$ respectively. They are given by

$$\begin{aligned} P_{ij,kl}^0 &= \frac{1}{3}\delta_{ij}\delta_{kl} \\ P_{ij,kl}^1 &= \frac{1}{2}(\delta_{ik}\delta_{jl} - \delta_{il}\delta_{jk}) \\ P_{ij,kl}^2 &= \frac{1}{2}(\delta_{ik}\delta_{jl} + \delta_{il}\delta_{jk}) - \frac{1}{3}\delta_{ij}\delta_{kl}. \end{aligned} \quad (6.35)$$

The disentangled correlation functions for different spin channels are

$$\begin{aligned} C_{J/\Psi-\rho}^0(t) &= \frac{1}{3} \sum_{i,j=1}^3 C_{ii,jj}^{J/\Psi-\rho}(t), \\ C_{J/\Psi-\rho}^1(t) &= \frac{1}{6} \sum_{i,j=1}^3 (C_{ij,ij}^{J/\Psi-\rho}(t) - C_{ij,ji}^{J/\Psi-\rho}(t)), \\ C_{J/\Psi-\rho}^2(t) &= \frac{1}{10} \sum_{i,j=1}^3 (C_{ij,ij}^{J/\Psi-\rho}(t) + C_{ij,ji}^{J/\Psi-\rho}(t) - \frac{2}{3}C_{ii,jj}^{J/\Psi-\rho}(t)). \end{aligned} \quad (6.36)$$

For the s-wave $J/\Psi - N$ scattering, the spin can be $s=1/2$ and $s=3/2$. The four-point correlation function can be decomposed into spin-1/2 and spin-3/2 components

$$C_{ij}^{J/\Psi-N}(t) = C_{J\Psi-N}^{1/2}P_{ij}^{1/2} + C_{J/\Psi-N}^{3/2}P_{ij}^{3/2} \quad (6.37)$$

Ensemble	m007	m010	m020	m030
ΔE_{η_c-N}	-0.004(5)	-0.0012(9)	-0.000(2)	-0.0019(3)
$\Delta E_{\eta_c-\rho}$	0.0001(3)	-0.0004(3)	-0.0003(5)	-0.0011(3)
$\Delta E_{J/\Psi-N}^{1/2}$	-0.001(2)	-0.007(2)	-0.0033(6)	-0.0077(6)
$\Delta E_{J/\Psi-N}^{3/2}$	0.001(2)	-0.005(2)	-0.0028(5)	-0.0051(8)
$\Delta E_{J/\Psi-\rho}^0$	-0.0004(6)	-0.002(1)	-0.0007(2)	-0.0014(3)
$\Delta E_{J/\Psi-\rho}^1$	-0.0005(6)	-0.002(1)	-0.0007(2)	-0.0014(3)
$\Delta E_{J/\Psi-\rho}^2$	-0.0005(6)	-0.002(1)	-0.0007(2)	-0.0014(3)

Table 6.5: Fitted energy shifts of the scattering of η_c-N , $\eta_c-\rho$, $J/\Psi-\rho$ and $J/\Psi-N$. All values are in lattice units. The statistical errors are indicated in the parentheses.

The spin projection operators for spin-1/2 and spin-3/2 are given by

$$P_{ij}^{1/2} = \frac{1}{3}\gamma_i\gamma_j, \quad P_{ij}^{3/2} = \delta_{ij} - \frac{1}{3}\gamma_i\gamma_j. \quad (6.38)$$

Then, the spin-projected correlation functions are

$$\begin{aligned} C_{J/\Psi-N}^{1/2}(t) &= \frac{1}{3} \sum_{i,j=1}^3 \gamma_i\gamma_j C_{ji}^{J/\Psi-N}, \\ C_{J/\Psi-N}^{3/2}(t) &= \frac{1}{2} \sum_{i=1}^3 C_{ii}^{J/\Psi-N}(t) - \frac{1}{6} \sum_{i,j=1}^3 \gamma_i\gamma_j C_{ji}^{J/\Psi-N}(t), \end{aligned} \quad (6.39)$$

As we did for the scattering of charmed mesons with light pseudoscalar mesons, the energy shifts ΔE are obtained by fitting $R_{h_1 h_2}(t)$, which is the ratio of the four point correlation functions to the multiplication of the two relative two-point correlation functions, to a single exponential. The fitted values of ΔE with input charm quark mass $m_0 = 0.2034$ are presented in Table 6.5. The values of ΔE with charm quark mass $m_0 = 0.2100$ are very close to those with $m_0 = 0.2034$. We extrapolate ΔE linearly to the physical charm quark mass determined in Sec. 5.3.2. As typical examples, the effective energy shift plots for the ensemble m007 are shown in Fig. 6.2.

As seen in Table 6.5, the energy shifts are quite small. They are generally nega-

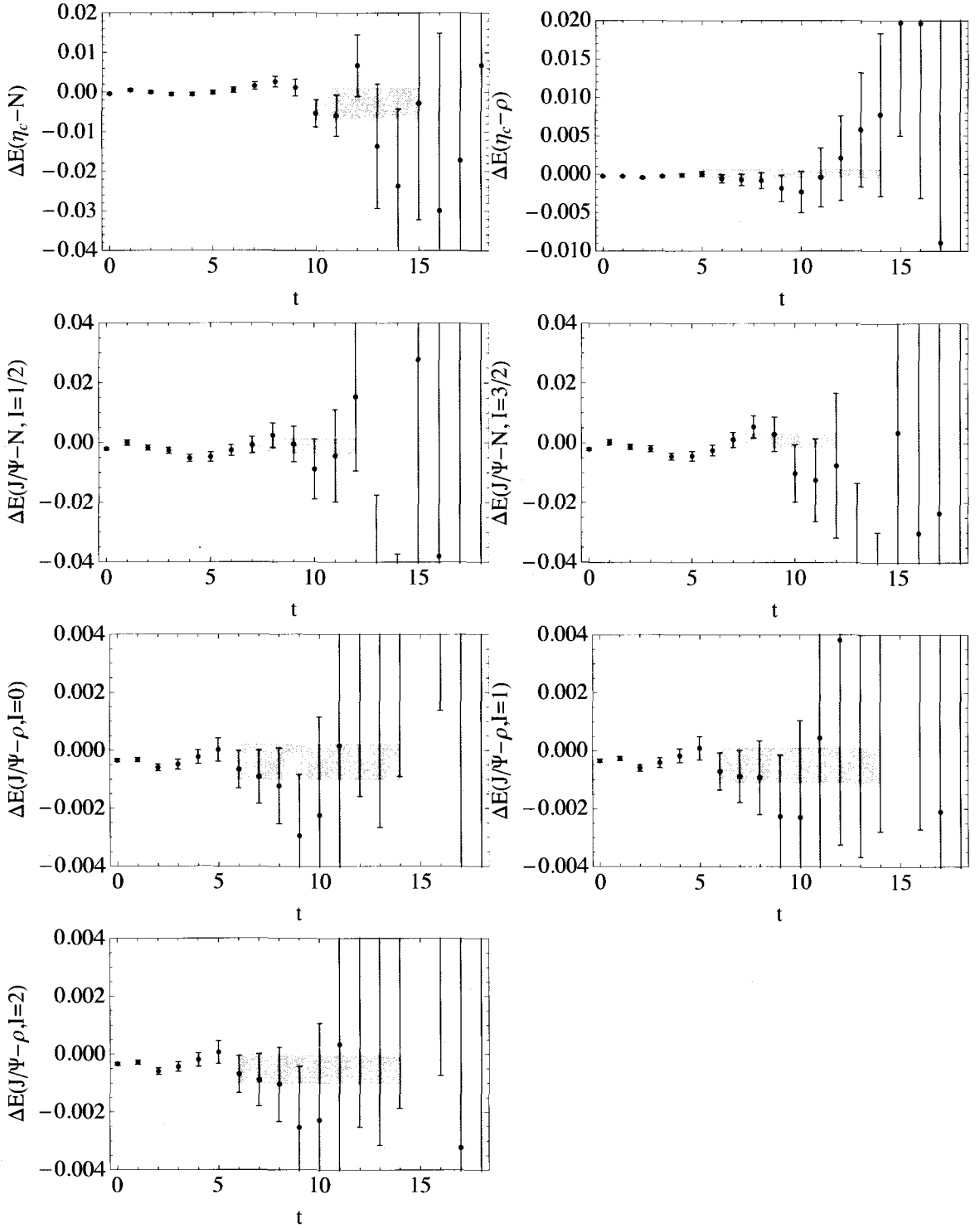


Figure 6.2: Effective energy shifts of the scattering of charmonium (η_c and J/ψ) with light hadrons (ρ and nucleon). All plots are for ensemble m007. The grey bars indicate the fitted energy shifts and the fitting ranges. The height of the grey bars show the statistical errors.

tive, which means that the interactions in these channels are attractive. However, the signals become very noisy at large t , which produce relatively large statistical error bars. In some channels, the energy shifts are consistent with zero within statistical error.

For each ensemble, the scattering length is calculated from Eq. 4.49. The scattering lengths have to be extrapolated to the physical light quark mass. Since the scattering processes of charmonium with light hadron have not been studied in chiral perturbation theory, we perform simple polynomial extrapolation

$$m_\pi(1 + \frac{m}{M})a = c_1 \frac{m_\pi^2}{f_\pi^2} + c_2 \frac{m_\pi^3}{f_\pi^3}, \quad (6.40)$$

where m is the mass of the light hadron, M is the mass of the charmonium. The factor $1 + \frac{m}{M}$ is inspired by the existing formulas for the scattering length of light-heavy scattering processes, e. g. Eq. 6.14 – Eq. 6.18. In the limit $m_\pi \rightarrow 0$, the scattering lengths should approach zero, so the lowest term in the expansion of a is $\sim m_\pi$. Considering that we only have four light quark masses, we keep the expansion to the second lowest order. Thus we have two coefficients c_1 and c_2 to be determined from the fits. The extrapolation is performed individually for each channel. The two coefficients are different for different channels. Fig. 6.3 shows the fits of all the channels. In these plots, the blue points are the data from lattice calculation. The shaded bands indicate the standard deviation allowed regions. The χ^2 per degree of freedom of the fits for all these channels range from $0.5 \sim 1.5$. In Fig. 6.3 we can see that the scattering lengths of all these channels approach zero at the lightest ensemble. The scattering lengths extrapolated to the physical point are all consistent with zero within statistical error except for the spin-3/2 $J/\Psi - N$ channel, which has very tiny non-zero scattering length $-0.002(1)\text{fm}$.

Some of the channels we study are mixed with other channels. The spin-1 $J/\Psi - \rho$ channel may contain contamination of the isospin-1 $D - \bar{D}^*$ channels. The spin-0 $J/\Psi - \rho$ channel is mixed with the isospin-1 $D\bar{D}$ channel. The spin-2 $J/\Psi - \rho$ channel does not contain any contamination. For the $J/\Psi - N$ system, the spin-3/2 channel is free of contamination, while the spin-1/2 channel is mixed with $\eta_c - N$ channel. Therefore, strictly speaking, the spin-2 $J/\Psi - \rho$ and spin-3/2 $J/\Psi - N$ channels are safe channels in extracting s-wave scattering lengths from Lüscher's formula. However, for the $J/\Psi - \rho$ system, we didn't find any difference among different spin channels. The mixed channel problem is expected to be treated more carefully in our future work by applying the variational method.

In conclusion, we find very weak interaction between the charmonium and the light hadrons. It is likely that the interaction of J/Ψ with nucleon is attractive. Statistics need to be improved to obtain more accurate data. Studying the volume dependence of the interaction will be helpful to determine whether there is a J/Ψ -nucleon bound state.

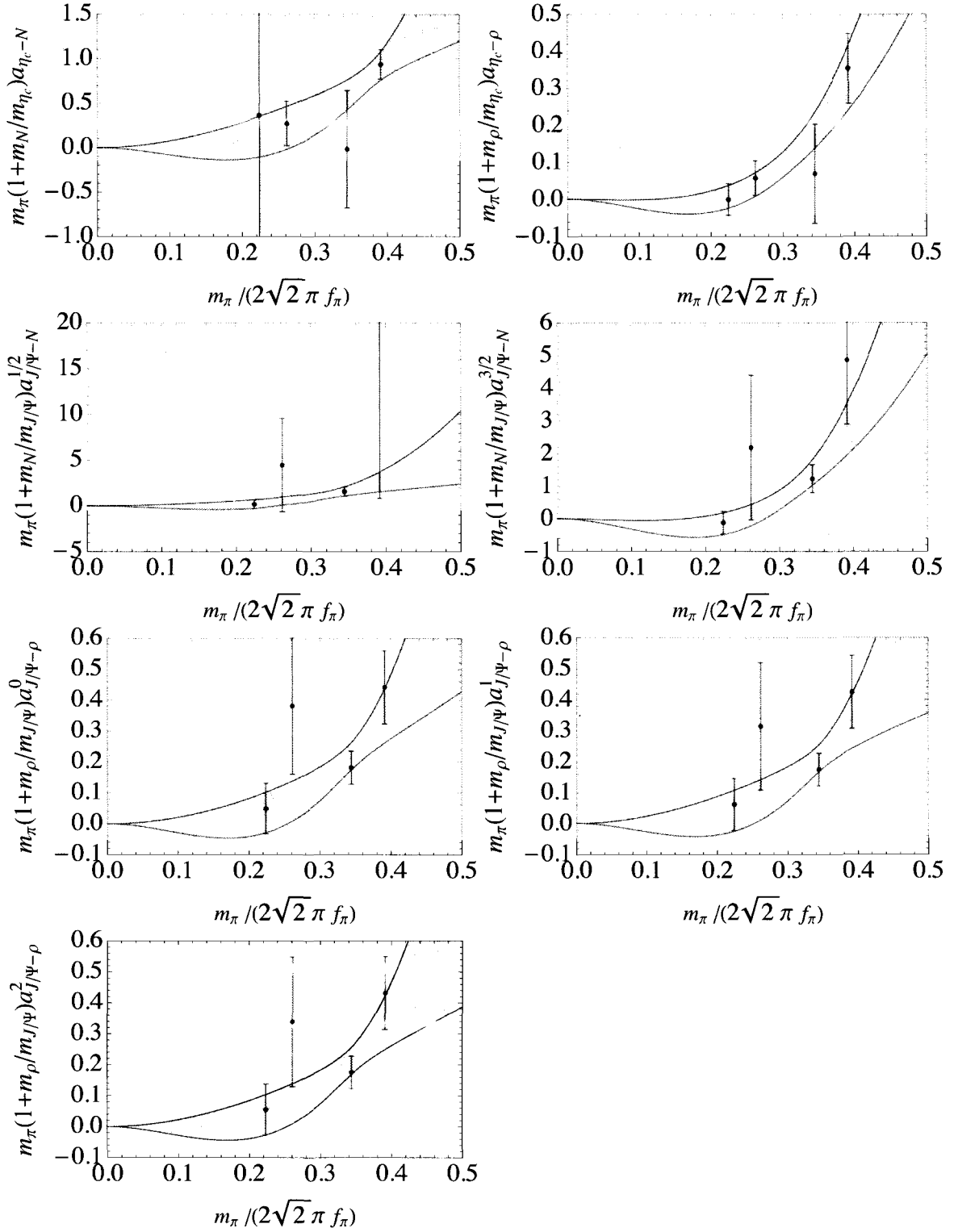


Figure 6.3: The scattering lengths of charmonium with light hadron fitted to Eq. 6.40. The blue points are the values from lattice calculation. The blue bands indicate the standard deviation allowed regions of the fits.

CHAPTER 7

Conclusions

In this work we study the charmed hadron spectrum and interactions in full lattice QCD. Relativistic heavy quark action is used for charm quark. For the light quarks we use domain-wall fermions in the valence sector and improved Kogut-Susskind sea quarks. The ensembles are generated by MILC collaboration at four values of light-quark masses with the corresponding pion mass range from 290 MeV to 590 MeV. In the heavy quark action, the anisotropy is tuned nonperturbatively by calculating the dispersion relation of charmonium and charmed mesons; the bare charm quark mass is determined from the spin-averaged mass of η_c and J/Ψ . The hyperfine splitting of J/Ψ and η_c as well as the masses of low-lying charmonium (χ_{c0} , χ_{c1} and h_c) are calculated to test the action.

The details of the calculations of the charmed baryon spectrum are presented in chapter 5. The baryon masses are extrapolated to the physical light quark mass using SU(2) HB χ PT formulas. The mass splittings between charmed baryons are calculated, providing an alternative way to estimate the charmed baryon masses using the experimental value of the mass of a reference state. We take the values determined from the mass splittings as our main results because the discretization errors are

partly canceled in the splittings. The discretization errors are estimated using various symmetries and power counting. Our results for singly charmed baryons are in good agreement with experiment within the systematics. For the doubly charmed baryons, the mass of Ξ_{cc} is determined to be $M_{\Xi_{cc}} = 3665 \pm 17 \pm 14_{-78}^{+0}$ MeV, which is higher than the experimental value 3519 MeV observed by SELEX collaboration. The mass of Ω_{cc} has not been measured in experiment, we predict it to be $3763 \pm 19 \pm 26_{-79}^{+13}$ MeV.

The main source of uncertainty in our calculation arises from discretization errors. Calculating the charmed baryon spectrum for several different lattice spacings and extrapolating to the continuum limit is the priority of our future plans. We also plan to extend our calculation to include the spin-3/2 charmed baryons and bottom baryons.

The charmed hadron interactions are studied in chapter 6. The scattering lengths are calculated using Lüscher's finite volume method, which is described in section 4.3. The scattering of charmed mesons with light pseudoscalar mesons has been studied in chiral perturbation theory, we use the formulas to extrapolate the scattering lengths to the physical light quark mass. We calculate the scattering lengths of isospin-3/2 $D\pi$, $D_s\pi$, D_sK , isospin-0 $D\bar{K}$ and isospin-1 $D\bar{K}$ channels on lattice. The scattering lengths of the isospin-0 and 1 DK , $D_s\bar{K}$ and isospin-1/2 $D\pi$ channels are predicted by the low-energy constants determined from the chiral fits. We find strong attractive interaction in the isospin-0 DK channel. This channel is closely related to the structure of the $D_{sJ}(2317)$ state. However, studying volume dependence of the interaction is needed to determine whether there is a bound state in this channel.

We also calculate the scattering lengths of the charmonium (η_c and J/Ψ) with light hadrons (ρ and N). Very weak attractive interactions are found in these channels. Particularly, for the $J/\Psi - N$ channel, in which the dominate interaction is attractive gluonic van der Waals and it could lead to molecular-like bound states, we

find the scattering length is tiny comparing to the predictions from some hadronic models. In the future, we plan to improve the statistics and extend the calculation to multiple volumes to obtain more definite information about this channel.

Bibliography

- [1] A. Walker-Loud et al. Light hadron spectroscopy using domain wall valence quarks on an Asqtad sea. *Phys. Rev.*, D79:054502, 2009.
- [2] C. Amsler et al. Review of particle physics. *Phys. Lett.*, B667:1, 2008.
- [3] Heechang Na and Steven Gottlieb. Heavy baryon mass spectrum from lattice QCD with 2+1 dynamical sea quark flavors. *PoS*, LATTICE2008:119, 2008.
- [4] W. Roberts and Muslema Pervin. Heavy baryons in a quark model. *Int. J. Mod. Phys.*, A23:2817–2860, 2008.
- [5] A. P. Martynenko. Ground-state triply and doubly heavy baryons in a relativistic three-quark model. *Phys. Lett.*, B663:317–321, 2008.
- [6] D. Ebert, R. N. Faustov, V. O. Galkin, and A. P. Martynenko. Mass spectra of doubly heavy baryons in the relativistic quark model. *Phys. Rev.*, D66:014008, 2002.
- [7] J. G. Korner, M. Kramer, and D. Pirjol. Heavy baryons. *Prog. Part. Nucl. Phys.*, 33:787–868, 1994.
- [8] V. V. Kiselev, A. K. Likhoded, O. N. Pakhomova, and V. A. Saleev. Mass spectra of doubly heavy Omega Q Q-prime baryons. *Phys. Rev.*, D66:034030, 2002.

- [9] V. V. Kiselev and A. E. Kovalsky. Doubly heavy baryons Omega(Q Q-prime) versus Xi(Q Q-prime) in sum rules of NRQCD. *Phys. Rev.*, D64:014002, 2001.
- [10] R. Roncaglia, D. B. Lichtenberg, and E. Predazzi. PREDICTING THE MASSES OF BARYONS CONTAINING ONE OR TWO HEAVY QUARKS. *Phys. Rev.*, D52:1722–1725, 1995.
- [11] M Gell-Mann. A Schematic Model of Baryons and Mesons. *Phys. Lett.*, 8:214, 1964.
- [12] M Gell-Mann. Symmetries of Baryons and Mesons. *Phys. Rev.*, 125:1067, 1962.
- [13] G Zweig. An SU(3) Model for Strong Interaction Symmetry and Its Breaking. *Developments in the Quark Theory of Hadrons, Vol. 1*, pages 22–101, 1964.
- [14] S. K Choi et al. Observation of a narrow charmonium - like state in exclusive $B^+ \rightarrow K^+ \pi^+ \pi^- J/\psi$ decays. *Phys. Rev. Lett.*, 91:262001, 2003.
- [15] B. Aubert et al. Evidence for $X(3872) \rightarrow \psi(2S)\gamma$ in $B^\pm \rightarrow X(3872)K^\pm$ decays, and a study of $B \rightarrow c\bar{c}\gamma K$. *Phys. Rev. Lett.*, 102:132001, 2009.
- [16] D. Acosta et al. Observation of the Narrow State $X(3872) \rightarrow J/\psi\pi^+\pi^-$ in $\bar{p}p$ Collisions at $\sqrt{s} = 1.96\text{TeV}$. *Phys. Rev. Lett.*, 93:072001, 2004.
- [17] B. Aubert et al. Study of the $B^- \rightarrow J/\psi K^- \pi^+ \pi^-$ Decay and Measurement of the $B^- \rightarrow X(3872)K^-$ Branching Fraction. *Phys. Rev.*, D71:071103, 2005.
- [18] S. K Choi et al. Observation of a near-threshold $\omega J/\psi$ mass enhancement in exclusive $B \rightarrow K\omega J/\psi$ decays. *Phys. Rev. Lett.*, 94:182002, 2005.
- [19] T. Aaltonen et al. Evidence for a Narrow Near-Threshold Structure in the $J/\psi\phi$ Mass Spectrum in $B^+ \rightarrow J/\psi K^+$ Decays. *Phys. Rev. Lett.*, 102:242002, 2009.

- [20] B. Aubert et al. Observation of a Broad Structure in the $\pi^+\pi^-J/\psi$ Mass Spectrum around 4.26 GeV/ c^2 . *Phys. Rev. Lett.*, 95:142002, 2005.
- [21] Michael Creutz. *Quarks, Gluons and Lattices*. Cambridge University Press, 1983.
- [22] István Montvay and Gernot Münster. *Quantum Fields on a Lattice*. Cambridge University Press, 1994.
- [23] Thomas DeGrand and Carleton DeTar. *Lattice Methods for Quantum Chromodynamics*. World Scientific Publishing, 2006.
- [24] K. Osterwalder and R. Schrader. Axioms for euclidean green's functions. *Comm. Math. Phys.*, 31:83, 1973.
- [25] K. Osterwalder and R. Schrader. Axioms for euclidean green's functions ii. *Comm. Math. Phys.*, 42:81, 1975.
- [26] K. G. Wilson. Confinement of quarks. *Phys. Rev.*, D10:2445, 1974.
- [27] C. Gattringer and C. B. Lang. *Quantum Chromodynamics on the Lattice: An Introductory Presentation*. Springer, Berlin Heidelberg, 2010.
- [28] H. B. Nielsen and M. Ninomiya. A no-go theorem for regularizing chiral fermions. *Phys. Lett.*, B105:219, 1981.
- [29] Herbert Neuberger. Exactly massless quarks on the lattice. *Phys. Lett.*, B417:141, 1998.
- [30] Herbert Neuberger. More about exactly massless quarks on the lattice. *Phys. Lett.*, B427:353, 1998.

- [31] David B. Kaplan. A Method for simulating chiral fermions on the lattice. *Phys. Lett.*, B288:342–347, 1992.
- [32] David B. Kaplan. Chiral fermions on the lattice. *Nucl. Phys. Proc. Suppl.*, 30:597, 1993.
- [33] Yigal Shamir. Chiral fermions from lattice boundaries. *Nucl. Phys.*, B406:90–106, 1993.
- [34] Vadim Furman and Yigal Shamir. Axial symmetries in lattice QCD with Kaplan fermions. *Nucl. Phys.*, B439:54–78, 1995.
- [35] Howard Georgi. AN EFFECTIVE FIELD THEORY FOR HEAVY QUARKS AT LOW- ENERGIES. *Phys. Lett.*, B240:447–450, 1990.
- [36] S. Weinberg. Phenomenological lagrangians. *Physica*, A96:327, 1979.
- [37] J. Gasser and H. Leutwyler. Chiral Perturbation Theory to One Loop. *Ann. Phys.*, 158:142, 1984.
- [38] J. Gasser and H. Leutwyler. Chiral Perturbation Theory: Expansions in the Mass of the Strange Quark. *Nucl. Phys.*, B250:465, 1985.
- [39] Aneesh V. Manohar and Mark B. Wise. Heavy quark physics. *Camb. Monogr. Part. Phys. Nucl. Phys. Cosmol.*, 10:1–191, 2000.
- [40] M. Neubert. Heavy Quark Symmetry. *Phys. Rept.*, 245:259, 1994.
- [41] E. Jenkins and A. V. Manohar. Baryon chiral perturbation theory using a heavy fermion lagrangian. *Phys. Lett.*, B255:258, 1991.
- [42] E. Jenkins and A. V. Manohar. Chiral corrections to the baryon axial currents. *Phys. Lett.*, B259:353, 1991.

- [43] E. Jenkins and A. V. Manohar. Baryon chiral perturbation theory. *Talk presented at the workshop on Effective Field Theories of the Standard Model, Dobogoko, Hungary, Aug 1991.*
- [44] W. Rarita and J. S. Schwinger. On a theory of particle with half integral spin. *Phys. Rev.*, 60:61, 1941.
- [45] Brian C. Tiburzi. Baryon masses in partially quenched heavy hadron chiral perturbation theory. *Phys. Rev.*, D71:034501, 2005.
- [46] Feng-Kun Guo, Christoph Hanhart, and Ulf-G Meier. Interactions between heavy mesons and goldstone bosons from chiral dynamics. *Eur. Phys. J.*, A40:171–179, 2009.
- [47] Yan-Rui Liu, Xiang Liu, and Shi-Lin Zhu. Light pseudoscalar meson and heavy meson scattering lengths. *Phys. Rev. D*, 79:094026, 2009.
- [48] Claude W. Bernard et al. The QCD spectrum with three quark flavors. *Phys. Rev.*, D64:054506, 2001.
- [49] Mark G. Alford, W. Dimm, G. P. Lepage, G. Hockney, and P. B. Mackenzie. Lattice QCD on small computers. *Phys. Lett.*, B361:87–94, 1995.
- [50] Kostas Orginos, Doug Toussaint, and R. L. Sugar. Variants of fattening and flavor symmetry restoration. *Phys. Rev.*, D60:054503, 1999.
- [51] Kostas Orginos and Doug Toussaint. Testing improved actions for dynamical Kogut-Susskind quarks. *Phys. Rev.*, D59:014501, 1999.
- [52] D. Toussaint and K. Orginos. Tests of improved Kogut-Susskind fermion actions. *Nucl. Phys. Proc. Suppl.*, 73:909–911, 1999.

- [53] J. F. Lagae and D. K. Sinclair. Improved staggered quark actions with reduced flavour symmetry violations for lattice QCD. *Phys. Rev.*, D59:014511, 1999.
- [54] G. Peter Lepage. Flavor-symmetry restoration and Symanzik improvement for staggered quarks. *Phys. Rev.*, D59:074502, 1999.
- [55] K. Orginos, R. Sugar, and D. Toussaint. Improved flavor symmetry in Kogut-Susskind fermion actions. *Nucl. Phys. Proc. Suppl.*, 83:878–880, 2000.
- [56] Satchidananda Naik. ON-SHELL IMPROVED LATTICE ACTION FOR QCD WITH SUSSKIND FERMIONS AND ASYMPTOTIC FREEDOM SCALE. *Nucl. Phys.*, B316:238, 1989.
- [57] Silas R. Beane, Kostas Orginos, and Martin J. Savage. Hadronic Interactions from Lattice QCD. *Int. J. Mod. Phys.*, E17:1157–1218, 2008.
- [58] Anna Hasenfratz and Francesco Knechtli. Flavor symmetry and the static potential with hypercubic blocking. *Phys. Rev.*, D64:034504, 2001.
- [59] Thomas A. DeGrand, Anna Hasenfratz, and Tamas G. Kovacs. Improving the chiral properties of lattice fermions. *Phys. Rev.*, D67:054501, 2003.
- [60] Thomas A. DeGrand. Kaon B Parameter in Quenched QCD. *Phys. Rev.*, D69:014504, 2004.
- [61] Stephan Durr, Christian Hoelbling, and Urs Wenger. Staggered eigenvalue mimicry. *Phys. Rev.*, D70:094502, 2004.
- [62] Oliver Bar, Claude Bernard, Gautam Rupak, and Noam Shoreh. Chiral perturbation theory for staggered sea quarks and Ginsparg-Wilson valence quarks. *Phys. Rev.*, D72:054502, 2005.

- [63] Brian C. Tiburzi. Baryons with Ginsparg-Wilson quarks in a staggered sea. *Phys. Rev.*, D72:094501, 2005.
- [64] Jiunn-Wei Chen, Donal O’Connell, and Andre Walker-Loud. Two meson systems with Ginsparg-Wilson valence quarks. *Phys. Rev.*, D75:054501, 2007.
- [65] Kostas Orginos and Andre Walker-Loud. Mixed meson masses with domain-wall valence and staggered sea fermions. *Phys. Rev.*, D77:094505, 2008.
- [66] Jiunn-Wei Chen, Donal O’Connell, and Andre Walker-Loud. Universality of Mixed Action Extrapolation Formulae. *JHEP*, 04:090, 2009.
- [67] Jiunn-Wei Chen, Maarten Golterman, Donal O’Connell, and Andre Walker-Loud. Mixed Action Effective Field Theory: an Addendum. *Phys. Rev.*, D79:117502, 2009.
- [68] Weon-Jong Lee and Stephen R. Sharpe. Partial Flavor Symmetry Restoration for Chiral Staggered Fermions. *Phys. Rev.*, D60:114503, 1999.
- [69] Dru Bryant Renner et al. Hadronic physics with domain-wall valence and improved staggered sea quarks. *Nucl. Phys. Proc. Suppl.*, 140:255–260, 2005.
- [70] Robert G. Edwards et al. Hadron structure with light dynamical quarks. *PoS*, LAT2005:056, 2006.
- [71] Aida X. El-Khadra, Andreas S. Kronfeld, and Paul B. Mackenzie. Massive Fermions in Lattice Gauge Theory. *Phys. Rev.*, D55:3933–3957, 1997.
- [72] K. Symanzik. Continuum Limit and Improved Action in Lattice Theories. 1. Principles and ϕ^4 Theory. *Nucl. Phys.*, B226:187, 1983.

- [73] Ping Chen. Heavy quarks on anisotropic lattices: The charmonium spectrum. *Phys. Rev.*, D64:034509, 2001.
- [74] G. Roepstorff. *Path Integral Approach to Quantum Physics*. Springer, Berlin Heidelberg, 1996.
- [75] L. Brown. *Quantum Field Theory*. Cambridge University Press, 1992.
- [76] M. Lüscher and U. Wolff. How To Calculate The Elastic Scattering Matrix In Two-Dimensional Quantum Field Theories By Numerical Simulation. *Nucl. Phys.*, B339:222, 1990.
- [77] B. Blossier et al. On the Generalized eigenvalue method for energies and matrix elements in lattice field theory. *JHEP*, 0904:094, 2009.
- [78] L. Maiani and M. Testa. Final state interactions from Euclidean correlation functions. *Phys. Lett.*, B245:585, 1990.
- [79] M. Lüscher. Volume dependence of the energy spectrum in massive quantum field theories II: Scattering states. *Commun. Math. Phys.*, 105:153, 1986.
- [80] M. Lüscher. Two particle states on a torus and their relation to the scattering matrix. *Nucl. Phys.*, B354:531, 1991.
- [81] S. R. Beane, P. F. Bedaque, and M. J. Savage. Two Nucleons on a Lattice. *Phys. Lett.*, B585:106, 2004.
- [82] R. G. Newton. *Scattering Theory of Waves and Particles*. Springer, New York, 1982.
- [83] S. Sasaki and T. Yamazaki. Signature of S-wave Bound State Formation in Finite Volume. *Phys. Rev.*, D74:114507, 2006.

- [84] E. Barberio et al. Averages of b -hadron and c -hadron Properties at the End of 2007. 2008.
- [85] M. B. Voloshin. Charmonium. *Prog. Part. Nucl. Phys.*, 61:455–511, 2008.
- [86] T. Aaltonen et al. First observation of heavy baryons Σ_b and Σ_b^* . *Phys. Rev. Lett.*, 99:202001, 2007.
- [87] V. M. Abazov et al. Direct observation of the strange b baryon Xi_b^- . *Phys. Rev. Lett.*, 99:052001, 2007.
- [88] M. Mattson et al. First observation of the doubly charmed baryon Xi_{cc}^+ . *Phys. Rev. Lett.*, 89:112001, 2002.
- [89] A. Ocherashvili et al. Confirmation of the double charm baryon $Xi_{cc}(3520)^+$ via its decay to $p D^+ K^-$. *Phys. Lett.*, B628:18–24, 2005.
- [90] T. Aaltonen et al. Observation and mass measurement of the baryon Xi_b^- . *Phys. Rev. Lett.*, 99:052002, 2007.
- [91] G. Peter Lepage, Lorenzo Magnea, Charles Nakhleh, Ulrika Magnea, and Kent Hornbostel. Improved nonrelativistic QCD for heavy quark physics. *Phys. Rev.*, D46:4052–4067, 1992.
- [92] Sinya Aoki, Yoshinobu Kuramashi, and Shin-ichi Tominaga. Relativistic heavy quarks on the lattice. *Prog. Theor. Phys.*, 109:383–413, 2003.
- [93] Norman H. Christ, Min Li, and Huey-Wen Lin. Relativistic heavy quark effective action. *Phys. Rev.*, D76:074505, 2007.
- [94] Huey-Wen Lin and Norman Christ. Non-perturbatively determined relativistic heavy quark action. *Phys. Rev.*, D76:074506, 2007.

- [95] Andreas S. Kronfeld. Heavy quarks and lattice QCD. *Nucl. Phys. Proc. Suppl.*, 129:46–59, 2004.
- [96] Matthew Wingate. Status of lattice flavor physics. *Nucl. Phys. Proc. Suppl.*, 140:68–77, 2005.
- [97] Masataka Okamoto. Full determination of the CKM matrix using recent results from lattice QCD. *PoS*, LAT2005:013, 2006.
- [98] Tetsuya Onogi. Heavy flavor physics from lattice QCD. *PoS*, LAT2006:017, 2006.
- [99] Michele Della Morte. Standard Model parameters and heavy quarks on the lattice. *PoS*, LAT2007:008, 2007.
- [100] Elvira Gamiz. Heavy flavour phenomenology from lattice QCD. 2008.
- [101] K. C. Bowler et al. Heavy Baryon Spectroscopy from the Lattice. *Phys. Rev.*, D54:3619–3633, 1996.
- [102] J. M. Flynn, F. Mescia, and Abdullah Shams Bin Tariq. Spectroscopy of doubly-charmed baryons in lattice QCD. *JHEP*, 07:066, 2003.
- [103] Ting-Wai Chiu and Tung-Han Hsieh. Baryon masses in lattice QCD with exact chiral symmetry. *Nucl. Phys.*, A755:471–474, 2005.
- [104] Randy Lewis, Nilmani Mathur, and R. M. Woloshyn. Charmed baryons in lattice QCD. *Phys. Rev.*, D64:094509, 2001.
- [105] Nilmani Mathur, Randy Lewis, and R. M. Woloshyn. Charmed and bottom baryons from lattice NRQCD. *Phys. Rev.*, D66:014502, 2002.

- [106] Heechang Na and Steven A. Gottlieb. Charm and bottom heavy baryon mass spectrum from lattice QCD with 2+1 flavors. *PoS*, LAT2007:124, 2007.
- [107] Liuming Liu, Huey-Wen Lin, and Kostas Orginos. Charmed Hadron Interactions. *PoS*, LATTICE2008:112, 2008.
- [108] Gilberto Colangelo, Stephan Durr, and Christoph Haefeli. Finite volume effects for meson masses and decay constants. *Nucl. Phys.*, B721:136–174, 2005.
- [109] Mark B. Wise. Chiral perturbation theory for hadrons containing a heavy quark. *Phys. Rev.*, D45:2188–2191, 1992.
- [110] Gustavo Burdman and John F. Donoghue. Union of chiral and heavy quark symmetries. *Phys. Lett.*, B280:287–291, 1992.
- [111] Tung-Mow Yan et al. Heavy quark symmetry and chiral dynamics. *Phys. Rev.*, D46:1148–1164, 1992.
- [112] Peter L. Cho. Chiral perturbation theory for hadrons containing a heavy quark: The Sequel. *Phys. Lett.*, B285:145–152, 1992.
- [113] Peter L. Cho. Heavy hadron chiral perturbation theory. *Nucl. Phys.*, B396:183–204, 1993.
- [114] Martin J. Savage. Charmed baryon masses in chiral perturbation theory. *Phys. Lett.*, B359:189–193, 1995.
- [115] Jie Hu and Thomas Mehen. Chiral Lagrangian with heavy quark-diquark symmetry. *Phys. Rev.*, D73:054003, 2006.
- [116] Martin J. Savage. Heavy-meson observables at one-loop in partially quenched chiral perturbation theory. *Phys. Rev.*, D65:034014, 2002.

- [117] Thomas Mehen and Brian C. Tiburzi. Doubly heavy baryons and quark-diquark symmetry in quenched and partially quenched chiral perturbation theory. *Phys. Rev.*, D74:054505, 2006.
- [118] Brian C. Tiburzi and Andre Walker-Loud. Hyperons in Two Flavor Chiral Perturbation Theory. *Phys. Lett.*, B669:246–253, 2008.
- [119] C. Aubin et al. Light pseudoscalar decay constants, quark masses, and low energy constants from three-flavor lattice QCD. *Phys. Rev.*, D70:114501, 2004.
- [120] Silas R. Beane, Paulo F. Bedaque, Kostas Orginos, and Martin J. Savage. $I = 2$ $\pi\pi$ scattering from fully-dynamical mixed-action lattice QCD. *Phys. Rev.*, D73:054503, 2006.
- [121] A. Bazavov et al. Full nonperturbative QCD simulations with 2+1 flavors of improved staggered quarks. 2009.
- [122] Jozef J. Dudek, Robert G. Edwards, Nilmani Mathur, and David G. Richards. Charmonium excited state spectrum in lattice QCD. *Phys. Rev.*, D77:034501, 2008.
- [123] Benjamin Grinstein. THE STATIC QUARK EFFECTIVE THEORY. *Nucl. Phys.*, B339:253–268, 1990.
- [124] Adam F. Falk, Howard Georgi, Benjamin Grinstein, and Mark B. Wise. HEAVY MESON FORM-FACTORS FROM QCD. *Nucl. Phys.*, B343:1–13, 1990.
- [125] Huey-Wen Lin. Charmed spectroscopy from a nonperturbatively determined relativistic heavy quark action in full QCD. *PoS*, LAT:184, 2006.
- [126] L. Levkova and Carleton E. DeTar. Contributions of charm annihilation to the hyperfine splitting in charmonium. 2008.

- [127] Steven Gottlieb et al. Onium masses with three flavors of dynamical quarks. *PoS, LAT2005:203*, 2006.
- [128] Fu-Jiun Jiang and Brian C. Tiburzi. Hyperon Axial Charges in Two-Flavor Chiral Perturbation Theory. 2009.
- [129] Maxim Mai, Peter C. Bruns, Bastian Kubis, and Ulf-G. Meissner. Aspects of meson-baryon scattering in three- and two- flavor chiral perturbation theory. 2009.
- [130] B. C. Tiburzi. Two-Flavor Chiral Perturbation Theory for Hyperons. 2009.
- [131] Andre Walker-Loud. New lessons from the nucleon mass, lattice QCD and heavy baryon chiral perturbation theory. 2008.
- [132] Brian C. Tiburzi and Andre Walker-Loud. Decuplet baryon masses in partially quenched chiral perturbation theory. *Nucl. Phys.*, A748:513–536, 2005.
- [133] Elizabeth Ellen Jenkins. Heavy Baryon Masses in the $1/m_Q$ and $1/N_c$ Expansions. *Phys. Rev.*, D54:4515–4531, 1996.
- [134] Roger F. Dashen, Elizabeth Ellen Jenkins, and Aneesh V. Manohar. The $1/N(c)$ expansion for baryons. *Phys. Rev.*, D49:4713–4738, 1994.
- [135] Elizabeth Ellen Jenkins and Richard F. Lebed. Baryon mass splittings in the $1/N_c$ Expansion. *Phys. Rev.*, D52:282–294, 1995.
- [136] Elizabeth Ellen Jenkins, Aneesh V. Manohar, John W. Negele, and Andre Walker-Loud. A Lattice Test of $1/N_c$ Baryon Mass Relations. 2009.
- [137] B. Aubert et al. Search for doubly charmed baryons Ξ_{cc}^+ and Ξ_{cc}^{++} in BABAR. *Phys. Rev.*, D74:011103, 2006.

- [138] R. Chistov et al. Observation of new states decaying into $\Lambda/c + K^- \pi^+$ and $\Lambda/c + K^0(S) \pi^-$. *Phys. Rev. Lett.*, 97:162001, 2006.
- [139] Mehmet B. Oktay and Andreas S. Kronfeld. New lattice action for heavy quarks. *Phys. Rev.*, D78:014504, 2008.
- [140] B. Sheikholeslami and R. Wohlert. Improved Continuum Limit Lattice Action for QCD with Wilson Fermions. *Nucl. Phys.*, B259:572, 1985.
- [141] Mark G. Alford, T. Klassen, and P. Lepage. The D234 action for light quarks. *Nucl. Phys. Proc. Suppl.*, 47:370–373, 1996.
- [142] Ting-Wai Chiu. Optimal domain-wall fermions. *Phys. Rev. Lett.*, 90:071601, 2003.
- [143] S. P. Ratti. New results on c-baryons and a search for cc-baryons in FOCUS. *Nucl. Phys. Proc. Suppl.*, 115:33–36, 2003.
- [144] Kazuo Yokokawa, Shoichi Sasaki, Tetsuo Hatsuda, and Arata Hayashigaki. First Lattice Study of Low-energy Charmonium-hadron interaction. *Phys. Rev.*, D74:034504, 2006.
- [145] G. Meng et al. Low-energy $D^{*+} D_1^0$ Scattering and the Resonance-like Structure $Z^+(4430)$. *Phys. Rev.*, D80:034503, 2009.
- [146] Shi-Lin Zhu. New hadron states. *Int. J. Mod. Phys.*, E17:283, 2008.
- [147] S. J. Brodsky, I. A. Schmidt, and G. F. de Teramond. Nuclear Bound Quarkonium. *Phys. Rev. Lett.*, 64:1011, 1990.
- [148] M. E. Luke, A. V. Manohar, and M. J. Savage. A QCD calculation of the interaction of quarkonium with nuclei. *Phys. Lett.*, B288:355, 1992.

- [149] S. J. Brodsky and G. A. Miller. Is J/Psi-nucleon scattering dominated by the gluonic van der waals interaction? *Phys. Lett.*, B412:125, 1997.